EXPERIMENTAL AND THEORETICAL INVESTIGATION ON WATER DESALINATION USING MEMBRANE DISTILLATION

BY

HAFIZ MUHAMMAD AHMAD

A Thesis Presented to the
DEANSHIP OF GRADUATE STUDIES

KING FAHD UNIVERSITY OF PETROLEUM & MINERALS

DHAHRAN, SAUDI ARABIA

In Partial Fulfillment of the
Requirements for the Degree of

MASTER OF SCIENCE

In

MECHANICAL ENGINEERING

MAY 2015

KING FAHD UNIVERSITY OF PETROLEUM & MINERALS
DHAHRAN- 31261, SAUDI ARABIA
DEANSHIP OF GRADUATE STUDIES

This thesis, written by **HAFIZ MUHAMMAD AHMAD** under the direction his thesis advisor and approved by his thesis committee, has been presented and accepted by the Dean of Graduate Studies, in partial fulfillment of the requirements for the degree of **MASTER OF SCIENCE.**

A. Khalifa

Dr. Atia E. Khalifa
(Advisor)

Dr. Zuhair M. Gasem
Department Chairman

M Antar

Dr. Mohammed A. Antar
(Member)

Dr. Salam A. Zummo
Dean of Graduate Studies

Dr. Tahar Laoui
(Member)

3/6/15
Date

EXPERIMENTAL AND THEORETICAL INVESTIGATION ON WATER DESALINATION USING MEMBRANE DISTILLATION

HAFIZ MUHAMMAD AHMAD

MECHANICAL ENGINEERING DEPARTMENT

MAY 2015

This work is dedicated to my beloved family

ACKNOWLEDGMENTS

I would like to thank King Fahd University of Petroleum and Minerals (KFUPM) for funding my research work and providing me the environment to achieve this level of study. I would like to express my gratitude and sincere thanks to my thesis advisor Dr. Atia Khalifa. He is not only helpful with deep vision and understanding but also most importantly a kind person. I honestly consider him as a friend rather than my advisor. Because a friend can be helpful in good and hard times. He has been such a great motivator for me throughout thesis work. I sincerely thank him for his exemplary guidance and encouragement. My profound and special thanks goes to my thesis committee members in the person of Dr. Mohammed Antar and Dr. Tahar Laoui for their support, guidance and constructive advice which really help me to successfully complete my thesis. And especially Dr. Antar, who has been praising all the times even for very minute achievements.

Many thanks to Mr. Mohammed Karam for his technical support throughout this work. My appreciation goes to Mr. Ali Kamal who assisted in machining the MD modules. My thanks also goes to Mr. Ibrahim Bahaaeldin, Mr. Syed Saber Ali and Mr. Thunaiyan for their technical support.

My appreciation goes to Professor M. Khayet of Universidad Complutense de Madrid (UCM), Spain and his group for carrying out membrane characterization test. I would like to acknowledge the support provided by Deanship of Scientific Research (DSR). My gratitude goes to people of Mechanical Engineering Department. I would equally like to thank all my friends and colleagues for their encouragement.

I am very grateful to the entire Pakistani and all Muslim community at KFUPM for their moral support and encouragement. Lastly, I would like to thank my mother, father and

sisters, brother, who taught me the value of hard working by their own example. They always encouraged me whenever I feel down myself. They rendered me enormous support whenever I needed it the most.

Table of Contents

LIST OF TABLES

LIST OF FIGURES

LIST OF ABBREVIATIONS

A : Area, m^2

C_p : Specific Heat J/kg-K

D_h : Hydraulic Diameter, m

D_{pore} : Pore Diameter, m

D_e : Diffusion Coefficient, m^2/s

% EE : Percent Evaporative Efficiency

h : Convective Heat Transfer Coefficient W/m^2-K

ΔH : Enthalpy or Latent Heat of vaporization of water, kJ/kg

k : Thermal Conductivity, W/m-K

k_s : Solute Mass Transfer Coefficient, m/s

Mol : Molecular Weight g/mol

J_w : Mass Flux kg/m^2-s

k_b : Boltzman constant, 1.3807×10^{-23}J/K

K_n : Knudsen Number

P : Pressure, Pa

r : Radius of membrane pore, m

R : Universal gas constant, 8314 J/kmol-K

Nu : Nusselt number

Re : Reynolds number

Sc : Schmidt number

Sh : Sherwood number

SEC : Specific energy consumption (kW-hr/m^3)

T : Absolute temperature, K

U : Overall heat transfer coefficient, W/m^2-K

x : Mole Fraction

Greek Symbols

α : Contribution of Knudsen diffusion to mass transfer

β : Concentration Polarization coefficient

δ : Membrane Thickness , m

ε : Porosity, %

μ : Viscosity Pa-s

ρ : Density kg/m^3

γ : Salt activity coefficient

τ : Membrane Tortuosity

λ : Mean Free path of water molecule, (m)

Subscripts

Ch : Channel

f : Feed side

p : Permeate side

bf : Bulk Feed

bp : Bulk Permeate

mf : Membrane Feed Surface

mp : Membrane permeate Surface

c : Conduction

m : Mean or Average Property

mem. : Membrane

k : Knudsen

M : Molecular

v : Vapors/ Vaporization

w : Water

w-a : Water in Air

ABSTRACT (English)

Full Name : Hafiz Muhammad Ahmad
Thesis Title : Experimental and Theoretical Investigation on water desalination using Membrane Distillation
Major Field : Mechanical Engineering
Date of Degree : April 2015

Membrane Distillation (MD) is a potential source of water desalination. This process is quite simple, easy to achieve, adoptable and also viable. In MD, a hydrophobic membrane is separated by two streams of waters. One is the hot feed saline water stream, and on the other side of membrane a cooling media that is used to condense the water vapours passing through the membrane pores. Water vapours are produced because of temperature and partial pressure difference on both sides of membrane. Depending upon the cooling media, the configuration of MD process can be classified. MD has many advantages but the important one is that 40-90 ^{o}C of temperature is required for the feed side and 10-30 ^{o}C temperature is required for the coolant side, and this temperature can be obtained easily by waste or renewable energy resource e.g. solar heating. It can also perform well at atmospheric pressure. The other main advantage of MD is that it gives good water product in terms of its flux and quality. e.g. very high salt rejection value, which is good for drinking purpose.

The main objectives of the present study is to establishing a setup at laboratory scale to perform different tests for Direct Contact (DCMD), Air Gap (AGMD) and Water Gap Membrane Distillation configurations (WGMD), then compare the performances of the DCMD and AGMD system for the same module design. Another comparison is made for

WGMD and AGMD for another design module. Investigation of the effects of different parameters like feed temperature, coolant temperature, feed flow rate, coolant flow rate, gap width on the permeate flux were conducted for different MD configurations. One of the most important objectives is to develop a valid mathematical heat and mass transfer model to predict flux and performance of the MD system.

ABSTRACT (Arabic)

ملخص الرسالة

الاسم : حافظ محمد أحمد

عنوان البحث : دراسة عملية ونظرية لتحلية الماء عن طريق التقطير باستخدام الغشاء

التخصص : الهندسة الميكانيكية

تاريخ منح الدرجة : أبريل 2015

تعتبر طريقة التقطير باستخدام الغشاء مصدرا واعدا لتحلية المياة. تتميز هذه الطريقة بالبساطة و سهولة التطبيق. في هذه الطريقة يفصل الغشاء بين تياري ماء أحدهما ساخن ومالح بينما على الجانب الآخر يوجد وسيط التبريد الذي يستخدم لتكثيف بخار الماء الذي يمر عبر مسام الغشاء. يتم توليد بخار الماء بسبب الفرق في درجة الحرارة والضغط الجزئي بين جانبيي الغشاء. يتم تصنيف عملية التقطير باستخدام الغشاء بناء على طبيعة وسيط التبريد. تمتلك هذه الطريقة عدة مميزات أهمها انخفاض درجة الحرارة المطلوبة والمقدرة بحوالي (40-90) درجة مئوية على جانب التغذية (جانب الماء الساخن) والتى يمكن الحصول عليها بسهولة من مخلفات الطاقة أو مصادر الطاقة المتجددة مثل الطاقة الشمسية. يمكن أيضا أن تعمل هذه الطريقة بصورة جيدة عند ضغط مساوي للضغط الجوي. من مميزات هذه الطريقة ايضا أنها تعطي انتاجية جيدة من الماء من حيث الكمية والجودة كما انها تتميز بمعدل طرد عالي للأملاح (مناسبة لأغراض الشرب).

الغرض الأساسي من الدراسة الحالية هو عمل منظومة لإجراء عدد من الإختبارات المختلفة على منظومات الإتصال المباشر (DCMD)، فجوة الهواء (AGMD) وفجوة الماء (WGMD) ثم مقارنة أداء منظومتي فجوة الماء والهواء لنفس التصميم. أيضا تمت مقارنة أداء المنظومتين باستخدام تصاميم مختلفة. تمت دراسة تأثير عدد من المتغيرات مثل درجة حرارة ماء التغذية(الماء الساخن)، درجة حرارة وسيط التبريد، معدل سريان ماء التغذية، معدل سريان وسيط التبريد وسمك الفجوة على معدل تدفق الماء

الناتج لمنظومات مختلفة. أحد أهم أهداف هذه الدراسة هو تطوير نموذج رياضي لإنتقال الكتلة و الحرارة لتقدير معدل السريان وأداء منظومة التقطير باستخدام الغشاء.

CHAPTER 1

INTRODUCTION

Clean drinking water is a basic need for everyone but unfortunately more than one in six people in the world is deprived of it. Of the total estimated volume of water of 1.4 billion km^3 (1018 m^3) in the world, more than 1.36 billion km^3 (97.5%) is seawater and only 35 million km^3 (2.5%) is fresh water. A substantial amount of the mentioned fresh water, about 24 million km^3 or 70%, is locked in the form of ice and permanent snow on the mountains, the Antarctic, and the Arctic region. UN document pegged the water "poverty level" at 1000 m3 per capita per year where nominally water is consumed by three major sectors of an economy, namely,

i) Irrigation 70%,

ii) Industry 22%

iii) Domestic 8%

Many countries in the semi desert and desert regions suffer from acute water shortage (500 m^3 per capita per year), caused by high population growth, diminishing underground water and increase rate of economic development Increase in fresh water demand exceeded 2% annually has been reported in many economies of the world, and such projections almost double the population growth rates of these countries [1]. With such trends, it is predicted that some regions of the world will be plagued by water scarcity, affecting more than 1.8 billion people by 2025, as compared to 0.25 billion presently in 2010 [2].

The famine of drinkable water for some regions or countries can be filled up by seawater desalination processes but each of the desalination process needs substantial amount of energy to be employed. However, the thermodynamic limit for desalination is dependent of the salinity and the temperature of seawater and the accepted specific energy consumption of seawater, with total dissolved solids (TDS) of 28,000 to 45,000 ppm, ranges from 0.78 to about 1 kWh/m3 [3], and major desalination methods found in the industry have specific energy consumption from 3 to 8 kWh/m3 [4]. Presently, the total desalination capacity in the world is 70 billion m3 per year, of which about 50 % is by membrane using the concept of reverse osmosis, and the remaining shares are by thermal processes such as the multi-stage flashing (MSF), the multi effect desalination (MED), vapor compression (VC) and adsorption desalination (AD). Although the non-membrane methods are lower in the world’s shares of desalination capacity, yet they are dominantly (70% share) used in the Gulf Cooperation Council (GCC) countries [5]. The percentages of thermal methods can be as high as 94% in some countries such as the Saudi Arabia, UAE, Qatar, Kuwait, etc. [6]. The major reasons for adopting the thermal methods in the GCC countries are; Firstly, the high feed salinity in the Gulf and the fouling susceptibility of membranes at high brine concentration limits the water recovery ratio of RO process. Secondly, the frequent occurrences of harmful algae blooms (HABs) in the water of Gulf tend to contain high concentration of toxins in seawater feed that may pass through the membrane pores, causing human illnesses and death if the toxins are ingested [7].

Thermal desalination methods are deemed more robust over the membrane or RO method. Both the MSF and MED processes hitherto are energy intensive because of the limitation in the top-brine and the ambient temperature levels. Recent hybridization trends of proven thermal methods to the adsorption processes and the effective anti-scallant dosing for sea-water feed have enabled better process design that leads to better cost competitiveness compared to ROs. The hybridization of thermal desalination systems is a novel concept because it latches on the proven thermally-driven processes by extracting low temperature waste or renewable heat sources for the AD cycles whist maintaining the same operational parameters for the conventional thermal processes. Hybrid desalination methods are new and no experimental results are available in the literature. There is a need of research to investigate the performance of hybrid desalination systems experimentally.

CHAPTER 2

LITERATURE REVIEW

2.1 Background

Fresh water is necessary not only for continuation of human life but also for economic development in the sectors such as agriculture, manufacturing and industries. The world population is increasing at a very high pace that indirectly increasing the straws into available fresh water sources. Fresh water available resources are being depleted due to pressure of increasing trend of population. Although more than half (70%) of earth is covered by water but there is still inadequate fresh water supply and this not only affects human life but is also the main bottleneck in economic development [8-10]. Most of the available water is in the form of sea and high salt concentration is the main hindrance of its direct utilization [11, 12].

"Desalination is a process that removes the excess amount of salt and minerals from sea water and brackish water to make it portable/drinkable". Desalination process actually separate the input water into two streams one with permissible limit of dissolved salts (the portable water stream) and the other containing the remaining high percentage dissolved salts (the rejected brine stream).

Membrane distillation is assumed to be one of the low grade energy utilization technology available for water desalination. Membrane Distillation is a potential source of water purification. This process is quite simple, easy to achieve, adoptable and also viable. There is a rapid growth in membrane technology that governs huge achievements in membrane distillation technology. It involves a hydrophobic microporous membrane that separates feed from permeate. Hydrophobicity of membrane disallows water in liquid form because of surface tension but vapor can pass through it by means of diffusion. The major reasons for adopting the thermal methods in the GCC countries are; firstly, the high feed salinity in the Gulf and the fouling susceptibility of membranes at high brine concentration limits the water recovery ratio of RO process. Secondly, the frequent occurrences of harmful algae blooms (HABs) in the water of Gulf tend to contain high concentration of toxins in seawater feed that may pass through the membrane pores, causing human illnesses and death if the toxins are ingested [7].

The driving force across membrane is the partial pressure of the two streams, which result in vapor formation. In DCMD , distillation process can be described as follows, vaporization occurring at the liquid-vapor interface at the membrane pore surface in the feed side, then these vapors diffuse in the pores from hot side to the cold side because of capillary action and then condensation occurs in the cold side[13]. DCMD is not only limited to water purification but can also be used for treatment of oilfield produced water [14]. Macedonio et el. reported that a good salt rejection factor can be obtained by desalinating water that is obtained after oilfield treatment by using PP and PVDF membranes at high flow rates of feed and coolant.

Manawi et. al. determined the effect of temperature polarization on the flux by measuring intermediate temperatures on membrane surface. He developed the multi-dimensional model in order to find temperatures at different points on membrane surface. Manawi et al. optimized the flux by minimizing temperature polarization co-efficient [15]. The effect of feed water salinity was studied by S.T. Hsu et. al. They experimented feed water as NaCl-H_2O solution and sea water and then compared the performances of both systems, and they also used ultrasonic technique for cleaning purpose [16].

Ali Boubakri et al. performed DCDM experiments with using PP (Polypropylene) membrane and reported a permeate flux of 2-3L/m^2-h on average subjected to a temperature difference of °C for sea and brackish water [17]. Shihong Lin et al. did a comprehensive energy analysis of MD-HX system and defined optimum relative flow rates and mass recovery rates and specific heat duty for the system. They coupled MD module with heat exchanger in order to recover latent of condensation of vapors in the coolant stream using a circular module [18]. Surapit srisurichan et al investigated the mass transport and fouling mechanism in direct contact membrane distillation system. They suggested that molecular diffusion model is the best one for diffusion in fouling related phenomenon [19]. The effect of coolant velocity is not much explained well in literature. Some researchers have point of view of decreasing flux by increasing permeate velocity and rest has opposite [20]. Gayathri Naidu et al. found values of 0.8-1.2 m/s as optimum for feed and permeate velocities.

The effect of channel smoothness and direction of flow was discussed by Chii Dong Ho et.al. They used eddy promoter to make roughened surface channels for feed and permeate. counter-current direction flow gives more flux than concurrent [21].

L. Martinez and F. J. Florido Diaz developed a model depending on dusty gas model of gas transport through membrane pores [18]. It was showing good agreement between assumed model and experimental values. M. Qtaishata et.al. provided a detailed analysis of the heat transfer in direct contact membrane distillation (DCMD). The influence of mass transfer on heat transfer flux was identified in the feed thermal boundary layer, across the membrane and through the permeate thermal boundary layer. A mathematical model was proposed to evaluate the experimental values of the thermal boundary layers' heat transfer coefficients, the membrane/liquid interface temperatures, the temperature polarization coefficient, the membrane mass transfer coefficient and the evaporation efficiency [22]. Olof investigated different form of dusty gas models were utilized for mass transfer Different heat and mass transfer correlations were tested in order to find the best correlation [13] and then came up with transitional model to be the best one. The same model was also used by Dahiru et. al. [23].

Air gap membrane distillation is a common membrane distillation configuration. A new module design for membrane distillation, namely material gap membrane distillation (MGMD), for sea water desalination has been proposed and successfully tested. It has been observed that employing appropriate materials between the membrane and the condensation plate in an air gap membrane distillation (AGMD) module enhanced the water vapor flux significantly [24]. An increase in the water vapor flux of about 200–800% was observed by filling the gap with sand and DI water at various feed water temperatures. While Khalifa [25] reported an increase of 80-140 % in flux. However, insulating materials such as polypropylene and polyurethane have no effect on the water vapor flux. The MGMD consists of filling the gap between the membrane and the condensation plate with different materials having different characteristics such as polyurethane (sponge), polypropylene mesh sand, and de-ionized water. If the filling media comes out to be water , it is treated as water gap membrane distillation (WGMD) or liquid gap membrane distillation (LGMD) [26]. The effect of these materials on the water vapor flux during the MGMD process has been studied and compared with AGMD flux under the same operating conditions. The effect of material thickness and feed flow rate on water vapour flux have been investigated and reported. AGMD/MGMD water vapor flux performance comparison using commercially available membranes provided by different manufacturers at different feed inlet temperatures.

MGMD configuration is comparable to the DCMD configuration in terms of heat transfer mainly due to the high heat loss through conduction[24] . Moreover, the temperature polarization effect is expected to increase at the permeate side for the following reasons:

1. There is no forced-convective heat transfer at the permeate side as it is the case in the DCMD configuration.

2. There is no heat transfer through vapor mass transfer as it is the case in the AGMD configuration. Hence, all the heat should be transferred by conduction through the filling material. However, this new configuration still maintains the AGMD configuration advantages, mainly separating the permeate from the cooling medium. Hot feed solution rolls over the hydrophobic membrane surface. liquid gap membrane distillation (LGMD) were considered in order to enhance the water production rate and the thermal efficiency of the MD technology[27, 28] . There is temperature difference across the membrane surface that causes partial pressure difference that generates water vapours. These vapours condense over the cooling surface and accumulate in the permitted gap. After filling the gap with condensed vapours it act as water gap and then extra water comes from top of the gap as fresh water[26]. In the cold side, coolant enters and rolls over the condensation plate to

keep temperature of condensing plate down as much as possible, so that condensation can be enhanced in order to produce maximum flux.

Researchers are thus pressurized from both the community and the industry to develop new techniques to produce fresh water form seawater or brackish water. This would fulfill the water demand especially for economic development. Many methods have been introduced in the past few years namely: 1) conservation, 2) management and 3) re-use of fresh water but there is a prediction that all these solution still cannot meet the world water demand. To utilize the seawater, desalination is the only solution to fuel the population and to supply water to industry for economic growth in future. The sections below will highlight the water secrecy, desalination methods and a novel desalination cycle.

2.2 Water Distribution Globally

More than 70% of earth surfaces are covered with water but the maximum portion (>97%) is in the form of ocean and deep ground water. According to World Health Organization (WHO), water having TDS less than 500ppm is drinkable and in some cases it can be up to 1000 ppm [29]. Standard seawater salt concentration varies from 35,000~45,000ppm and cannot be used as a portable or process water due to high TDS. Out of 3% of fresh water, more than 2% is locked in icecaps and glaciers and is very difficult to recover for use. Figure 2.1 shows the distribution of earth surface water and it can be seen that only less than 1% of fresh water is available in the form of lake and rivers [30]. This small amount of fresh water is not sufficient to fulfil the demand in different sectors of life cycle such as to quench the thrust of large World population, industrial development and agricultural purposes. Table 1 shows the amount of water in volume as fresh and salt water available in different form on earth surface. A large quantity of water is not useable because of high TDS and millions of people will be sacrificed in near the future due to poor water quality.

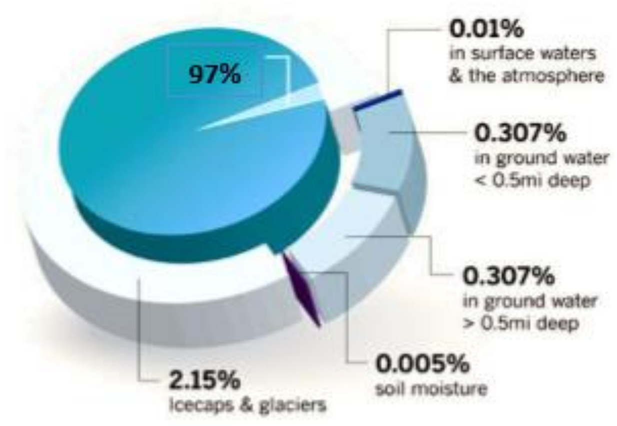

Figure 2. 1 Water distribution on earth surface

Table 2. 1 Global Water Distribution on the surface of earth [14]

Source	**Volume, in km^3**	
	Fresh water	Salt water
Oceans, Seas, & Bays	0	1,338,000,000
Ice Sheets, Glaciers, & Permafrost	24,364,000	0
Groundwater	10,530,000	12,870,000
Surface Water	122,210	85,400

Atmosphere	12,900	0
Totals	35,029,110	1,350,955,400
	Grand Total (rounded)	1,386,000,000

2.3 Water Demand in the world

Population dynamics is an important factor that affects the fresh water demand. World population growth is very fast as shown in Figure 2.2 and it is expected that it will grow up to 9 billion in 2050 compared to 7 billion in 2013 [31](The World Bank Group survey). The spread of population growth is not even in the world and most of population is concentrated in the developing countries.

Only a small percentage of global population (about 20%) have access to running water because of over pumping their non-replenish aquifers while over one billion people do not have access to clean water and this insufficient water supply results more than 15 million death annually. In the developing countries, almost 80% diseases are due to water quality and leading to more than 3 million deaths annually [32]. Figure 2.3 shows total water related deaths with and without United Nation Millennium Goals (UN-MG) that is “to halve, by the year 2015, the proportion of people who are unable to acquire safe drinking water. It can be seen that water related death rate may be increase from 5 million in 2000 to 120 million in 2050 without UN-MG. This trend can be reduced to 80 million by 2025 by achieving UN-MG [33]. These developing countries have greater demand for life commodities even with poor technologies. With increase in global population, pressure on water demand is also increasing and it almost doubles in every twenty years, a rate that is twice than the pace of growth of population. In the developing regions, the water consumption is very high as compared to the developed part of the world and it is due to three main factors such as

1) High population growth

2) Industrialization thrust

3) Agricultural need

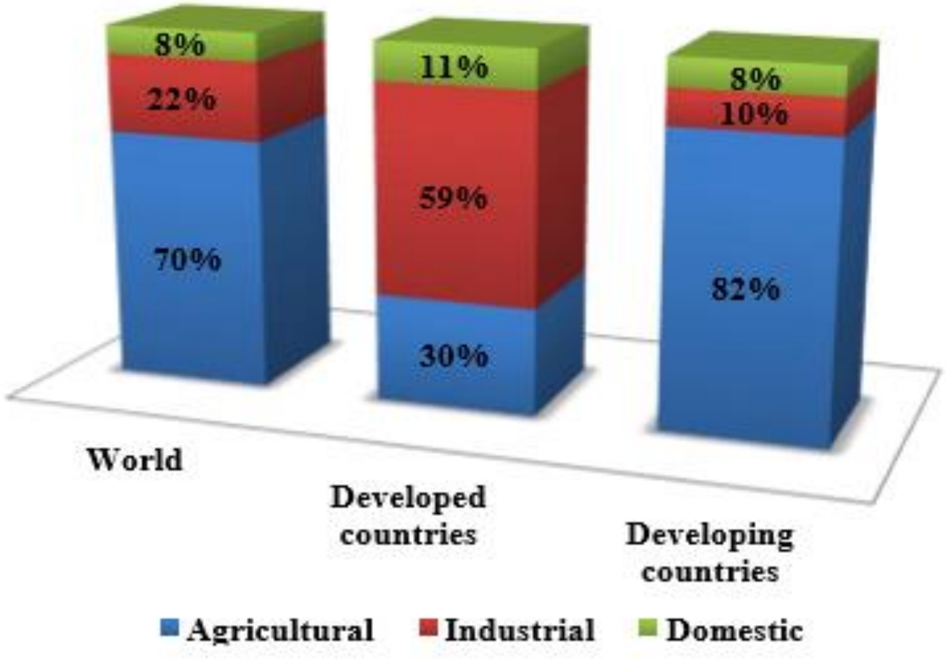

Figure 2. 2 Share of different sectors (%age) for water consumption [18]

Fresh water consumption in these sectors is different in different part of the World. Figure 2.2 shows the water consumption in each sector in developed and developing countries.

Developing countries are using most of the fresh water for agricultural purposes to feed their huge population while developed countries utilized them for industrial processes to enhance their economic growth [34]. Figure 2.3 shows fresh water requirement in billion cubic meters (Bm^3) per year in different parts of the world. It can be seen that major contribution is by Asian developing countries that is more than 50% of the world requirement followed by America and Europe [35, 36]. The gluttony of high GDP of highly dense populated regions i.e. developing countries is exerting more pressure on water demand and because of maximum intake the world water demand is increasing exponentially. Even though many measures are taken to handle the water problem like: implementing the technologies and policies for water re-use and conservation, improved water usage and population control, but as fresh water is very limited and not renewable so it cannot fulfil the world water demand. The unlimited source of water "the ocean" can only fulfil the world water demand in all sectors of life. Excess salt needs to be removed before using by desalination methods to convert high TDS saline water to low TDS portable water. Although desalination is not new, but the available technologies such as thermal and membrane are need to develop for most energy efficient and environment friendly processes. Fresh water shortfall and desalination methods are discussed in the following sections.

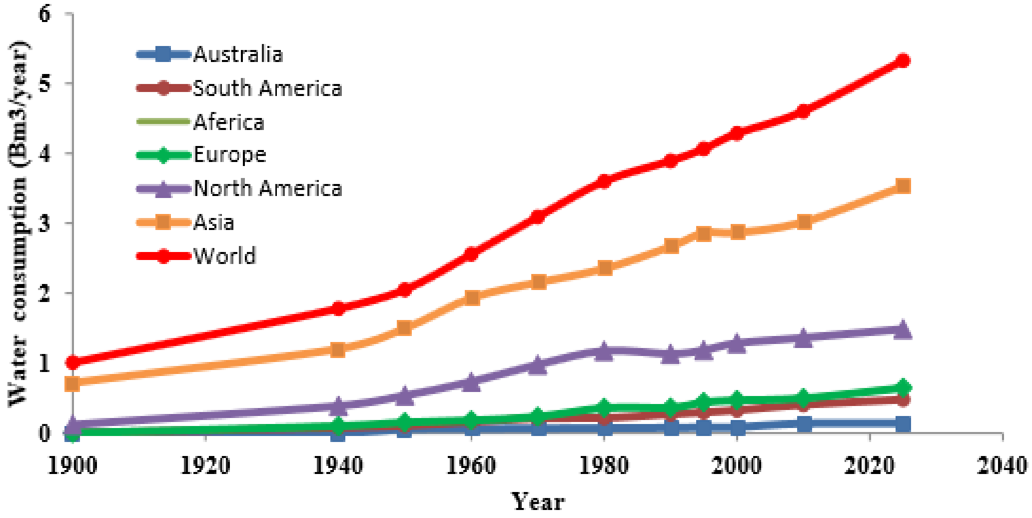

Figure 2. 3 Fresh water consumption in different parts of world [20]

2.4 Water Deficit and Desalination-An Overview

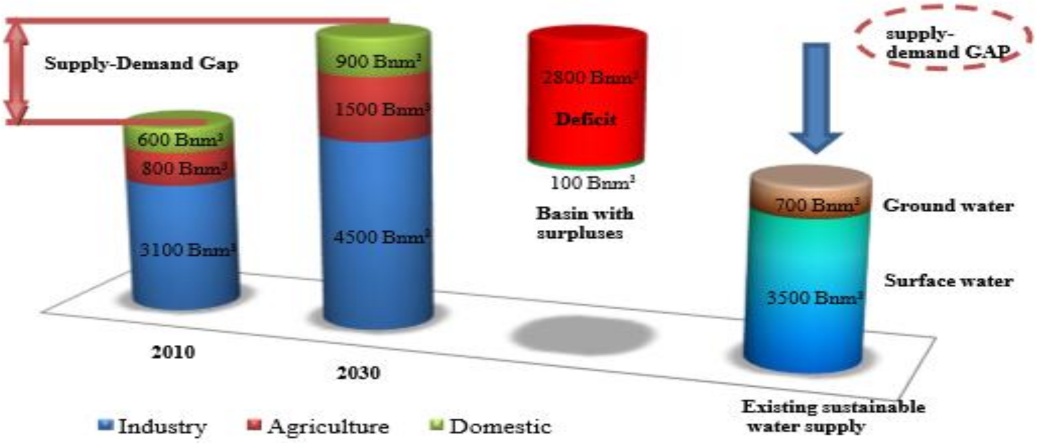

Figure 2. 4 Available global fresh water; consumption in in future [5, 6]

In 2010, the sustainable supply of fresh water from the Earth's natural water cycle was 4500 billion cubic meters (Bm3) and it is predicted to increase up to 6,900 Bm3 by 2030 with 2% annual increment due to population growth and industrialization thrust[7, 37] . At the present era, the total water demand has increased by 40% than current accessible reliable supply as shown in Figure 2.6 [7, 38]..

For agriculture and industry to maintain its rate to 2030 for economic development, promotion in water efficiency can only provide 20 percent of the supply-demand gap, leaving a huge deficit to be filled. Similarly, a business-as-usual supply build-out as shown in Figure 2.7, assuming constraints in infrastructure rather than raw resources, will stress only a further 20 percent of the gap. Even after considering these two measures, there is still a large gap between water supply and demand[38] .

Most developing and developed countries focus on addressing the water challenge by considering alternative sources in many cases through extensive energy measures such as desalination.

In the water depriving regions, fresh and clean water is produced by the desalination of seawater, brackish and recycled water. Basically “Desalination is a process that removes the excess amount of salt, ions of sodium, potassium and minerals from sea water and brackish water to make it portable/drinkable”. Desalination processes actually distributes the input stream of raw water into two streams of different concentrations ; one with acceptable limit of dissolved salts (the portable or fresh water stream) and the other containing the remaining high percentage dissolved salts (the rejected solution of high concentration with brine stream). Figure 2.8 shows the basic concept of a desalination process.

Since “the ocean” is the un-limited source of water, seawater desalination is being applied at 58% of installed capacity worldwide, followed by brackish water desalination accounting for 23% of installed capacity. Fig.2.9 outlines the global desalting capacities by feed water sources[39, 40]. The global desalination capacities are increasing at a rapid pace and according to International Desalination Association (IDA) 20th inventory the total global installed desalination capacities were increased from 44 million cubic meters per day (Mm3/day) in 2006 [41] to 69 Mm3/day in 2010 and is expected to double by 2015 [42]. Figure 2.10 shows the projected growth of the desalination market including all sources of feed water [43]. It can be seen that the growth rate is higher in gulf and GCC countries as compared to rest part of the world.

More than half (65%) of desalination capacities in the world are installed in the Middle East and Gulf Cooperation Council (GCC) countries [41]. Despite a higher desalination market share in GCC, the fresh water availability is dropping rapidly to below the acute water poverty level of 500 m3 per capital per [42] year for all consumption, caused by an exponential growth in population boom. Figure 2.11 shows the annual fresh water available per capita in desalination production and water demand requirements of GCC countries, spanning from the early decades in 1950 to the future years up to 2025 [43-45] .It can be seen that the available fresh water sources and present desalination capacities are not sufficient even to supply the water to meet acute water poverty level. Water production by desalination processes can have a significant effect on the energy requirement and environment. The intricate nexus between water, energy and environment has encouraged scientists and engineers to innovate desalination methods with better energy efficiency and environment friendly processes. The overview of presently available desalination technologies is provided in the following sections.

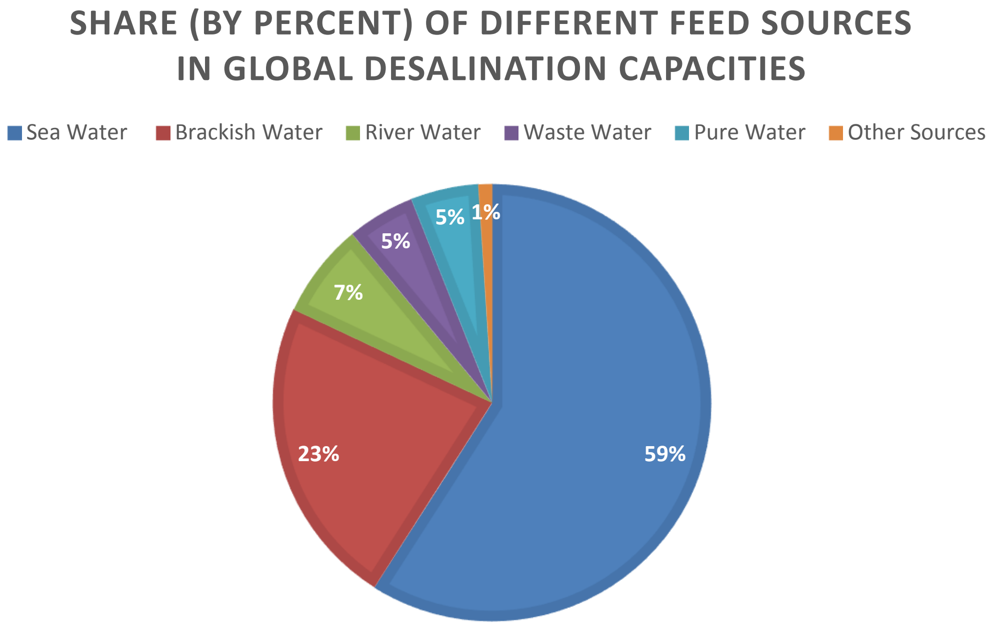

Figure 2. 5 Share of different feed sources in global desalination capacities [26]

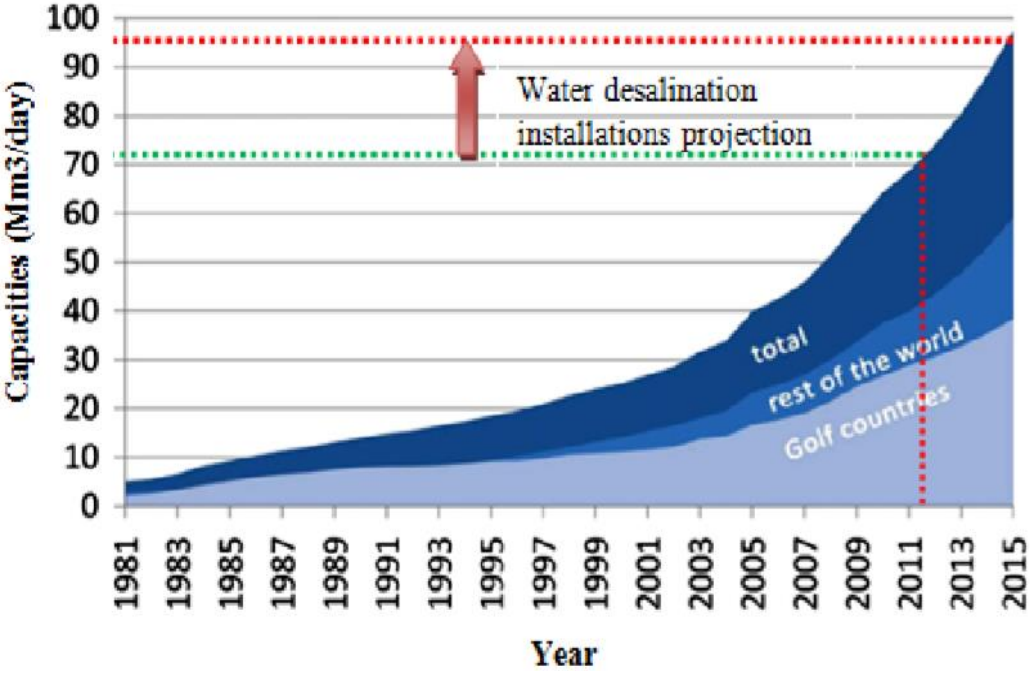

Figure 2. 6 Desalination capacities in past and estimated trend increase in future [33]

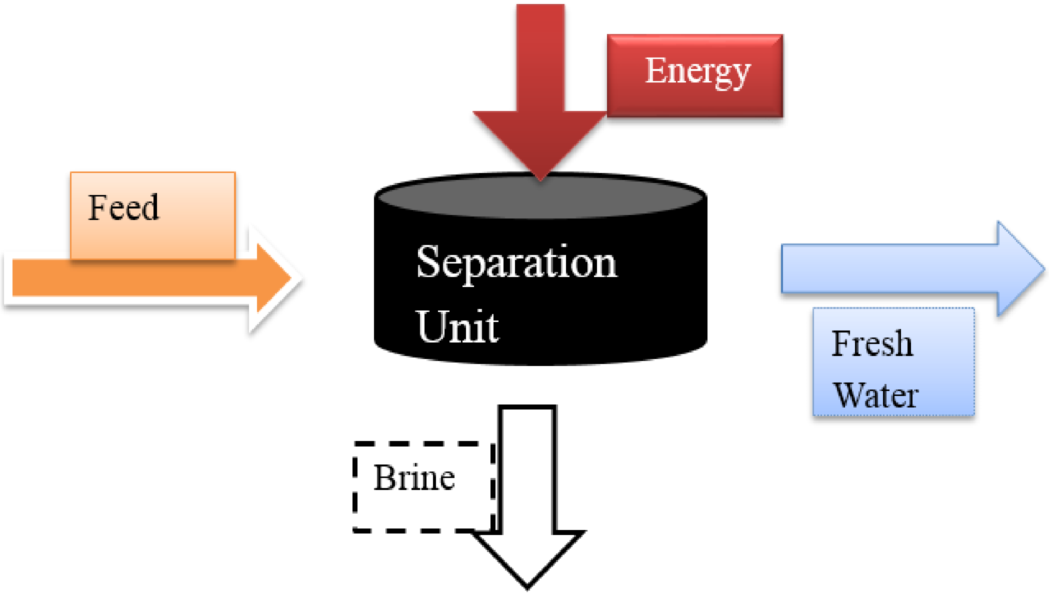

Figure 2. 7 Basic Desalination process

2.5 Desalination Technologies

Conventional desalination methods are divided into three major categories, namely:

1) Thermal desalination systems (MED, MSF, AD and MED-TVC) which utilize thermal and electric energy

2) Membrane desalination systems (RO) which utilize the pressure energy and

3) chemical desalination systems (ion-exchange, liquid- liquid extraction and gas hydrates) which utilize the chemical potential [46, 47]

Fig. 2.5.1 shows an general overview of the main desalination process categories [48].

1-Thermal desalination systems:

In thermal desalination, seawater or brackish water is evaporated and then fresh water is produced by condensing these vapors. This is actually an energy re-use or energy recovery process and number of recoveries depends on number of stages.

Thermal desalination includes multi-effect desalination (MED), multi stage flash desalination (MSF), mechanical vapor compression (MVC) and adsorption desalination (AD). The MED process is an old method and has been used since the late 1950s and early 1960s [49]. Multi-effect distillation uses the principles of evaporation and condensation at progressively reduced pressure and it occurs in a series of vessels (effects). In the MED, the vapour produced at the first effect/stage is used as evaporating medium for the next stage because water evaporates at the lower temperature as the pressure is reduced. This process continues and the last stage vapours are condensed in the separate water cooled condenser. The performance ratio of the MED system is directly related to number of effects. MED stages vary from eight to sixteen [47]. The process schematic of conventional MED system is shown in Figure 2.13.

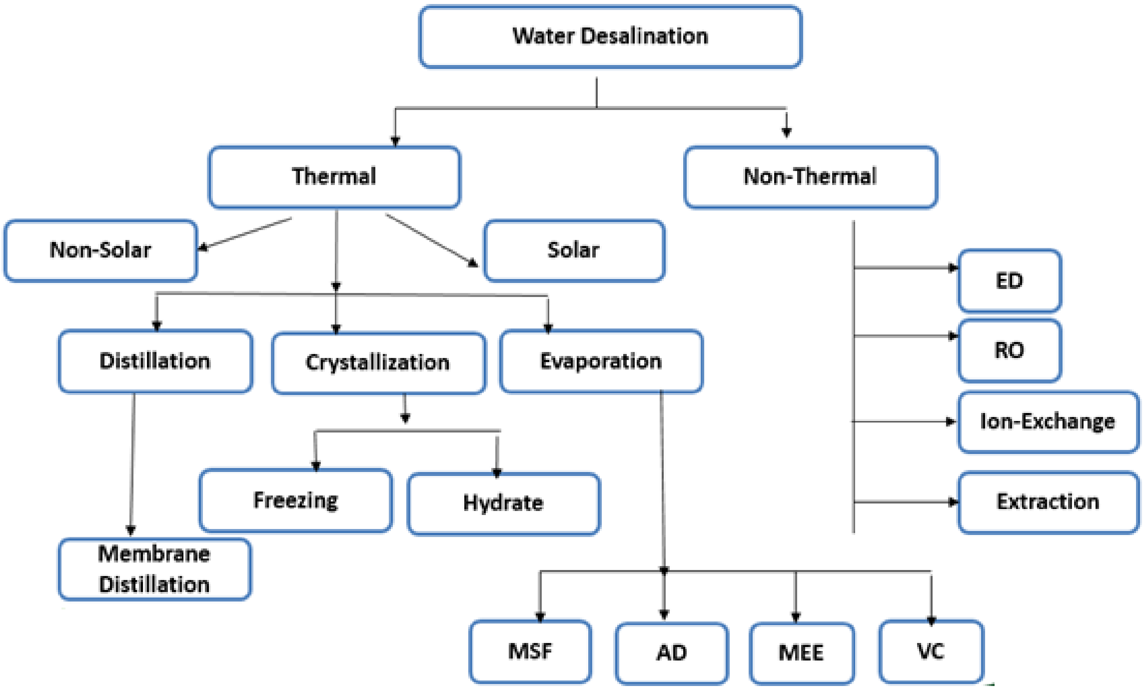

Figure 2. 8 Desalination classification [7]

MED units can be classified as horizontal tube, vertical tube or vertically stacked tube bundles on the basis of heat exchanger tubes arrangement in the effect/stage. It can also be classified as forward feed, backward feed and parallel feed on the basis feed supply. Extensive literature is available on MED systems. El-Desouky et. al. [50] and Hisham et. al. [51] analyzed the thermal performance of MED system with different configurations. Their model includes all the parameters effect as in real plant namely: 1) temperature, 2) salt concentration, 3) temperature depression due to pressure losses, 4) non-condensable gases and 5) flash boxes effects. They found that the specific power consumption decreases with higher heat input temperature. Many researchers [52, 53] have provided the theoretical modelling and simulation codes for MED different parameter calculations at steady state conditions. E1-Nashar et al [52] used the real plant data at Abu Dhabi, UAE and he found good agreement with simulated results. However, dynamic operation modelling in provided by Aly et. al. [54].MSF was first patented by R.S. Silver after his major improvement over the 1st Westinghouse design. Westinghouse designed a four stage MSF in 1957 and was installed in Kuwait [55], but later R.S. Silver improved the design by providing the partitions to decrease the capital cost of the system . The MSF invention gave the new direction to desalination industry in which evaporation can occur by flashing from large amount of feed water. MSF has higher performance because the heat of condensation is utilized to pre-heat the feed before flashing in the chamber.

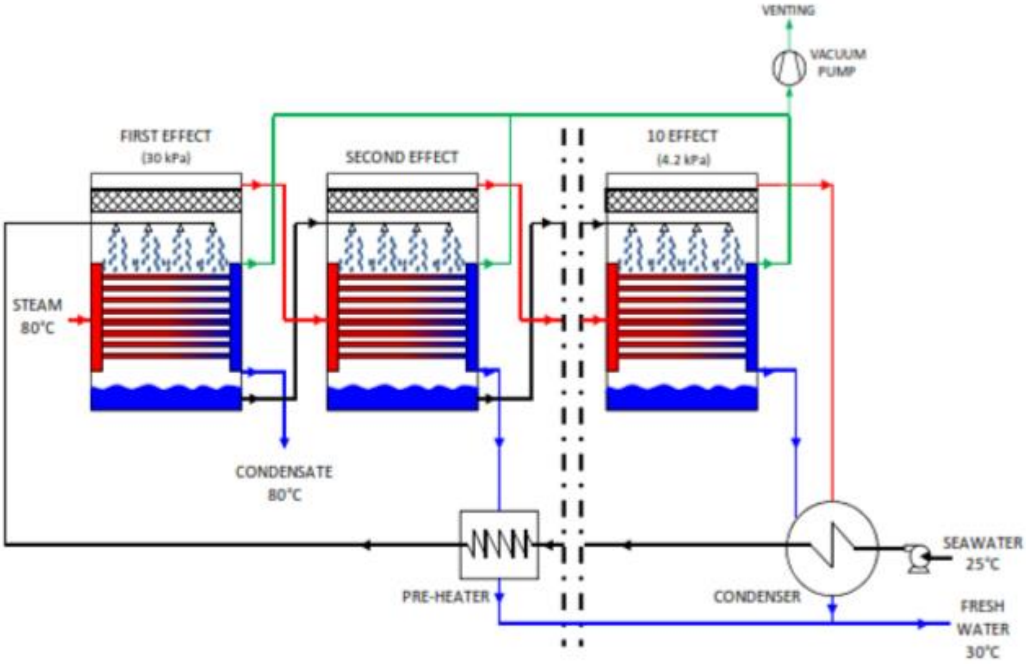

Figure 2. 9 Schematic process flow diagram of MED System

The MSF plant can also be coupled with steam power plants to operate the system and to enhance the power plant energy utilization [64, 65]. In the Gulf and MENA region this process was very attractive because of its low corrosion and fouling benefits. The MSF process considers the production of distilled water through a finite number of chambers/stages and each next chamber/stage operates at progressively lower pressures. The heated feed water is introduced to the first flash chamber where the low pressure of chamber causes rapid evaporation (called flashing) of the portion of water. This process (flashing) of evaporation of a portion of the feed water continues in each successive stage, because the pressure at each stage is lower than in the previous stage. The feed water that passes through the tubes of pre-heaters causes the condensation of vapour produced due to flashing in that chamber [56]. The basic concept of MSF is shown in Figure 2.5.3. MSF distillation plants can be further divided into two categories ‘once-through’ or ‘recycled’ process on the basis of feed system.[67].

Aly et. al. [57] conducted the thermal performance analysis of MSF system and developed the mathematical modelling for steady state operation. They incorporated all possible factors such as; 1) stage design, 2) correlations/mechanisms for heat transfer and 3) liquid properties variation with salt concentration and temperature. The results of a real MSF plant “Sidi-Krir” at west Alexandria having 17 stages are compared with the model and found to be in good agreement. MSF performance is limited to 10 [58] . Due to serious problems with MED plants such as; severe corrosion and fouling, initially, MSF overtaken desalination market but later researchers developed new anti-corrosive materials and helped MED to gain its position in market again. MED processes are thermodynamically more efficient than MSF processes and they have great potential for large scale plant. However, there are a number of limitations/drawbacks of MED and MSF processes such as; 1) thermal processes are energy intensive, 2) high corrosion and fouling rate due to high heat source temperature, 3) high capital cost due to very big hardware and 4) low recovery ratio [59] .

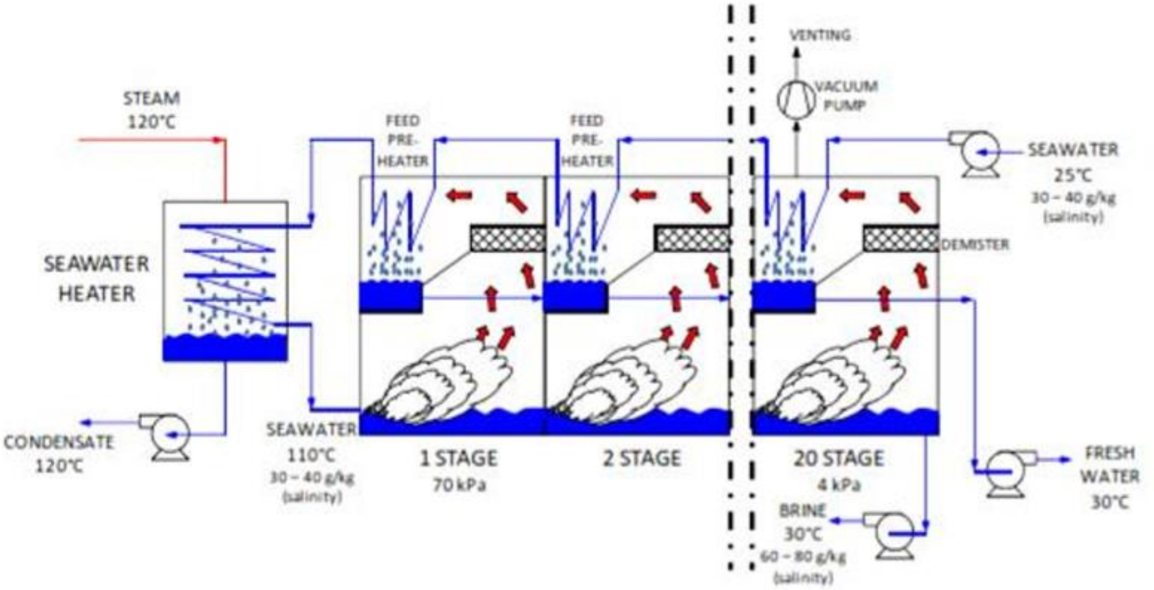

Figure 2. 10 Schematic flow process of MSF system

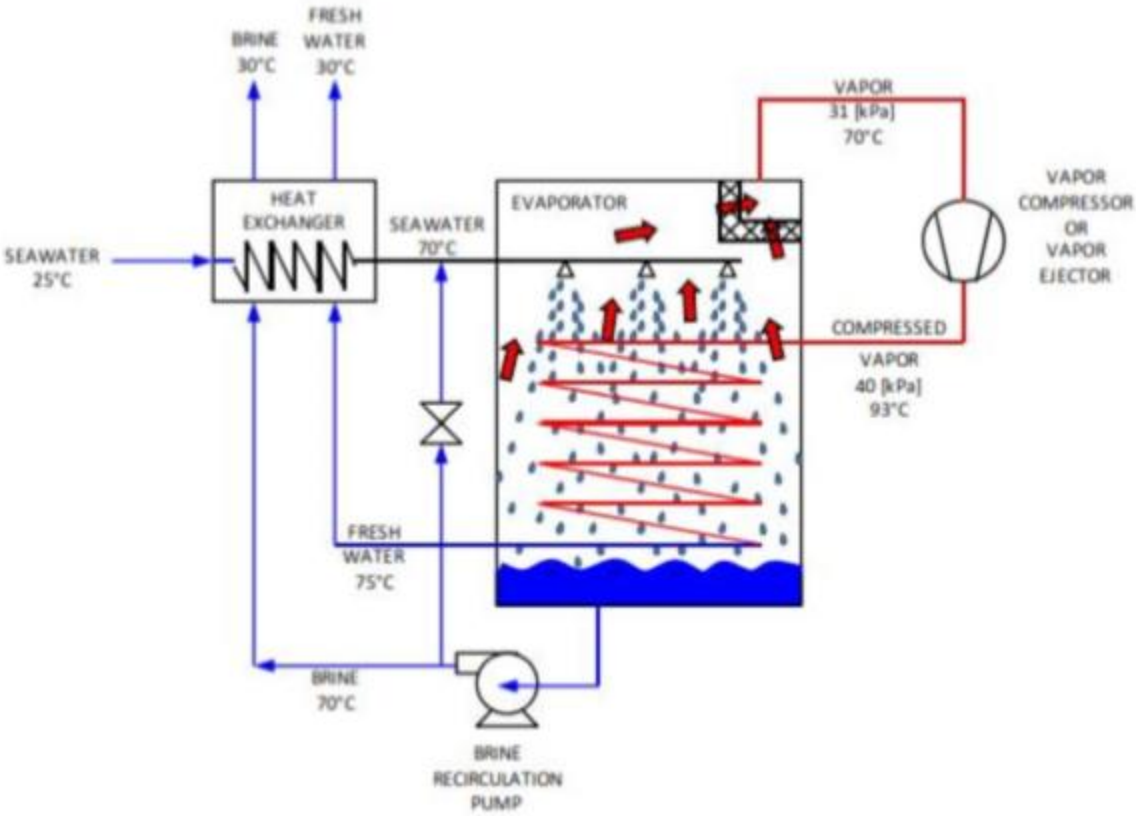

Figure 2. 11 Typical process flow diagram of MED-TVC

In the MED-TVC, MED is used in conjunction with vapor compression (VC) to improve efficiency and performance ratio. Vapor compression processes recompress the vapor produced in the effect to reuse this vapor heat. The vapor produced in one stage is partially recompressed either with thermal (TVC) or mechanical compressor (MVC) and divert to first cell to use the heat of these compressed vapors. The motive steam at higher pressure is bled from steam turbine for thermal vapor compression [74].

The maximum advantages can be obtained from small to medium installations by incorporating vapour compression processes. The production capacity of MVC units typically ranges in size up to about 3,000m3/day while TVC units may range in size to 20,000 m3/day [74]. The thermal performance of MED-TVC system was investigated by M.A. Darwish [60]. This performance model incorporated all necessary parameters such as; 1) evaporator heat transfer area, 2) heat transfer area of heat exchangers, 3) feed temperature, 4) vapors lines pressure drop and 5) evaporator temperatures. Specific energy consumption expression is also proposed in this model.

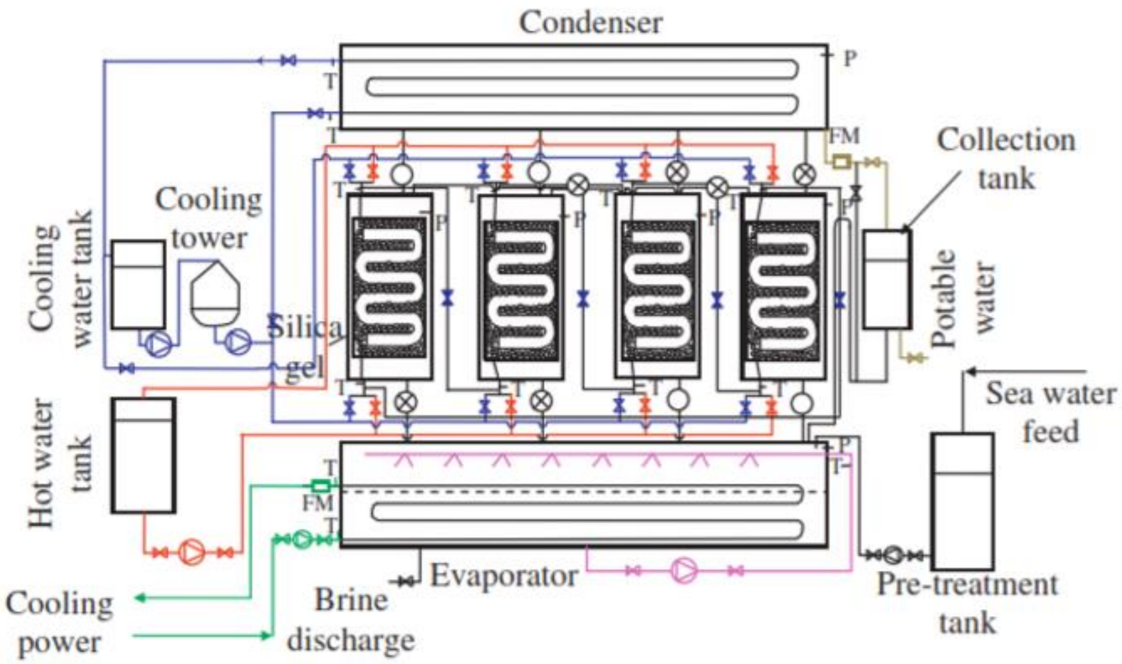

Figure 2. 12 Typical AD Cycle operational flow schematic [4]

The performance ratio of MED is directly connected with the number of effects and is always less than the number of effects.. This PR of MED can be increased by VC system. By bridging the VC unit to a certain number of effects, the performance ratio will increase to 11: 1 or even higher. The production could be increased 20% higher than nominal rated output by installing VC process [61]. The process diagram is shown in Figure 2.12. Adsorption processes are introduced by Kayser in 1881 for gases condensation on a free surface [77]. Adsorption is a process of adhesion of gas or liquid atoms or molecules to solid surfaces. These cycles utilize an adsorbate-adsorbent pair. Adsorption desalination (AD) is another thermal desalination method that can overcome the limitations of conventional thermal desalination namely; MED and MSF [62-64] . The AD cycle can produce high grade portable water with lowest specific energy consumption typically ≈ 1.5 KWh/m^3. It utilizes the low grade waste heat, solar or geothermal energy for sorption process that require 45^{o}C – 85^{o}C [65-68].

AD cycles operation is a batch operation with adsorption assisted evaporation and desorption assisted condensation [69, 70]. The adsorption desalination process for low grade waste heat or solar energy has been patented by Ng. et. al [64]. Adsorption desalination was developed to overcome the limitations of conventional thermal desalination systems. Typical AD system consists of four major components namely; 1) the evaporator, 2) silica-gel beds, 3) condenser and 4) pumping unit [71]. AD operation is cyclic steady operation so to get continuous water production multi-bed scheme is used. Figure 2.12 shows the major components and operation of an AD system. There are many advantages of AD processes namely; 1) low maintenance cost because of no moving parts, 2) low operational cost because of low level waste heat utilization, 3) less corrosion and fouling chances because of low operational temperature and 4) cooling effect in addition to water production. At chilled water temperature 12^{o}C, AD process can produce 4.7 kg of potable water per kg of silica gel [62]. An extensive literature is available on theoretical modelling and simulation of AD cycle [65, 72, 73]. Many researchers also conducted the experiments at different heat source temperatures to investigate the performance of AD cycle and to find the optimum operational parameters. The performance analysis based on isotherm, kinetics and energy balance is provided by many researchers . They found good agreement of results.

2-Membrane methods:

These processes employ polymeric membranes that filter the dissolved salts when subjected to a pressure gradient or different in electrical potential across the membrane surfaces. Membrane technologies can be vastly distributed into two categories: Electro dialysis or Electro dialysis Reversal (ED/EDR) and Reverse Osmosis (RO).

Reverse Osmosis (RO) processes are dominant in pressure activated desalination. In reverse osmosis (RO) or membrane separation process the pure/drinkable water is recovered from the pressurized saline solution (greater than osmotic pressure) by passing it through semi permeable membrane. The RO membrane filters out the water from pressurized solution keeping the high concentrated solution on other side of membrane. The invention of RO processes was the breakthrough in the desalination industry that changed the whole market because these processes do not require evaporation. The semi-permeable membranes used in RO are made by cellulose acetates, polyamides, polyamides, and poly-sulfones and hold in strong structure.

Most of the energy required for the RO process is to pressurize the saline water. As the pressure needed to increase the fluid pressure and the pressure required for separation is directly related to the salt concentration, usually reverse osmosis is preferable when brackish water is present in free, because they can operate on intermediate pressure. The osmotic pressure of seawater is about 25 bars. The RO desalinators operate from 10 – 15 bar pressure for brackish and from 50 to 80 bar pressure for seawater desalination. As the brine concentration increases the pressure required to recover additional water also increases so the water recovery rate of RO systems tends to be low. Typical, only 40% recovery is possible by RO systems [74]. The main portion of energy supplied is wasted in the form of compressed brine rejection. A device to recover the compression energy from compressed brine is therefore developed and a new RO plant now equipped with these devices to improve the energy efficiency. The pre-treatment of feed water in very important in the RO process because the membranes are very sensitive to pH, oxidizers, a wide range of organics, algae, and bacteria. The cost of the RO process is very much affected by almost 60% discharging of pre-treated water. The process block diagram of RO process is shown in Figure 2.5.6. RO processes consists pre-treatment, RO membrane and post treatment process. The world largest RO plant in 1969 was a 380m3/day in Dallas, Texas using brackish water. Today, RO has largest single capacity of 330,000m3/day and it consists of 27,000 membrane elements having active surface area about 99ha. This plant total area is equivalent to 132 Olympic size swimming pools and the filter surface area is equivalent to about 200 football fields. These membranes need to replaced 3-7 years [75].

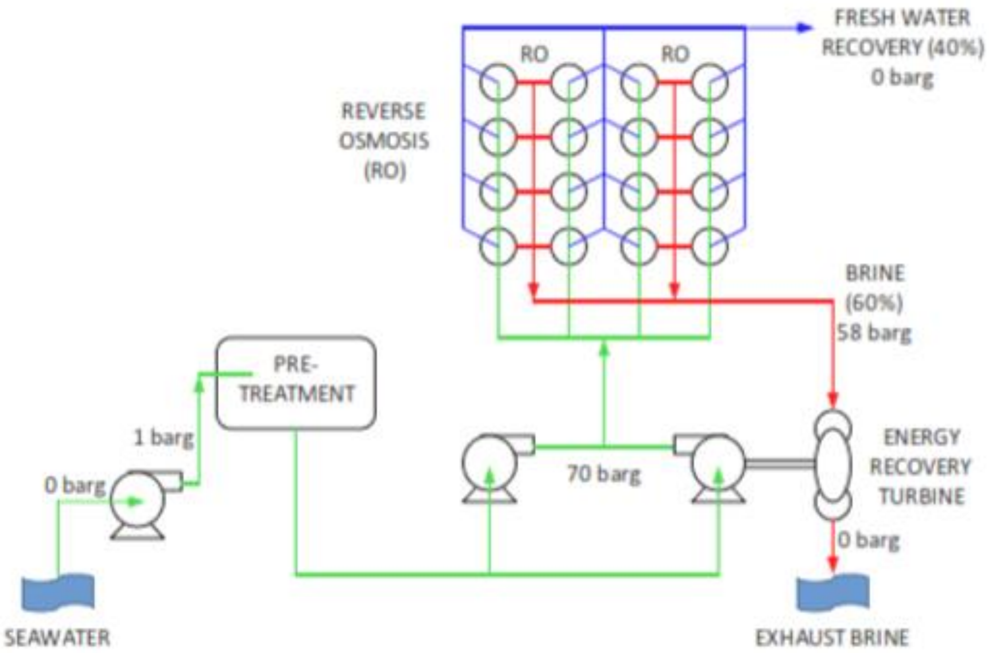

Figure 2. 13 Typical RO cycle operational flow schematic [4]

2.6 Installed Desalination Plants Worldwide -An Overview

The share of each desalination process in global installed capacities is shown in Figure 2.6.1.This percentage of share is based on all kind of feed water such as seawater and brackish water. It can be seen that RO is leading with 60% share followed by thermal processes 35% and others as 5%.

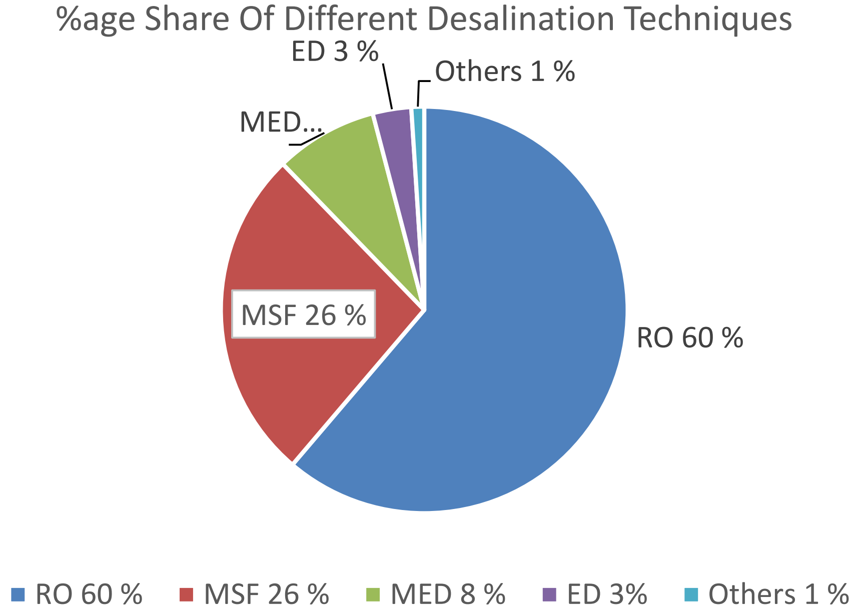

Figure 2. 14 %age share of different desalination methods

Although RO processes are dominant, it has certain limitations with respect to local conditions: For example, the frequent maintenance issues from high operating pressure, water quality problems in term of residuals of boron, chlorides and bromides and the severe fluctuations in the seawater intake quality are some of the challenges faced by the RO membranes. In the GCC region, frequent occurrence of harmful algae blooms (HABs) in the seawater where the microbes of HABs may contain high doses of neuroparalytic and diarrheic toxins. Such toxins are carried by algae contaminated water that may pass through the pores of membranes, possibly leading to health problems. During an algae event, RO plants face shut down periods up to several weeks leading to severe water shortage as most Gulf Cooperation Council (GCC) countries have water storage of less than a week. Large fluctuations in the feed water quality have direct implications to the operation and maintenance costs of RO plants [7] . Owing to the uncertainty of RO plant operation, thermal desalination are deemed as the dominant processes employed in desalination market in the GCC countries, and more than 70% of water is produced by thermal methods. Table 2.2 shows the desalination capacities in the GCC and non-GCC countries [76] .Seawater is the major source of feed for desalination capacities and more than half of installed desalination capacities (58%) are using seawater as feed water shown in Figure 2.8. Thermal desalination processes are leading with 61% share in seawater desalination market in the world followed by RO with 35% share as shown in Figure 2.6.2 [77]

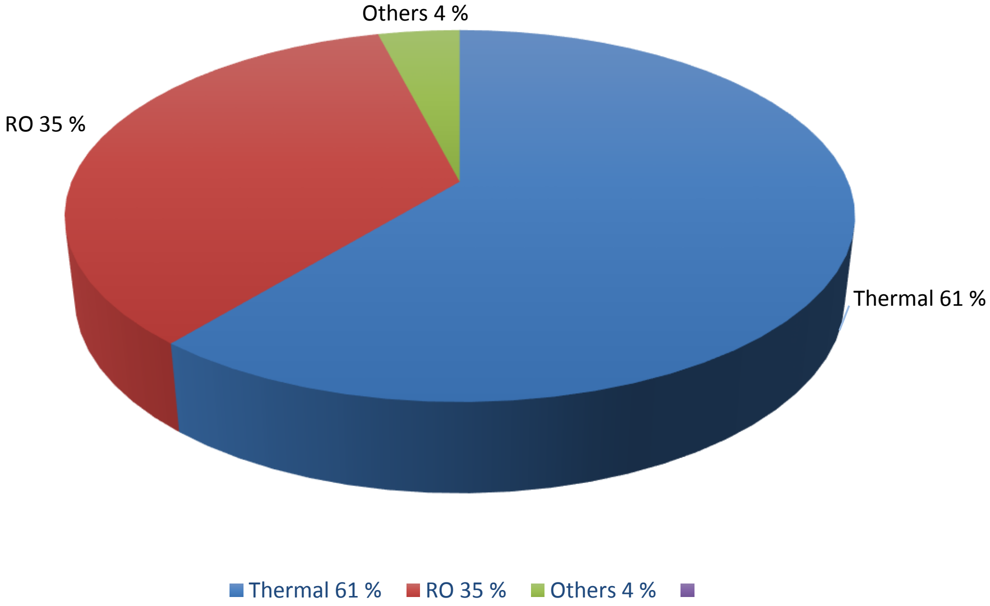

Figure 2. 15 %age share of desalination techniques on the basis of feed- sea water [66]

A bird eye’s view of global desalination installations on the basis of feed water type is shown in Figure 2.20 and Table 2.3 list the desalination plant size according to capacities and their share in installed capacities [104, 105].

Table 2. 2 Over view of desalination capacities in GCC and non-GCC Countries[7]

Year	SWRO(Mm^3/day)		Thermal(Mm^3/day)		Total (Mm^3/day)
	GCC	Non-GCC	GCC	Non-GCC	
1950	-	-	0.03	0.01	0.04
1960	-	0.005	0.06	0.03	0.1
1970	-	0.04	0.13	0.12	0.29
1980	0.1	0.65	1.9	1.4	4.05
1990	0.6	1.6	6.45	2.0	10.65
2000	1.0	2.1	8.3	2.95	14.35
2010	4.3	13.2	17.2	4.1	28.80

Table 2. 3 Desalination plant capacity according to daily production [64]

Plant Size	Production (m^3/day)	% share in Market
Very Large Plant(XL-Sized)	XL >= 50000	49 %
Large Plant (L-Sized)	50000<=L>=10000	25 %
Medium Plant (M-Sized)	10000<=M>=1000	22 %
Small Plant(S-Sized)	S<=1000	4 %

2.7 Membrane Distillation (MD)

Membrane distillation (MD) is arising technique for water cleaning. It is a separation process which is run by thermal gradient over the membrane surface, and in which separation is enabled due to phase change. Membrane distillation is a process that used thermal gradient to generate vapour pressure difference across membrane surface for evaporation and then permeation is followed by condensation process on the opposite side of membrane. MD is also useful foe non-volatile constituents present in the influent water. In the following sub sections some advantages and limitations of MD technology are explained well.

2.7.1 Why Membrane Distillation

The main features of membrane distillation are as, because of which MD technology is so commonly used.

- Low energy consumption
- Degradation of membrane is low in MD process as compared to pressure drive process such as RO.
- Reduced operating temperatures as compared to other traditional desalination processes.
- Quality of permeate is high enough to produce 100% salt rejection factor almost.
- Polymeric membrane of low requiring membrane properties demanded for operation.
- Directly sea water can be used for operation without requiring any pre-treatment process.

2.8 Membrane Distillation Configurations

In membrane distillation, several MD configuration had been employed depending on its application. The existing configuration differs from each other from the manner its distillates channels (modules) or the way in which this channels operate. The basic differences in MD configuration is found in the permeate side of the modules since all the available configuration operate in the same principle on the feed side of the membrane material. Basically MD has four configurations, which include Direct contact membrane distillation (DCMD), Air-gap membrane distillation (AGMD), Sweeping gas membrane distillation (SGMD) and Vacuum membrane distillation (VMD). All configurations have similar types of feed side flow, only difference comes from condensation process type. One basic modification is made in AGMD is that instead of air in between the gap, some liquid water is placed in between the gap, so that the condensation rate can be enhanced by decreasing the resistance to the vapor mass flux.

2.8.1 Direct Contact Membrane Distillation (DCMD)

In DCMD, active side of membrane comes in contact with high temperature, high, high concentration feed while the supporting side of membrane is in direct contact with the distilled water. Produced water vapours permeates through the membrane pores and condense by the distilled water flowing over the supporting side of membrane. Usually active side of membrane is made hydrophobic so that it may not allow water to come in contact, while the supporting side of membrane is made hydrophilic so that coolant water stays in contact with the coolant fluid in order to enhance condensation process. Because of simplicity in nature of module assembling for DCMD, it is always preferred. However DCMD shows more heat loss in the form of membrane conduction and diffusion, and latent of heat of fusion of the vapours.

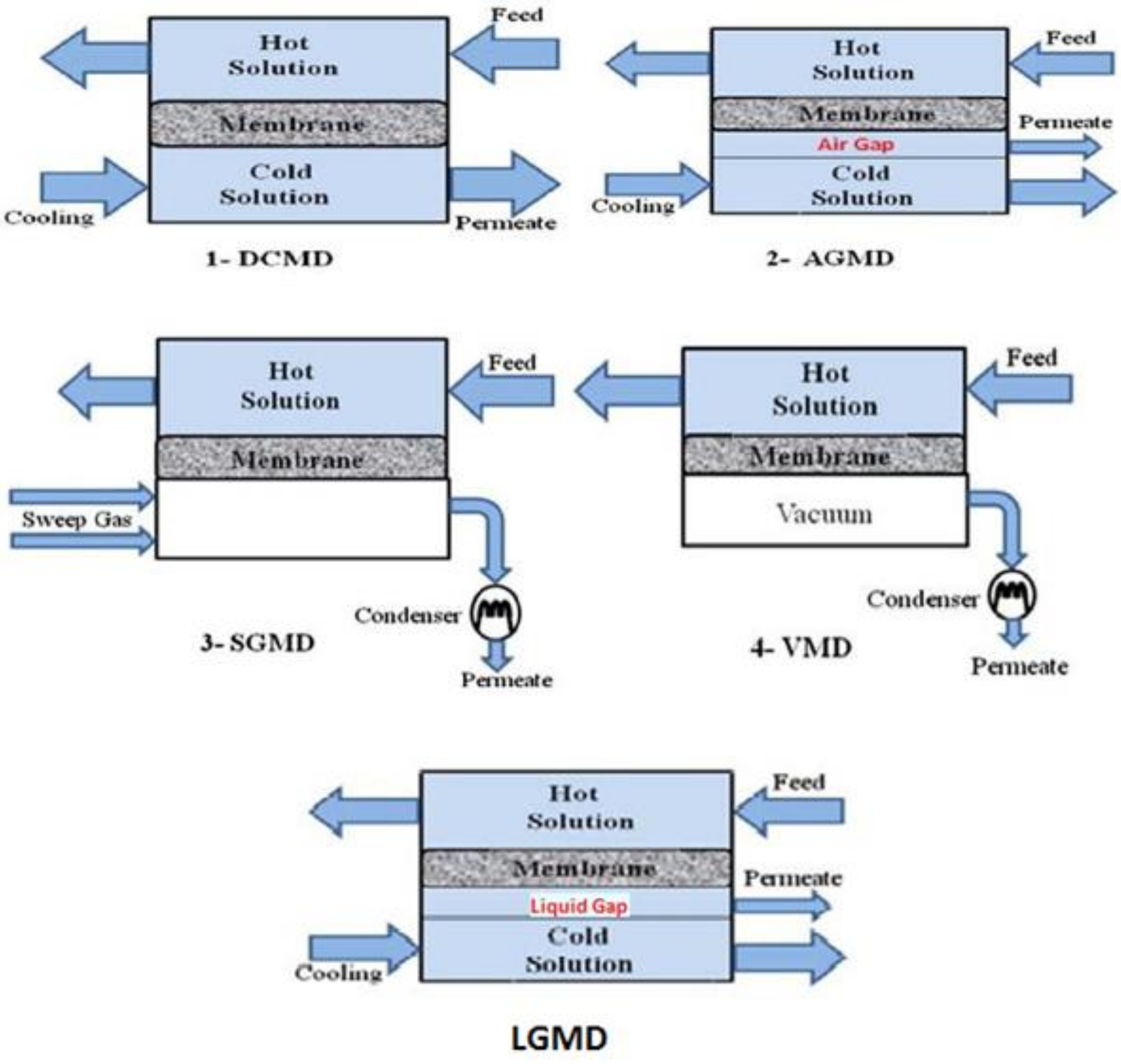

Figure 2. 16 Different configurations of membrane distillation

2.8.2 Air-Gap Membrane Distillation (AGMD)

In AGMD, active side behaves similar to what we studied in DCMD, but difference lies in condensation process of the vapours. In AGMD, vapours pass thorough membrane pore and cover another resistance offered by the air barrier between the supporting layer and condensation plate of module. As soon as these vapours comes in contact with the condensation plate, they condensed down towards the permeate cavity in the bottom of the module. AGMD gives low heat loss because of good thermal insulation caused by the air entrapped between the gap.

2.8.3 Sweeping gas membrane distillation (SGMD)

Sweeping-gas MD, also known as air st1ripping, introduces a channel similar to what we have in AGMD. But in AGMD , inside the gap there is stagnant air that causes resistance to the vapours to condense. But in SGMD, an inert gas is swept between the gap, that not only assist the condensation process but also reduces the resistance to vapours molecules. The gas which is swept is chemically inactive and does not react chemical with the permeate leaving it safer to drinking purpose. Comparing AGMD with SGMD , SGMD possess forced circulation of gas thorough gap intends to generate more flux as compared to AGMD for constant operating conditions. But the disadvantage of SGMD is that undissolved particles of inert gas can fill the pores of micro membrane which can reduce the flux.

2.8.4 Vacuum Membrane Distillation (VMD)

VMD is another advancement of AGMD after SGMD. In VMD, suction is provided in the condensation channel. The same gap design is made, but an extra pump is applied so that any vapour produce can be sucked out of the module to be condensed. VMD gives more flux as compared SGMD and AGMD but less than DCMD. E chief benefit of VMD over SGMD is that applied suction pressure is greater than equilibrium vapour pressure so condensation happens outside of module, and also there is no inert gas inserted between the gap so there is no chance of pore blocking by inert gas insertion in SGMD.

2.8.5 Material Gap Membrane Distillation (MGMD)

It has been observed that employing appropriate materials (like sand, water, and sponge) between the membrane and the condensation plate in an air gap membrane distillation module enhances the water vapor flux significantly [26]. An increase in the water vapor flux of about 200–800% was observed by filling the gap with sand and deionized water at various feed water temperatures. Also, an increase in the water gap width from 9 mm to 13 mm increases the water vapor flux. Another comparative study between air and water gap membrane distillation designs is presented [25].

Material gap membrane distillation is quite similar to air gap membrane distillation. The main difference lies in the media present between the cooling plate and membrane surface on the permeate side. In LGMD this media is stagnant water. LGMD gives more flux as compared to AGMD but less than the DCMD. The reason is that in AGMD, air offers more resistance to the vapour flux to pass through because of low heat capacity and low thermal conductivity. But water has higher heat capacity and higher thermal conductivity. Although no much work is done in WGMD but still it needs improvements.

CHAPTER 3

THEORETICAL ANALYSIS OF HEAT & MASS TRANSFER IN DCMD SYSTEM FOR FLUX PREDICTION

3.1 Mass transfer modeling

Figure 3.1 shows the configuration of direct contact membrane distillation system (DCMD). In DCMD system, there is hot fluid stream (Feed @ 40-90 ^{o}C) is run over a hydrophobic membrane. On the other side of membrane, cold fluid (Permeate @ 15-30 ^{o}C) flows. Due to temperature difference on the membrane surface, a difference of partial pressure is produced which causes some water to evaporate.

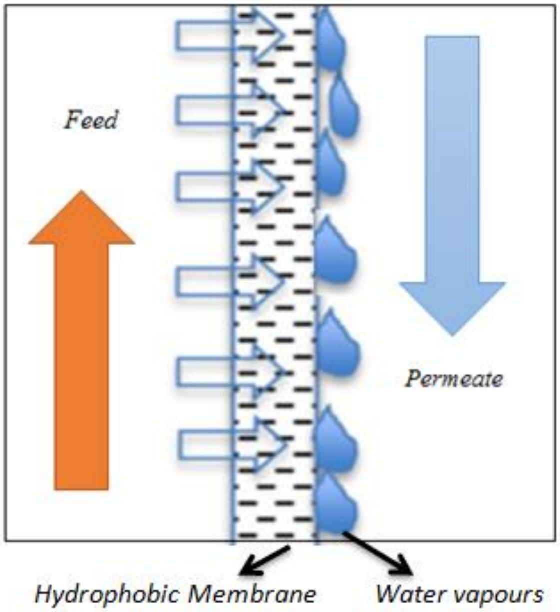

Figure 3. 1 Direct contact membrane distillation

Vapours produced, pass through membrane pores, where permeate used to condense down these vapours. The permeate mass flux produced depends mainly on equivalent diffusion coefficient (D_e) and difference of vapour pressure of water in feed and permeate side. The permeate mass flux can be given as [78-80];

$$J_w = D_e * \Delta p_m = D_e * (P^o{}_{wf} - P^o{}_{wp}) \tag{1}$$

Where J_w is the mass flux of permeate, ~~and D_e is th~~e equivalent diffusion coefficient. ΔPm is the vapour pressure difference at transmembrane surface. Powf and Powp are the partial pressures of feed and permeate sides at the membrane surface.

Where J_w is the mass flux of permeate, and D_e is the equivalent diffusion coefficient. ΔP_m is the vapor pressure difference at transmembrane surfaces. $P^o{}_{wf}$ and $P^o{}_{wp}$ are the vapor pressures of feed and permeate sides at the membrane surfaces; respectively, and they can be calculated using the Antoine equation as follows:

$$p^0{}_{wf} = exp\left((23.1964) - \frac{3816.44}{T_{mf} - 46.13} \right) \tag{2}$$

$$p^0{}_{wp} = exp\left((23.1964) - \frac{3816.44}{T_{mp} - 46.13} \right) \tag{3}$$

If we consider the effect of salinity in the feed then the above relation can be modified as,

$$J_w = D_e \cdot \left(p^o{}_{wf} \cdot \gamma_{wf} \cdot x_{wf} - p^o{}_{wp} \right) \tag{4}$$

Where γ_{wf} is activity coefficient and x_{wf} is the mole fraction of water in feed. Activity coefficient represents the variation of substances from their ideal behavior due to impurities, and mole fraction is the ratio of no. of moles of any specie to the total no. of moles present in solution.

For an aqueous solution of NaCl and is given as [79, 81]

$$\gamma_{wf} = 1 - (0.5 \cdot x_{NaCl}) - (10 \cdot x_{NaCl}{}^{2}) \tag{5}$$

Where xNaCl is the mole fraction of NaCl in water solution. As the sum of the mole fractions in a binary solution is taken as unity, so the mole fraction of salt in aquesous solution of NaCl can be obtained as ,

$$x_{wf} + x_{NaCl} = 1 \tag{6}$$

Now coming to pressure of air molecules inside the membrane pores, which can be simply taken as algebraic difference of total pressure of mixture (air and water vapours) and pressure of water vapours. The partial pressure exerted by the water vapours inside the pores can be found out by using Antoine equation [82]

$$P_{w,v,p} = exp\left((23.1964) - \frac{3816.44}{T_m - 46.13} \right) \tag{7}$$

Where Tm is the mean or average temperature across the membrane surface and can be taken as

$$T_m = \frac{T_{mf} + T_{mp}}{2} \tag{8}$$

Considering air and water vapours filling the pores then the partial pressure of air inside the membrane pores can be taken as

$$P_{air,pore} = P_{pore} - P_{w,v,p} \tag{9}$$

Pw,v,p shows the partial pressure of water vapours inside the pores and Ppore is the total pressure inside the pores and is assumed to be the average of feed and permeate side bulk pressures.

$$P_{pore} = \frac{P_f + P_p}{2} \tag{10}$$

Diffusion is transfer of matter from one surface to the another surface through some media. The driving force is concentration gradient and partial pressure difference between the two surfaces [17].

Three different models can be utilized in order to predict the diffusion coefficient the membrane. Knudsen diffusion model, Poiseullie flow model and molecular diffusion model [81]. The selection of diffusion model depends upon the Knudsen Number which is defined as the ratio of the mean free path to the characteristic length.

$$Kn = \frac{\lambda_w}{d_{pore}} \tag{11}$$

Where λ_w represents the mean free path which is the average distance between one molecule to the other molecule before it collides, or the distance between one molecule to the wall of membrane before collision, and d_{pore} is the pore size of membrane. Mean free path of water molecules in vapour form is given as [82];

$$\lambda_w = \frac{k_b * T_m}{\sqrt{2} * \pi * P_m * (\sum w)^2} \tag{12}$$

Mean free path can also be found from the following expression [83];

$$\lambda_w = \frac{k_b \cdot T_m}{\pi \cdot \left(\frac{\Sigma_W + \Sigma_A}{2} \right)^2 \cdot P_m \cdot \left(1 + \left(Mol_w / Mol_a\right)\right)^{0.5}} \tag{13}$$

Where k_b is the Boltzmann constant, P_m is the mean pressure within the membrane pores, Tm is mean temperature across membrane surface of feed and permeate side, and Σ_w is collision diameter of water molecule and is Σ_A collision diameter of air molecule. If the mean free path (The average distance between the molecule-molecule before collision happens) of the transported water molecules in vapour phase is greater than the membrane pore size (i.e. Kn>10 or dp<0.1λw), the molecule-pore wall collisions are taking over the molecule-molecule collisions and Knudsen diffusion will be causing the vapours transfer through membrane pores. It was considered that Knudsen type flow is prominent diffusion phenomenon when the ratio of the radius of pore to the mean free path (i.e. r_{pore}/λ_w) is lower than 0.05 as shown in figure 4 [82].

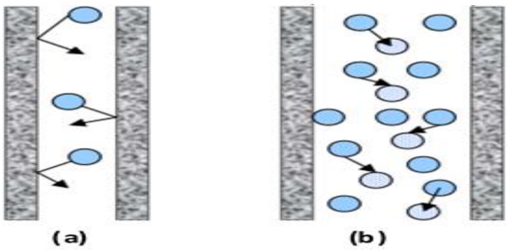

Figure 3. 2 (a) Knudsen type of flow and (b) Molecular type of flow [2]

Equivalent diffusion coefficient accounts both diffusion phenomenon, i.e. Knudsen and molecular. Essalhi et.al. [79] introduced the concept of combined (Knudsen and molecular) diffusion by introducing a factor α which is the ratio of Knudsen diffusion to mass diffusion and tells the dominance of phenomenon which is occurring in mass transfer. The value of α can vary between 0 to 1. This parameter covers the effect of combined diffusion[79].

Essalhi et. al calculated equivalent diffusion coefficient by the following expression

$$D_e = \left(\left(\frac{\alpha}{D_k} \right) + \left(\frac{1-\alpha}{D_m} \right) \right)^{-1} \tag{14}$$

Dk and Dm represents Knudsen and molecular diffusion coefficients respectively, and can found by the following expressions.[79]

$$D_k = \left(\left(3 \cdot \delta \cdot \frac{\tau}{2 \cdot \varepsilon \cdot d_{pore}} \right) \cdot \left(\pi \cdot R \cdot \frac{T_m}{8 \cdot Mol_w} \right)^{0.5} \right)^{-1} \tag{15}$$

$$D_m = \left(\frac{R \cdot T_m \cdot \delta \cdot \tau \cdot P_{air,pore}}{Mol_w \cdot \varepsilon \cdot PD_{w,a}} \right)^{-1} \tag{16}$$

Where δ is membrane thickness. ε is membrane porosity which shows the void volume fraction present in membrane, R is universal gas constant, Tm is the mean or average temperature across membrane surfaces d_{pore} is the pore diameter that is measured in accordance with the membrane tortuosity factor, Mol_w is the molecular weight of water molecules, PDw,a is the product of pressure and binary diffusion, and $D_{w,a}$ is pressure independent molecular diffusion coefficient for water and air or simply $D_{w,a}$ is diffusivity of vapours in air.

τ is the membrane tortuosity which represents the deviation of pore shape from circular to elliptical. Tortuosity depends upon the shape and looseness of pores. Two different relations are commonly used to calculate tortuosity. Ólöf Andrjesdóttir, S.B. Iversen et al. and Essalhi et al. [13, 79, 84] used the follwing expression to calculate tortuosity;

$$\tau = \frac{1}{\varepsilon} \tag{17}$$

Whereas Darwish and A.G. Fane [83, 85] suggested that the following expression is best suited for tortuosity;

$$\tau = \frac{(2-\varepsilon)^2}{\varepsilon} \tag{18}$$

Although both expressions don’t show much variations in flux predictions, anyone of the expressions cited above can be used depending upon the manufacturing method.

The membrane pore is filled with water vapours and air that was already entrapped in the pores. The product of pressure of air inside the membrane pores and ordinary diffusion of water vapours into air molecules affects the permeate flux. If the pressure of air inside the pores increases, the permeate flux decreases. Diffusivity of water vapours produced through the static air inside the membrane pores can be used as[13, 85, 86];

$$PD_{w,a} = 1.895 \times 10^{-5} \cdot T_m^{\ 2.072} \tag{19}$$

Yanbin Yun [87] developed his model for flux prediction by considering three resistances, i)membrane resistance ii) concentration polarization resistance iii) fouling resistance. Although later on he neglected the fouling resistance. DCMD mass transfer process is an intergradation diffusion, which includes Knudsen diffusion and molecular diffusion[87]

$$D_{e,Yun} = \frac{\tau \cdot \delta \cdot R \cdot T_m}{\varepsilon \cdot Mol_w \cdot D_k} + \frac{\tau \cdot \delta \cdot Y_{LN} \cdot R \cdot T_m}{\varepsilon \cdot Mol_w \cdot \left(P \cdot D_m\right)} \tag{20}$$

Where Y_{LN} which is logarithmic mean pressure of air , D_k is knudsen diffusion coefficient and D_m is molecular diffusion coefficient which Yun calculated from the following expressions,

$$D_k = 97 \cdot r_{pore} \cdot \left(T_m / Mol_a\right)^{0.5} \tag{21}$$

And molecular diffusion

$$D_m = \left(1.19 * 10^{-4}\right) \cdot \frac{T_m^{\ 1.75}}{P} \tag{22}$$

Where P is bulk feed pressure.

3.2 Heat Transfer Modeling

In feed side fluid at high temperature, high salinity flowing over the membrane surface.

The heat transfer in this side will be due to convection purely. Then on the permeate side the fluid is flowing, causing convective heat transfer to occur. But in the membrane pores due to mass flux, the heat transfer is due conduction and mass flux. So heat transfer in a DCMD system is occurring in three regions as shown in figure 3.3

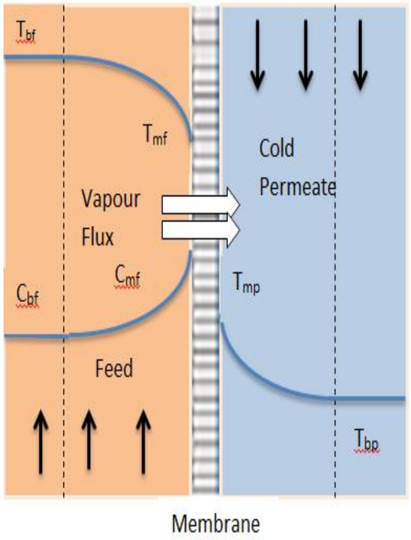

Figure 3. 3 Heat & mass transfer through membrane

1- Convective heat transfer in boundary layer region from the feed side to membrane surface. This heat transfer mechanism can be given by using Newton's law of cooling [21, 79, 85];

$$Q_f = h_f \cdot \left(T_{bf} - T_{mf}\right) \tag{23}$$

Where T_{bf} and Tmf are the bulk and membrane surface temperatures in the feed side and h_f is the convective heat transfer coefficient in feed side that can be calculated by using different correlations depending upon the flow type (laminar or turbulent).

2- Heat transfer through membrane matrix (solid part) by conduction and through the pores (Empty part) by evaporative mass flux in membrane.

3-Heat carried by the vapours (Evaporative heat transfer) is written as product of vapour mass flux (J_w) and enthalpy of vaporization (ΔH_v);

$$Q_v = J_w \cdot \Delta H_v \tag{24}$$

The Enthalpy of vaporization of water is taken as [87]

$$\Delta H_v = \left(\left(1.7535 \cdot T_{mf}\right) + 2024.3\right) \tag{25}$$

Where T_{mf} is temperature of the membrane surface of feed side.

Conductive heat transfer through membrane matrix can be represented by using Fourier's law of conduction as

$$Q_c = \left(\frac{k_m}{\delta}\right) \cdot \left(T_{mf} - T_{mp}\right) \tag{26}$$

Where T_{mf} and T_{mp} are membrane surface temperatures in feed and permeate side, membrane thickness is shown by δ and k_m is representing effective thermal conductivity of membrane.

There are three models available to calculate the effective thermal conductivity of membrane (membrane material and gases inside the pores).

- Series Model (Iso-Stress)
- Flux law Model
- Parallel Model (Iso-strain)

Using iso-stress or series model [24, 85] to determine the thermal conductivity of membrane matrix following relation can be taken into account as

$$k_m = \left(\left(\frac{\varepsilon}{k_{gas}}\right) + \left(\frac{1-\varepsilon}{k_{mem}}\right)\right)^{-1} \tag{27}$$

Using flux law model [88] to determine the thermal conductivity of membrane matrix which can be calculated as

$$k_m = k_{gas} \cdot \left(\frac{1+\beta_{s,g} \cdot (1-\varepsilon)}{1-\beta_{s,g} \cdot (1-\varepsilon)} \right) \tag{28}$$

Whereas dimensionless parameter βs,g can be formulated as

$$\beta_{s,g} = \frac{\left(\frac{k_{mem}}{k_{gas}} \right) - 1}{\left(\frac{k_{mem}}{k_{gas}} \right) + 2} \tag{29}$$

Darwish et. al. [85] is calculating the membrane conductivity as the volume average of both the conductivities (Vapours and membrane matrix).This is treated as Parallel model which can be taken as

$$k_m = (1-\varepsilon) * k_s + (\varepsilon * k_g) \tag{30}$$

Phattaranawik [85, 88] agreed upon series model. He believes membrane conductivity can be bitterly predicted on average basis instead of volume average, which is series model.[88]. The comparison shows that flux law model and series model give almost similar results but parallel law model shows slight decrement in flux output, which may not be a good option to choose.

The net heat transfer across the membrane is simply the addition of the conductive and evaporative heat transfer through the membrane.

$$Q_m = Q_c + Q_v \tag{31}$$

3- Convective Heat transfer in boundary layer region from bulk permeate stream to membrane surface can be given as

$$Q_p = h_p \cdot \left(T_{mp} - T_{bp}\right) \tag{32}$$

Where T_{bp} and T_{mp} shows bulk permeate and membrane permeate surface temperatures and h_p is the convective heat transfer coefficient in permeate side that can be calculated by using different correlations.

Under steady state condition, following conservation of energy, when heat transfer through feed, membrane and permeate side becomes equivalent to each other, the temperatures at the membrane surfaces can be calculated by using equations 17,18,20,25, and 26 as [79, 82] ;

$$T_{mf} = \frac{k_m \cdot \left(T_{bp} + h_f / h_p \cdot T_{bf}\right) + \left(\left(\delta \cdot \left(h_f \cdot T_{bf} - J_w \cdot \Delta H_v\right)\right)\right)}{\left(k_m\right) + \left(h_f \cdot \left(\delta + \left(k_m / h_p\right)\right)\right)} \tag{33}$$

$$T_{mp} = \frac{k_m \cdot \left(T_{bf} + h_p / h_f \cdot T_{bp}\right) + \left(\left(\delta \cdot \left(h_p \cdot T_{bp} + J_w \cdot \Delta H_v\right)\right)\right)}{\left(k_m\right) + \left(h_p \cdot \left(\delta + \left(k_m / h_f\right)\right)\right)} \tag{34}$$

3.3 Effect of concentration:

As the concentration of salts in bulk feed stream is different from the concentration of salts at the feed membrane surface, another parameter ‘concentration polarization coefficient’ can be defined which is the ratio of concentration of salt at the membrane surface to the concentration of salt in the bulk feed that can be given as [79]

$$\beta = C_{mf} / C_{bf} \tag{35}$$

Whereas the concentration at membrane surface is calculated as [87, 89] ;

$$C_{mf} = C_{bf} \cdot exp\left(\frac{J_w}{k_s \cdot \rho_{bf}} \right) \tag{36}$$

Where ρbf is the density of bulk feed and ks is the solute mass transfer coefficient for the diffusive mass transfer through the concentration boundary layer in the feed side and can be calculated as

$$k_s = Sh \cdot D_e / D_h \tag{37}$$

Where D_h is hydraulic diameter of feed channel and Sh is the Sherwood number which is a dimensionless parameter used for mass transfer. Sherwood number represents the ratio of convective to diffusive mass transport. Sherwood Number is a function of Reynolds number and Schmidt number. It is analogous to Nusselt number which is used for convective heat transfer.[87].

For Laminar Flow Sherwood number is given as[87, 90] which is Graetz–Lévêque equation

$$Sh = 1.86 * \left(\mathrm{Re} * Sc * \mathrm{D_h} / \mathrm{L} \right)^{1/3} \tag{38}$$

Where D_h is the hydraulic diameter, L is the channel length [87] and Sc is Schmidt number which is the ratio of momentum diffusivity to the mass diffusivity and can be written as

$$Sc = \frac{\mu_{mf}}{\rho_{bf} \cdot D_e} \tag{39}$$

For Turbulent Flow Sherwood number is calculated by using Dittus–Boelter equation[87]

$$Sh = 0.023 \cdot \left(Re_f \right)^{0.8} \cdot \left(Sc \right)^{0.33} \tag{40}$$

Table 3.1 shows different correlations have been utilized for Sherwood number depending upon flow types

Table 3. 1 Sherwood number correlations

Correlations	Type of Flow	Reference
$Sh = 1.86 * \left(\mathrm{Re} * Sc * \frac{D_h}{L} \right)^{0.33}$	Laminar	[91]
$Sh = 2 * \mathrm{Re}^{0.483} * Sc^{0.33}$	Laminar	[92]
$Sh = 1.62 * \left(\mathrm{Re} * Sc * \frac{D_h}{L} \right)^{0.33}$	Laminar	[93, 94]
$Sh = 0.023 * \mathrm{Re}^{0.875} * Sc^{0.25}$	Turbulent	[95]
$Sh = 0.023 * \mathrm{Re}^{0.8} * Sc^{0.33}$	Turbulent	[87, 91, 95]
$Sh = \frac{c}{\left(\frac{L}{l} \right)^{1/9}} \left(Sc * Gr \right)^{n}$ For 2.1E5<Gr<1.1E7 c=0.07,n=0.33 For 2E4<Gr<2.1E5 c=0.20,n=0.25	Turbulent	[95]
$Sh = 0.082 * \mathrm{Re}^{0.69} * Sc^{0.33}$	Turbulent Gas-Liquid Dispersion	[95]
$Sh = 0.012 * (\mathrm{Re}^{0.87} - 280) * Sc^{0.40} * \left[1 + \left(\frac{D_h}{L} \right)^{2/3} \right]$	$10^4 < \mathrm{Re} < 10^6$ 1.5< SC (500)	[95]

3.4 Calculation of convective heat transfer coefficient (h):

By definition of convective heat transfer coefficient (h)

$$h = Nu \cdot k / D_h \tag{41}$$

Where k is the average thermal conductivity of fluid in feed or permeate and Dh is the hydraulic diameters of flow channels and Nu is dimensionless Nusselt number.

If the feed (Hot side solution) is turbulent flow, the Nusselt number is a function of Reynolds and Prandtl number and can be given as [96]

$$Nu = 0.027 \cdot \left(\left(Re_f\right)^{0.8}\right) \cdot \left(\left(Pr_f\right)^{0.4}\right) \cdot \left(\left(\mu_{bf} / \mu_{mf}\right)\right)^{0.14} \quad (42)$$

Where Re_f is Reynolds number of bulk feed stream in the feed channel ,μ_{bf} if dynamic viscosity of bulk feed stream and µmf is the viscosity of feed at the membrane surface and , Pr_f is Prandtl number which is the ratio of viscous diffusion rate to thermal diffusion rate and can be written as

$$\Pr = \frac{\nu}{\alpha} = \frac{\mu * c_p}{k} \quad (43)$$

For permeate side (Cold side solution) Nusselt No. can be written as

$$Nu = 0.027 \cdot \left(\left(Re_f\right)^{0.8}\right) \cdot \left(\left(Pr_f\right)^{0.3}\right) \cdot \left(\left(\mu_{bf} / \mu_{mf}\right)\right)^{0.14} \quad (44)$$

The difference in Nusselt numbers in feed and permeate sides is the exponent difference of Prandtl number. Sieder and Tate [90, 97]proposed the following relation for Nusselt Number for laminar flow

$$Nu = 1.86 * (\mathrm{Re} * \Pr * D_h / L)^{0.33} \quad (45)$$

Table 3.2 shows some of these correlations used by different references to determine dimensionless parameter of Nusselt Number.

Table 3. 2 Nusselt number correlations

Correlations	Types of Flow	Refrences
$Nu = 1.86 * \left(\mathrm{Re} * \Pr * \frac{D_h}{L}\right)^{0.33}$	Laminar	[90, 97]
$Nu = 3.36 + \frac{0.036 * \mathrm{Re} * \Pr * \frac{D_h}{L}}{1 + 0.0011 * \left(\mathrm{Re} * \Pr * \frac{D_h}{L}\right)^{0.8}}$	Laminar	[86, 88, 98]
$Nu = 1.86 * \left(\mathrm{Re} * \Pr * \frac{D_h}{L}\right)^{0.33} * \left(\frac{\mu}{\mu_s}\right)^{1/7}$	Laminar	[99]

$Nu = 1.86 * \mathrm{Re}^{0.33} * \mathrm{Pr}^{0.33}\left(\frac{D_h}{L}\right)^{1/3}$	Laminar	[100]
$Nu = 1.62 * \left(\mathrm{Re} * \mathrm{Pr} * \frac{D_h}{L}\right)^{0.33}$	Laminar	[101]
$Nu = 0.298 * \mathrm{Re}^{0.646} * \mathrm{Pr}^{0.316}$	Laminar	[102]
$Nu = 0.74 * \mathrm{Re}^{0.2} * \left(Gr * \mathrm{Pr}\right)^{0.1} * \mathrm{Pr}^{0.2}$	Laminar	[102]
$Nu = 1 + 1.44\left(1 - \frac{1708}{\mathrm{Re}}\right) + \left[\left(\frac{\mathrm{Re}}{5830}\right)^{1/3} - 1\right]$		[103]
$Nu = 0.036 * \mathrm{Re}^{0.8} * \mathrm{Pr}^{0.33}\left(\frac{D_h}{L}\right)^{0.055}$	Turbulent	[104]
$Nu = 0.036 * \mathrm{Re}^{0.96} * \mathrm{Pr}^{0.33}\left(\frac{D_h}{L}\right)^{0.055}$	Turbulent	[100]
$Nu = 0.027 * \mathrm{Re}^{4/5} * \mathrm{Pr}^{n} * \left(\frac{\mu}{\mu_s}\right)^{0.14}$ n=0.4 for Heating n=0.3 for Cooling	Turbulent	[103, 105]
$Nu = 0.023 * \mathrm{Re}^{0.8} * \mathrm{Pr}^{n}$ n=0.4 for Heating n=0.3 for Cooling	Turbulent	[97]
$Nu = 0.023 * \mathrm{Re}^{0.8} * \mathrm{Pr}^{0.33} * \left(\frac{\mu}{\mu_s}\right)^{0.14}$	Turbulent	[104]
$Nu = 0.023 * \left(1 + \frac{6D_h}{L}\right) * \mathrm{Re}^{0.8} * \mathrm{Pr}^{1/3}$	Turbulent	[86, 88, 98]

Referring to fig. 3.4 , the heat transfer processes through DCMD process can be visualized. Electrical circuit analogy is made representing by resistance circuit. The overall heat transfer coefficient in feed, membrane and permeate side in DCMD process can be determined as follows [106];

$$U = \left[\frac{1}{h_f} + \frac{1}{\left(\frac{k_m}{\delta}\right) + \frac{J_w \cdot \Delta H_v}{\left(T_{mf} - T_{mp}\right)}} + \frac{1}{h_p} \right]^{-1} \tag{46}$$

So the total heat transfer in the module can be taken as

$$Q_m = U \cdot \left(T_{bf} - T_{bp}\right) \tag{47}$$

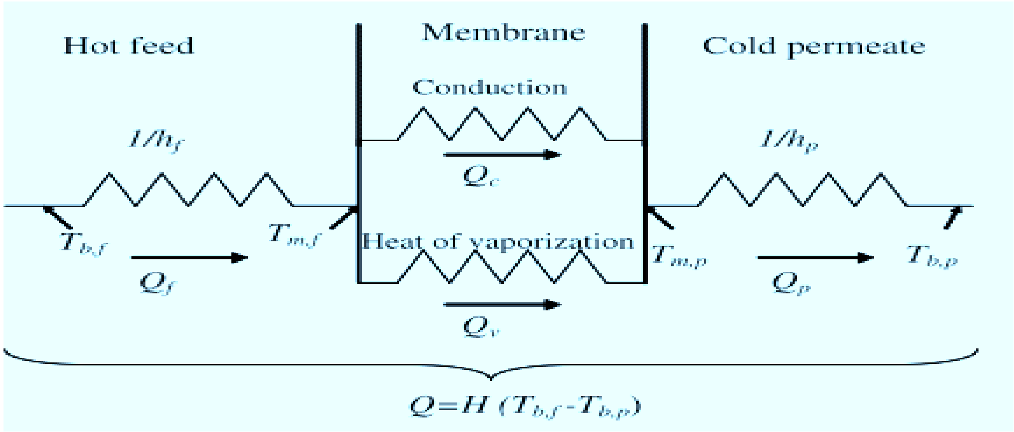

Figure 3. 4 Heat transfer analogy with electrical circuit [65]

The evaporative efficiency can be defined as the ratio of Evaporative heat transfer(latent heat required for evaporation at the hot feed liquid/vapor interface , Qv) due to mass transfer to the total heat transfer through module and can be given as [107]

$$\%EE = \left(\frac{Q_v}{Q_m}\right) * 100 = \left(\frac{J_w * \Delta H_v}{U * (T_{b,f} - T_{b,p})} * 100\right) \tag{48}$$

CHAPTER 4

EXPERIMENTAL SETUP

4.1 Introduction

In this chapter, the description of the direct contact membrane distillation (DCMD), and water gap membrane distillation (WGMD) setup will be explained. This chapter also illustrates the materials of the membranes used in the experiments. The components and instrumentations of the set-up, module design, selection of component and instrumentation will also be explained. Assembling of the DCMD module, WGMD and AGMD module, the assembling of the set up component will be discussed. The experimentation was done for DCMD, then compared the performance with AGMD configuration from Lawal's MS thesis [108] . In the second part, the experimentation will be done for WGMD and AGMD on the another membrane module made of HDPE [25] and then their performances will also be explained. Furthermore, the experimental plan will be outlined as well.

4.1.1 Description of set up

The DCMD system consists of two water closed cycles, hot and cold, connected to the MD module. The heart of the membrane distillation system is the membrane module. The MD module is made up of two Plexiglas (Poly methyl methacrylate PMMA having a melting point of 160 ^{o}C) flow compartments of 160×160mm and 25 mm thickness each as shown in fig 4.1. One compartment is used for hot saline water as feed and the other compartment is used for cold permeate side. Each flow compartment has three rectangular channel each channel has dimensions of 66 mm length, 24 mm width and 5 mm depth. Figure 4.1 shows the channel design and assembling of module. The membrane is supported by a net from hot side. The net is used between the feed stream and active side of membrane surface. This meshed net also ameliorates the performance of DCMD module. Figure 4.1, shows the channel design of module and assembling of module. Membrane is sandwiched between the two chambers.

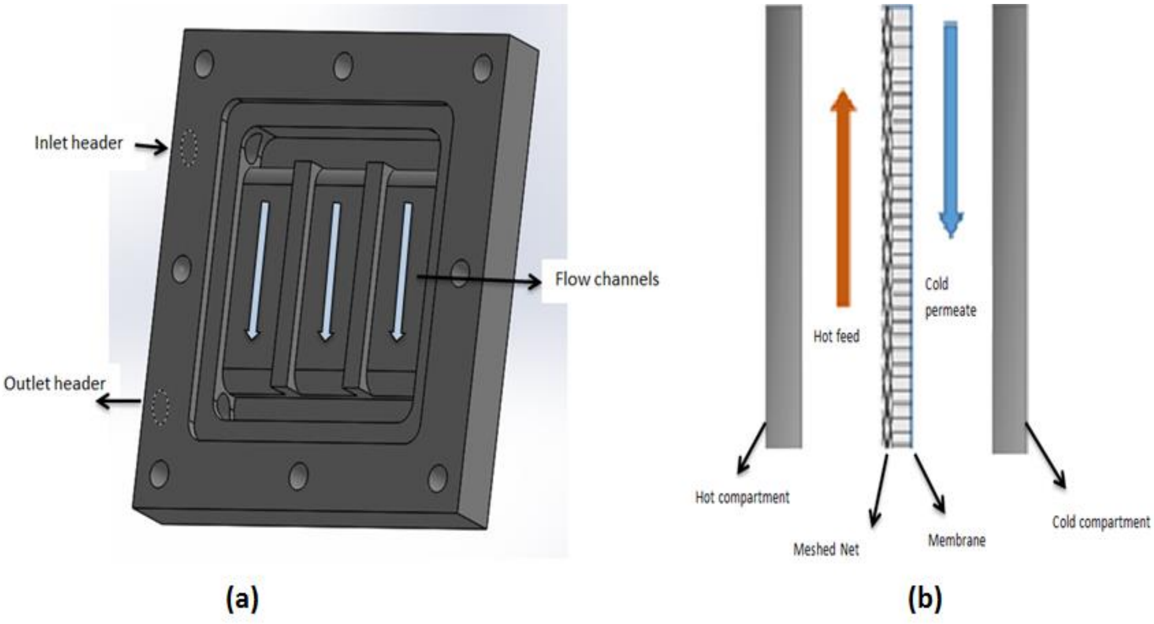

Figure 4. 1 Membrane module channel

(a) Module channel design (b) Sketched DCMD module (From L to R) Module Hot chamber, feed stream, meshed net, membrane , cold stream and cold chamber

The water enters through header and distributed into three channels. After passing over the membrane surface, the fluid is collected back into the exit header. Then it goes out of the module after producing vapours. Same process of flow happens in the cold side but in cold side instead of evaporation, condensation of vapours happens. The same chamber design is used for the cold side. Meshed net is also used between the feed stream and active side of membrane surface. There are two basic purpose of this net: 1) it supports the membrane and helping to avoid cracks at the sharp edges); 2) Enhance the turbulence level and heat transfer in the boundary layer of the feed side of the membrane.

In order to avoid internal and external leakage rubber sheet of 2mm was used as gasket. Internal leakage happens because of membrane rupture in the feed side. Because the active side of membrane is not much stronger than the supporting layer of membrane, by pressing the membrane, the sharp edges of the chamber can cause damage to membrane, which results in internal leakage.

The hot feed solution passes directly over the hydrophobic membrane; which is supported by the square meshed net. The effective membrane area that comes for vapor production is 6.192×10^{-2} m^2. A heater operated by a controlled head of Thermo-Fisher was used to provide constant flow rate and constant temperatures for the feed and permeate side. OMEGA FL 50000, float flow meter was used to measure feed flow rate and OMEGA turbine flow meter was used to measure the cold permeate flow rate. OMEGA CDH-287 conductivity meter was employed to measure salinity of feed, and permeate side. Pressure gauges are used to observe the inlet and outlet pressure of feed and permeate sides. National Instruments model NI 9211 Hi-Speed USB Carrier was used for data acquisition to record the data. K-type thermocouples were employed to measure the inlet and outlet temperatures of feed and permeate side. Figure 2 depicts the experimental setup of the used DCMD system. Pressure gauges and thermocouples are connected at the inlet and the outlet of the module to measure the temperatures and pressures of inlet and outlet for the hot and cold stream. A heated bath (equipped with a pump and heater) is used as the source of hot feed water. A rotameter is installed to measure the feed flow rate, and then measured feed flow is entering into the hot compartment and exiting. A circulated refrigeration bath is employed in accomplishing the desired temperature and flow of cold permeate. In addition, a turbine flow meter is installed in the path of cold flow to measure the flow of cold permeate. A small stainless steel welded pipe of 3 inch length and ¼ inch in diameter is attached to a port created in cold permeate bath to get the permeate flux out of the system. Before the start of experiment, the level of permeate is observed until extra water (permeates flux) comes out from the exit tube then the recording of experiment starts. Thermocouples are connected to data acquisition card to record and store the data. In order to observe the quality of permeate, a conductivity meter is used, that can measure the total dissolved solids (TDS) and conductivity of water.

Figure 4.2 and 4.3 depict the assembled and instrumented membrane module and whole experimental setup respectively. Pressure gauges and thermocouples are connected at the inlet and the outlet of the module to measure the temperatures and pressures at inlet and outlet for the hot and cold streams. Proceeding towards experimental setup in figure 4.3, actual setup is shown, where a heater is used as the source of hot feed water. Rotameter is installed to measure the flow rate of feed water, then measured feed flow is entering into the hot compartment and exiting. Similarly circulated refrigerator is employed in accomplishing constant flow of cold distilled water. A turbine flow meter is installed in the path of cold flow to measure the flow of cold fluid. A port is created in circulated refrigerator to get the permeate out of the system.

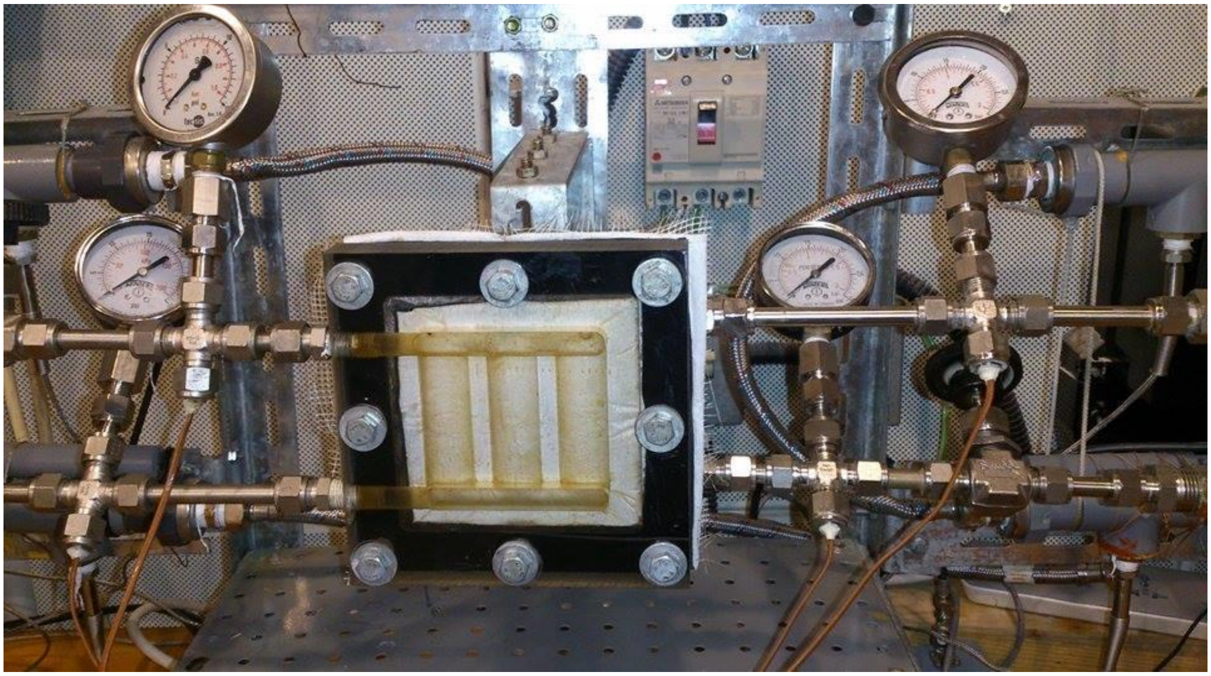

Figure 4. 2 Membrane Module

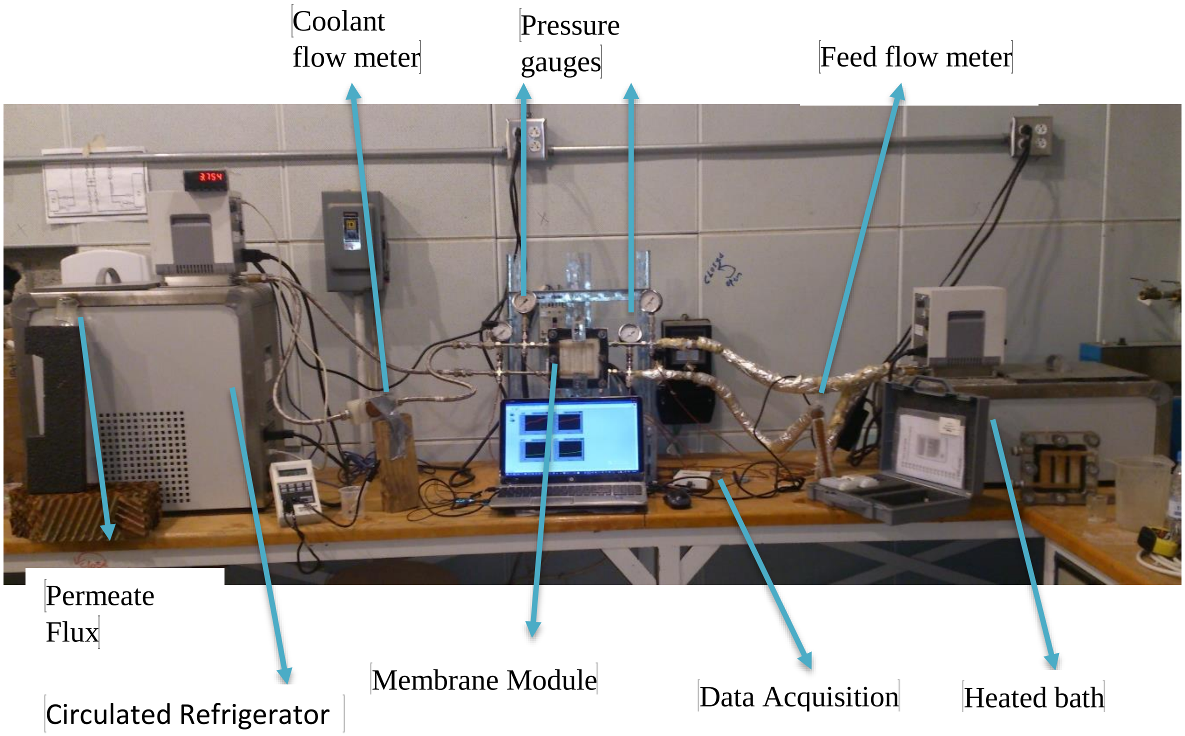

Figure 4. 3 Experimental setup-DCMD

4.1.2 Module Design

Same module design was used for DCMD and AGMD system for the sake of comparison. The actual design was implemented using the Solidworks software. It consists of two compartments: a hot feed compartment and cold permeate compartment, with three rectangular flow channels in each compartment. In-between every components within the module is a rubber gasket to prevent leakage prevention. The module flow channels were machined from Plexiglas material using CNC machine located at the main ME workshop. Presented in figure 4.4 is the module design, details and its dimensions for hot and cold compartments respectively. Both hot and cold compartments are similar to each other in terms of dimensions and design of channel.

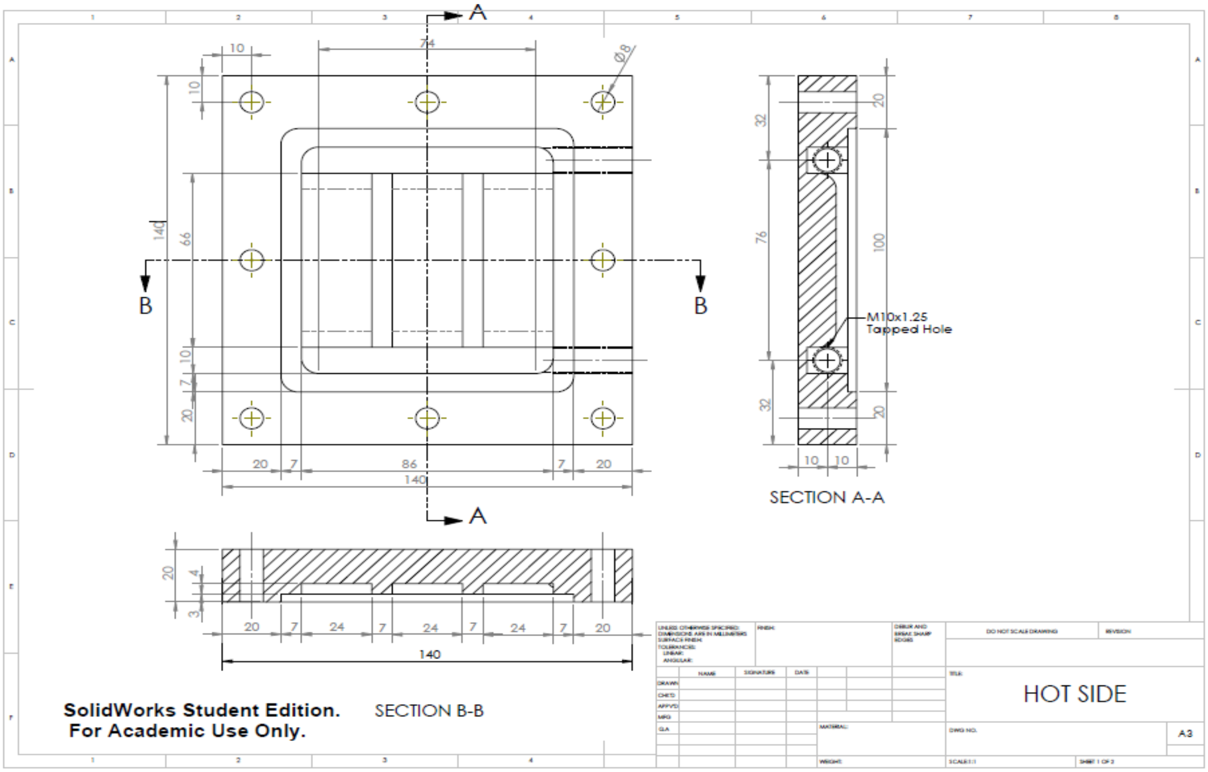

Figure 4. 4 Hot and cold compartments detailed sketch

The feed chamber and cooling chamber are identical with the following channels dimensions: 66 mm length, 24mm width, and depth of 5 mm. The cooling channel dimensions are 66 mm length, 24mm width, and depth of 5 mm. The effective membrane area of permeation is 6.192×10^{-2} m^2 with wetted perimeter and hydraulic diameter of 0.058 m and 0.08275 m respectively.

4.1.3 Assembly of the DCMD Module

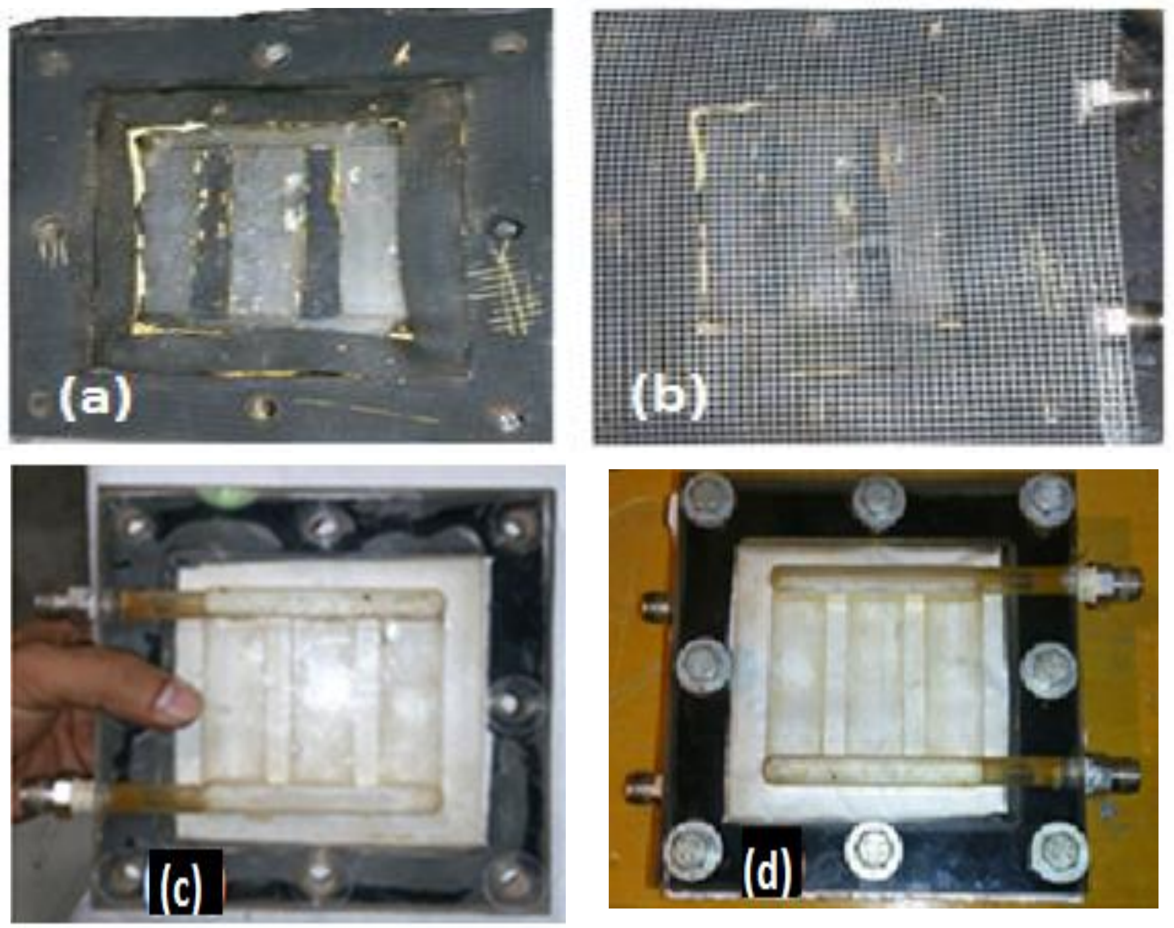

Figure 4. 5 Assembling of DCMD Module

(a) Hot side with rubber gaskets (b) Meshed Net wire in the hot side module (c) Cold side unassembled (d) Cold side assembled

Different parts of the used module are assembled as demonstrated in figure 4.5. Figure 4.5 (a) represents the placing of gaskets in the hot feed compartment. There are two basic purposes of the gaskets; 1- To avoid leakage while tightening 2- The other purpose is to smooth the sharp edges of the compartment that can damage the membrane active side while it is tightened up. Figure 4.5 (b) shows the squared meshed net in the feed side that will support the membrane. Figure 4.5 (c) shows the cold side of an unassembled module and Figure 4.5 (d) show the assembled module ready to be used for the experimentation.

4.2 Water Gap Membrane Distillation Setup (WGMD)

Figure 4.6 shows the schematic diagram of water gap membrane distillation (WGMD) configuration. Hot feed enters into the hot compartment, where hydrophobic membrane is fitted inside the module that is the core of the MD technology. This membrane is supported by a perforated brass plate of 1.75 mm. This supporting plate provides enough support to membrane against bending due to feed entering over the membrane. There is temperature difference across the membrane surface that causes partial pressure difference that generates water vapours. These vapours condense over the cooling surface and accumulate in the permitted gap. After filling the gap with condensed vapours it act as water gap and then extra water comes from top of the gap as fresh water, Whereas in the cold side of module, cooling fluid is recalculated so that the temperature of the condensation plate is kept low and condensation process can be effective. This condensation plate is made of brass. Figure 4.7 shows the exploded view of the membrane module. Two metallic stainless steel frame provides strength to compartments against tightening of screws. These frames are used so that the hot and cold compartments may not get broken while tightening.

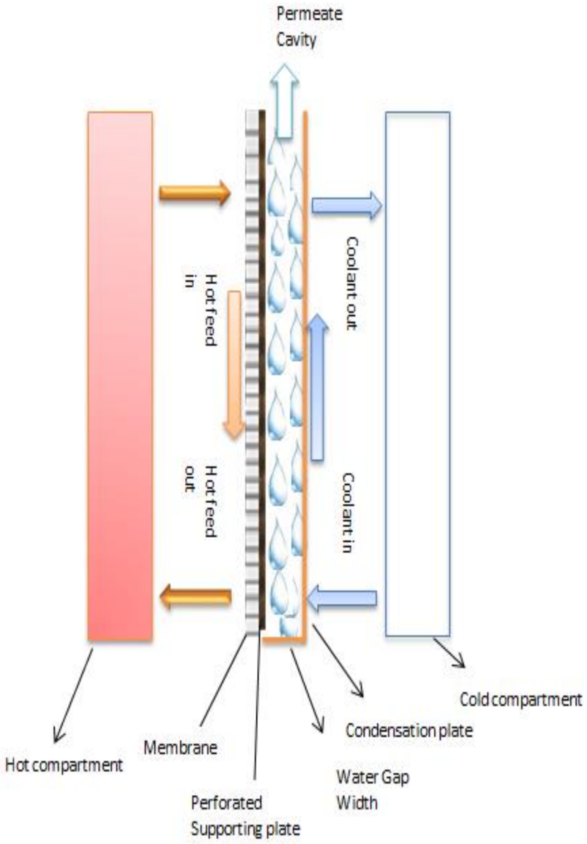

Figure 4. 6 Schematic diagram of Water Gap Membrane Distillation (WGMD

The MD module is made of two High-Density Polyethylene (HDPE) compartments with overall dimensions of 200 × 225 mm strength-to-density ratio and can withstand somewhat higher temperatures (120 ^{o}C and 110 ^{o}C continuously). One compartment is used for hot feed solution (water) and other compartment is used for permeate cold side. Each flow compartment has two rectangular channel of same dimension. The headers (15 x 150 mm) are used to collect the water at channels inlet and outlets. Each channel has dimensions of 60 x 120 mm. Figure 4.7 shows the exploded view of the membrane module that was used during experimentation of WGMD and AGMD configurations. The hot feed solution passes directly over the hydrophobic membrane. The effective membrane area that comes for vapor production is 7.24×10^{-2} m^2. Insulated steel pipes are used for inlet and outlet transmission pipes from heater and chiller.

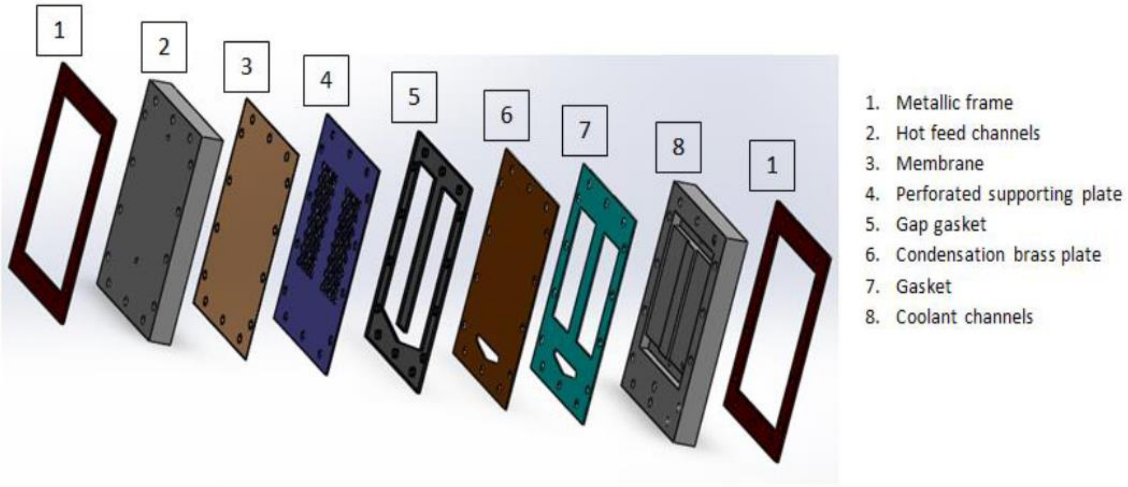

Figure 4. 7 Exploded view of membrane module (WGMD and AGMD)

Referring to figure 4.8, shows the channel design of module and assembling of module. Membrane is sandwiched between the two chambers. The water enters through header and distributed into two channels. After passing over the membrane surface, the fluid is collected back into the exit header. Then it goes out of the module after producing vapours. Same process of flow happens in the cold side but in cold side instead of evaporation, condensation of vapours happens. The same chamber design is used for the cold side. In order to avoid from internal and external leakage rubber sheet of 2mm was used as gasket. Internal leakage happens because of membrane rupture in the feed side. The distance between membrane support layer and condensing plate is called Gap width. This gap width is to be controlled by adjusting the gap gasket thickness and their numbers. For experimentation purpose, 2mm, 4mm, 6mm, 8mm and 12mm gap gaskets were tested.

Hydrophobic membrane

Perforated support plate

Gap gasket over supporting plate

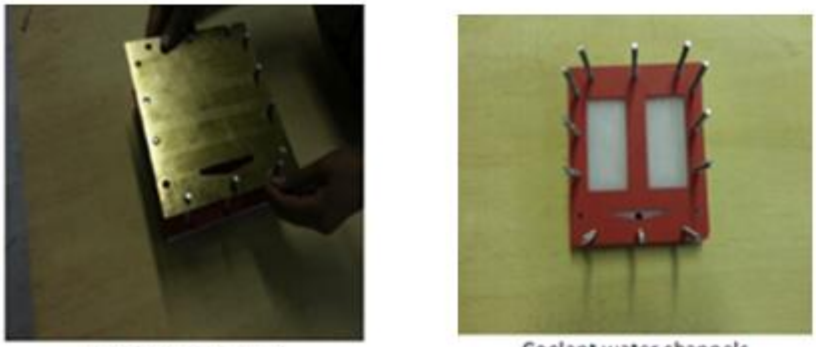

Condensation plate

Coolant water channels

Figure 4. 8 Steps to assemble the module

(From L to R 1st Row, Hydrophobic membrane over the hot compartment, then perforated brass supporting plate, then gap gasket with thermocouple, then solid brass condensation plate followed by cold channel compartment)

Figure 4.9 shows the instrumented membrane module. Pressure gauges and thermocouples are connected at the inlet and the outlet of the module to measure the temperatures and pressures of inlet and outlet for the hot and cold stream.

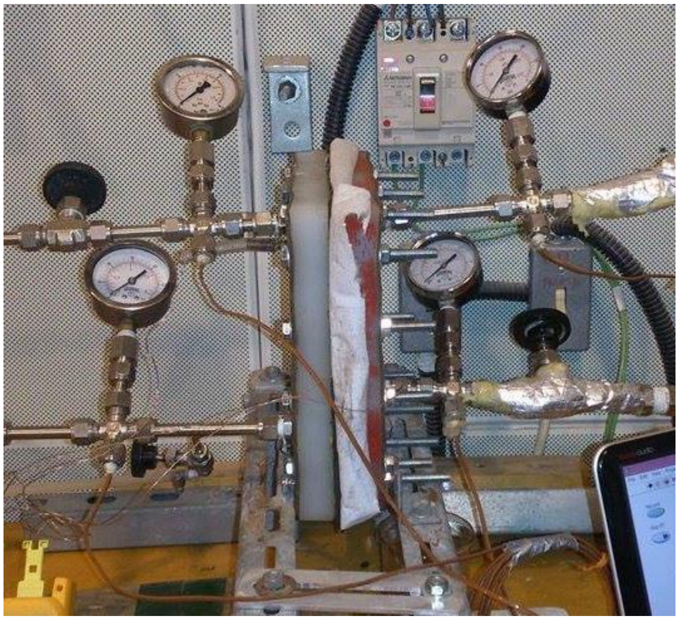

Figure 4. 9 Instrumented WGMD and AGMD Module

Figure 4.10 shows the experimental setup of WGMD and AGMD setups. The WGMD or AGMD system consists of two water closed cycles, hot and cold, connected to the MD module. The heart of the membrane distillation system is the membrane module. THERMOSCIENTIFIC heater operated by a controlled head of ThermoFisher was used to provide constant flow rate and constant temperatures for the feed and coolant side. OMEGA FL 50000, float flow meter was used to measure feed flow rate and OMEGA turbine flow meter was used to measure coolant flow meter**.** Then measured feed flow is entering into the hot compartment and exiting. Similarly circulated refrigerator is employed in accomplishing constant flow of cold distilled water. Also a turbine flow meter is put in the path of cold flow to measure the flow of cold fluid

OMEGA CDH-287 MICRO conductivity meter was employed to measure salinity of feed, coolant and permeate flux. Pressure gauges of are used to observe the inlet and outlet pressure of feed and permeate sides. National Instruments Hi-Speed USB Carrier was used for DAQ Data acquisition to record the data. And K-type thermocouples were employed to see the inlet, and outlet temperature of feed and coolant side. Membrane of TisCH scientific polyvinyl diflouiride (PVDF) and polytetraflouroethylene (PTFE) of 0.22µm and 0.45 µm were utilized for experimentations.

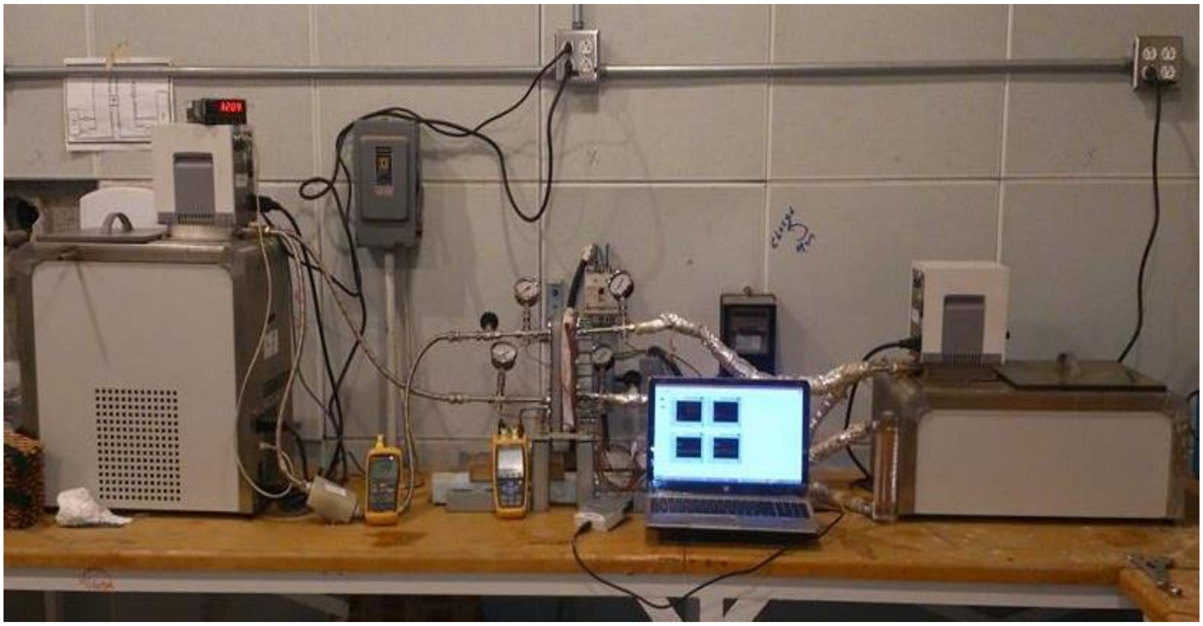

Figure 4. 10 Experiment Setup AGMD and WGMD

Figure 4.11 depicts the assembled and instrumented membrane module with cavities shown for flux collection in WGMD and AGMD configurations. Two cavities are provided to collect permeate from module. One on the bottom to that will be used when the module is acting as air gap, and the top cavity that will be used when the module is switched to liquid gap configuration.

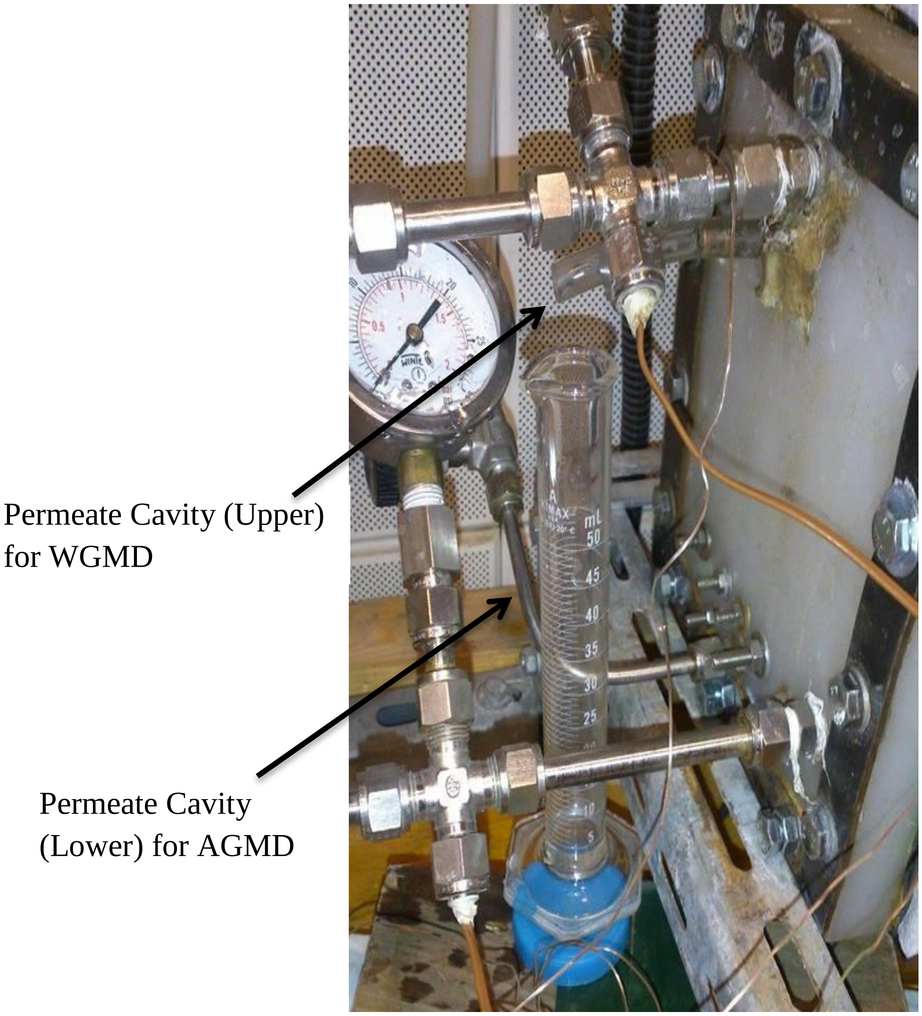

Figure 4. 11 Permeate Cavity for WGMD

Inside the gap, two thermocouples were fitted to see the temperature in the gaps, and one more thermocouple is employed in the cavity to see the temperature of cavity. Two thermocouple reader were used to read the temperatures for gap and cavity in air gap and liquid gap configuration. Then a gap gasket is inserted to maintain the gap between supporting plate and condensing plate.

Figure 4. 12 Cavity and Gap temperature readings

Figure 4.13 shows Data Acquisition system connected to the computer in order to record and save the data for the inlet and outlet of the hot and cold side of the MD systems.

Figure 4. 13 Data acquisition of membrane module inlet and outlet

4.3 General Description of Setup

The selection of appropriate component needed for the experimental setup is of paramount important. Table 4.1 presents the serial number, model number, short description, manufacturers, and the quantities of the main components and instrumentation used in the experiment.

Table 4. 1 Components and instruments used in system

Sr. No.	Component	Model No.	Description	Manufacturer	Quantity
1	Hi Speed USB carrier	9162	Channel	National Instruments	1

	(Slot Chassis)				
2	CDAQ (Thermo couple)	9211	4Channel,1.5V, -40^{o}C to 70 ^{o}C	National Instruments	1
3	Rotameter	FL 50000	2L/min to 20 L/min at 90 ^{o}C	OMEGA	1
4	Turbine flow meter or paddle wheel flow meter with digital display			OMEGA	1
5	conductivity meter	CDH-287		Ω OMEGA	
6	Pressure gauges		Capable of measuring 0-2 bar	Winter	2
7	Pressure gauges		Capable of measuring 0-1 bar	Tecsis	2
8	Thermocouples	SMPW-K-M	PATPEND K-type	OMEGA	7
9	Male Type K Miniature Connector	S PW-K M			
10	Membranes	SF 17386 PTFE 0.45 (260*300mm), SF 17386 PTFE 0.22 (260*300mm), SF17388	Hydrophobic	TisCH SCIENTIFIC	3 packs (50 pcs per pack)

		PVDF0.45 260*300mm)			
11	Water heater		100-115V,50-60 Hz, 1 Phase, 11.3 A	ThermoFisher SCIENTIFIC	1
12	Heater Controlled Head	HAKE AC 150		THERMOSCIENTIFIC	
13	Refrigerator circulator		115 V , 60 Hz,1 Phase, 11.7 A,R134A,6OZ, HIGH 300 PSIG, LOW 150 PSIG	ThermoFisher SCIENTIFIC	1
14	Refrigerator controlled head	HAKE AC 150		THERMOSCIENTIFIC	1
15	Control Valves	P316			2
16	Stainless steel fittings of ½ in				4
17	Measuring flasks	Glass and plastic beakers	20,40,50,100 and 250 mL	KIMAX	5
18	Data Logger Thermometer	HH147U	4 Channel	OMEGA	1
19	Thermometer	53 II	1 channel	FLUKE	1

4.4 Main components and sensors

The components of the DCMD system are depicted in figures 4.6 to 4.18. The components include; THERMOSCIENTIFIC heater operated by a controlled head of ThermoFisher was used to provide constant flow rate and constant temperatures for the feed and coolant side shown in fig 4.6 to 4.8. Also they are provided with a pump installed inside the chiller and heater that forces the fluid to flow. Both heater and chiller are equipped with digital regulator to control the pump speed, temperature and type of the fluid. A small port is created in the chiller so that extra water produced can be collected as permeate flux. And that flux will be collected in a measured beaker as shown in fig 4.9.

To measure the feed flow rate, a rotameter is installed before the inlet of the module as shown in fig 4.10. And at the inlet of the module (some inches away), a thermo-couple and a pressure gauge is installed to observe the inlet temperature and pressure of the feed fig 12. After passing through module, another thermocouple and pressure gauge is installed to measure the temperature and pressure at the outlet of the module. Similarly on the coolant side, two thermocouples and two pressure gauges are installed to see the temperature and pressure for the coolant inlet and outlet fig 4.13. In the path of coolant flow, a turbine meter is provided to check the inlet coolant flow rate as shown in fig 4.11.Paddle wheel or turbine flow meter is connected to a digital display meter to see the reading of actual coolant flow. Thermocouples at the inlet and outlet of hot and cold compartment are connected with data acquisition system a complete computer system for monitoring and storing data (figure 4.14 to figure 4.16). Inlet and outlet thermocouples are connected to Hi-Speed USB DAQ carrier in order for data acquisition. Programming of DAQ is done by using Lab View software and a block diagram of the program is shown in fig 4.16. Then graphical display of recorded data of inlet and outlet temperatures of feed and coolant is shown in graphical representation in fig 4.15. OMEGA CDH-287 MICRO conductivity meter was employed to measure salinity of feed, coolant and permeate flux as represented in fig 4.18. Different collecting beakers were used to measure the permeate flux as shown in fig 4.17.

Figure 4. 14 Feed heater provided with controlled head

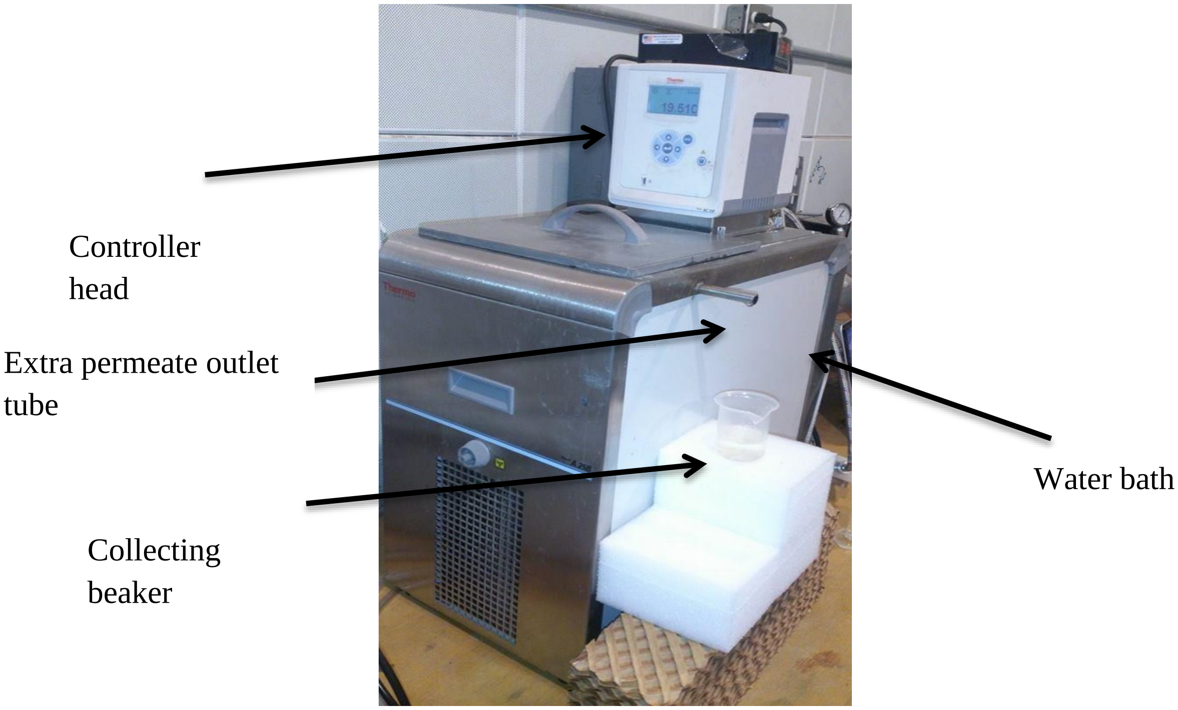

Figure 4. 15 Refrigerator circulator connected with controlled head

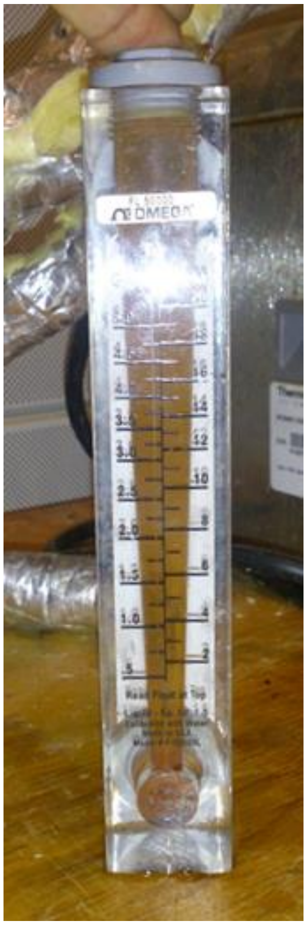

Figure 4. 16 Feed flow meter

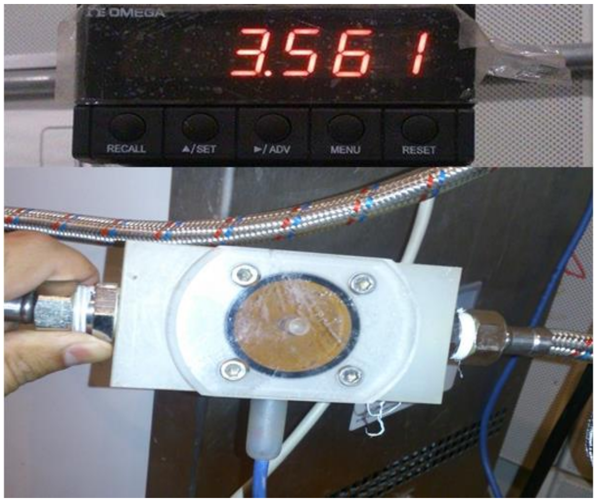

Figure 4. 17 Coolant flow meter with digital display

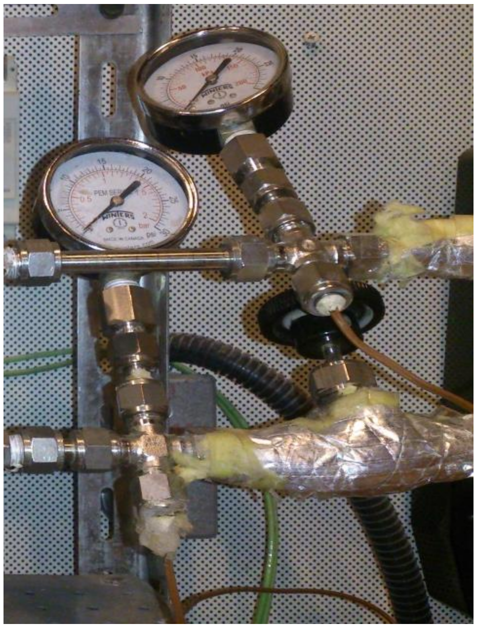

Figure 4. 18 Feed Inlet and outlet thermocouples and pressure gauges

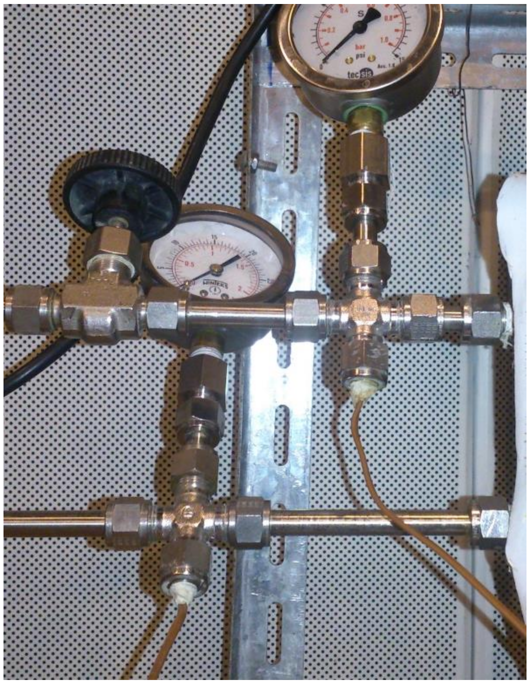

Figure 4. 19 Coolant inlet and outlet thermocouples and pressure gauges

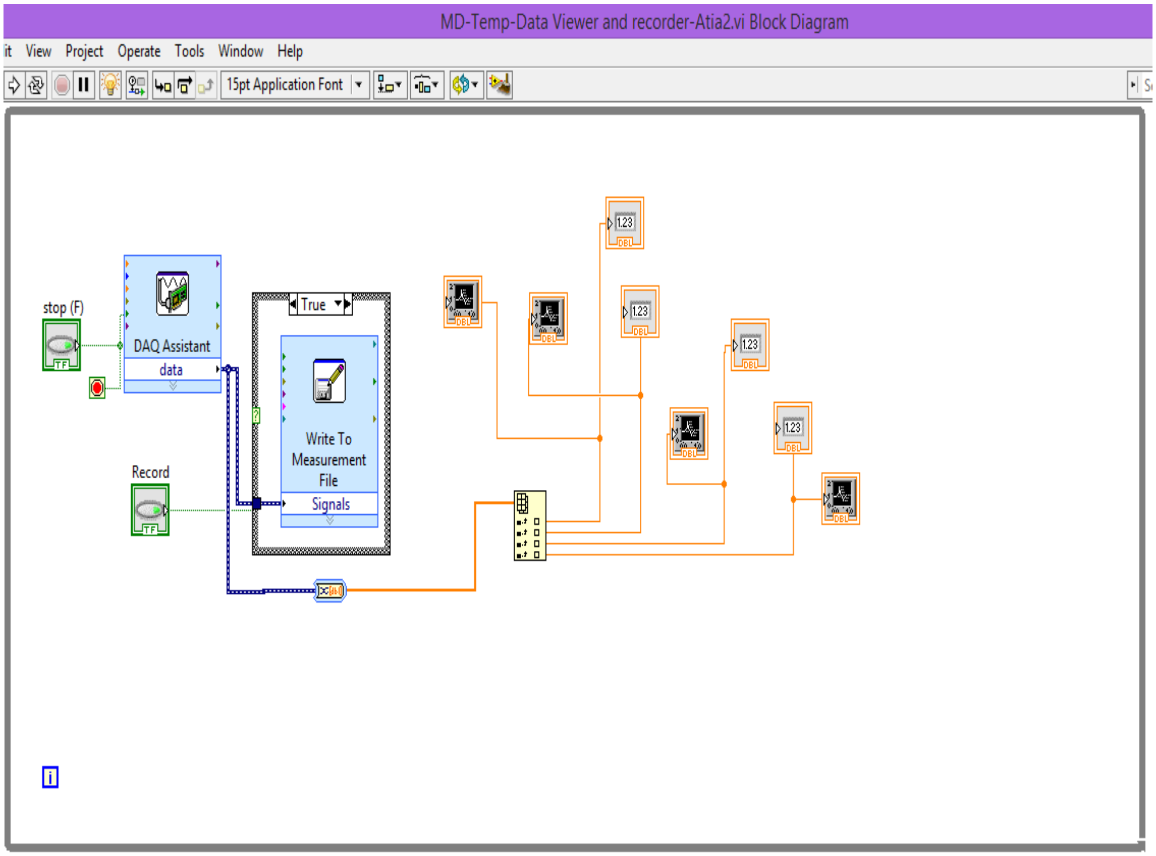

Figure 4. 20 Block diagram for LabVIEW code

Figure 4. 21 Collecting beakers

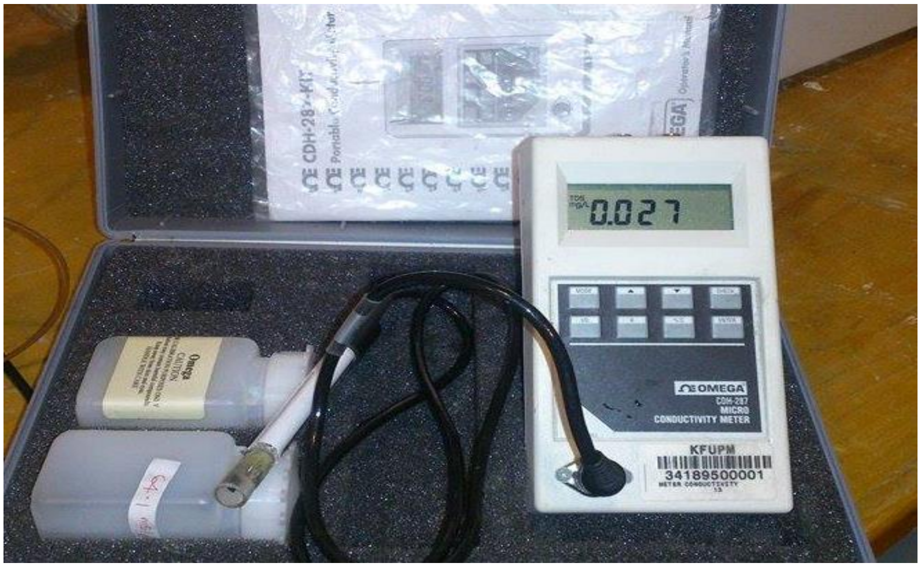

Figure 4. 22 Micro conductivity meter

4.5 Membrane Characterization

The membranes used in testing are polyvinydiflouiride and polytetraflouroethylene of 0.22 μm and 0.45 μm pore size acquired from TISH SCIENTIFIC. It is a composite membrane that is composed of an active layer and support layer. The characterization of membranes is done in Complutense de Madrid (UCM), Spain and results are tabulated in the following table 4.2.

Table 4. 2 Measured properties of used membranes

Membrane	**Parameters**							
	$\delta_{membrane}$ **(μm)**	δ_{teflon} **(μm)**	$\delta_{support}$**(μm)**	m_p **(nm)**	LEP_w **(bar)**	$LEP_{30\ g/L}$ **(bar)**	ε **(%)**	θ **(º)**
PTFE SF17385 (0.22)	159 ± 18	8 ± 2	143 ± 16	236	3,3 ± 0,1	3,5 ± 0,1	76	138
PTFE SF17386 (0.45)	154 ± 14	7 ± 2	141 ± 16	379	2,4 ± 0,1	2,6 ± 0,1	80	139
PVDF SF17388 (0.45)	105 ± 3	-	-	420	0,4 ± 0,1	0,4 ± 0,1	60	91

4.6 Proposed Research Work Plan

4.6.1 Objectives

The proposed work will be done to cover the following objectives.

1- Experimental investigation of the performance of Direct Contact Membrane Distillation (DCMD) unit under variable operating conditions of temperature, flow rate and salinity of feed . The objective is to build-up a setup for DCMD system, where the comprehensive study of all variable can be done to analyze the performance of DCMD system.

2- Experimental investigation of performance for Water Gap Membrane Distillation (WGMD) under variable operating and designed conditions. As WGMD is quite newer technology as compared to other conventional MD techniques so , we can build a module for LGMD , that can also be used for AGMD with slight modifications.

3- Modeling of DCMD. Engineering Equation Solver (EES) is a programming tool, which will be used for modeling purpose.

4- Comparing the performance of DCMD, LGMD, and AGMD configurations. After we build up the setup for DCMD, AGMD and LGMD, we can compare the performances of the systems simultaneously.

5- Energy and efficiency analysis for DCMD. Using 1st and 2nd law of thermodynamics we will be doing energy analysis for the MD systems.

4.6.2 Methodology

The methodology to meet the objectives specified above can be adapted by following these steps.

- Literature review

- Desalination-General overview
- Desalination with Membrane desalination (MD)
- Experimental testing for DCMD and LGMD
- Modeling of DCMD process
- Energy and efficiency analysis

4.6.3 Modeling

Following are the guidelines to develop a valid, best suited mathematical model for heat and mass transfer analysis of DCMD system.

- Study of available model in open literature to predict the performance of MD systems
- Investigate the used assumptions and correlations
- Adopt a final model for both DCMD and LGMD
- Improving the final adapted model
- Use of EES software for modeling

4.6.4 Experimental work plan

Experimental work was done by following the main steps outlined here;

- DCMD module (design and manufacturing)
- Study of the effect of operating and designed variables on the performance of the MED systems (Feed and permeate side)
- Use of different membranes materials and pore size (with repeated experiments)
- Membrane degradation with time (at least one experiment)
- Perform Experiments for Water Gap and Air Gap MD

- Comparing the performance of 3 techniques of DCMD, LGMD, AGMD

Following the methodology mentioned above, membrane distillation experiments were carried out. These are some equipment which will be brought under use for the experimentations purposes.

- Membrane materials

The membrane materials used in the membrane distillation experiment is Polytetraflouroethylene (PTFE), PVDF (Poly vinyl diflouiride), with pore sizes of membranes

- Module materials

The Membrane distillation module to be use will be designed and manufactured from locally available material like Plexiglas sheets, metal sheets, or plastics, and HDPE (highly dense polyethylene).

- Constant supply water heater and chiller

Constant hot water circulation and constant cold temperature circulation water bath will be used for the feed and coolant sides of MD module respectively. This will enable us to have control over the water supplied to the feed and coolant sides of the module.

- Sensor

The water supplied to the feed and coolant sides of MD module will be monitored by using the sensors given below;

- Thermocouples

For measuring temperature of water supplied to the feed and coolant sides of MD module.

- Pressure gages

For pressure measurement of water supplied to the feed and coolant sides of MD module.

- Flow meters

For measuring flow rate of water supplied to the feed and coolant sides of MD module.

- Data acquisition system (DAQ)

That was purchased and used for the automatic acquisition of data.

Other components that will be used in the experiment includes PVC pipes, T-connectors, Elbows joint, reducers, unions joint, hose, valves and water tanks.

A parametric study on the effect of different operating and design parameters on the permeate flux is carried out. This is done by varying one operating parameter while keeping the others constant. The investigation of feed solution concentration, membrane material type and membrane pore size on permeate flux is also carried out.

The investigated operating parameters are the feed temperature, feed flow rate, coolant temperature, coolant flow rate and air gap width. The table 4.3 below summarized the experimental condition. These stats based on the tested configurations. The data utilized for the sake of comparison for AGMD was taken from Dahiru Lawal's MS thesis [108] . In this comparison PMMA (Plexiglas) module of 3 channel was used. It must be mentioned here that the experimental data will be presented in combined effects to reduce the number of plots.

Table 4. 3 Comparison of operating parameters and ranges for DCMD and AGMD

Parameter	Range
Inlet feed temperature	40-80 ^{o}C
Inlet coolant temperature	15 – 30 ^{o}C
Feed flow rate	2,3 and 4.65 L/min
Coolant flow rate	2,2.85 and 3.65 L/min

Membrane material	PTFE,PVDF
Membrane pore size	0.45 µm, 0.22 µm
Gap width	3 mm-7mm (Applicable for AGMD only)
Concentration	0.140,2,43,100 g/L

In the later portion of the manuscript, another comparison was made between AGMD and WGMD configurations. Another 2 channel HDPE membrane module was utilized for their comparison. Operating variables and their ranges are well illustrated in table 4.4.

Table 4. 4 Comparison of operating parameters and ranges for WGMD and AGMD

Parameter	**Range**
Inlet feed temperature	50 – 90 ^{o}C
Inlet coolant temperature	5,15, 24 ^{o}C
Membrane material	PTFE,PVDF
Membrane pore size	0.45 µm, 0.22 µm
Gap width	2mm,4mm.6mm,8mm,12mm
Concentration	0.150,43 g/L

4.6.5 Analysis

Different kinds of analysis will be done on DCDM configurations in order to find thermal efficiency of the system, gain output ratio(GOR) of the module, entropy genertation and exergy destruction by applying first and second laws of thermodynamics. In general these analysis include;

- ✓ Energy consumption (Measured and calculated)
- ✓ Energy efficiency (in terms of thermal efficiency and GOR)
- ✓ Exergy analysis (Entropy generation, and effect of different operating parameters like inlet feed temperature, cold permeate temperature, feed flow rate, cold permeate flow rate on entropy generation or exergy destruction will be studied)

Table 4. 5 Proposed Time Plan

Se. No.	*TASKS*	*Months*																
		JAN 2014	**FEB 2014**	**MAR 2014**	**APR 2014**	**MAY 2014**	**JUN 2014**	**JUL 2014**	**AUG 2014**	**SEP 2014**	**OCT 2014**	**NOV 2014**	**DEC 2014**	**JAN 2015**	**FEB 2015**	**MAR 2015**	**APR 2015**	**MAY 2015**
1	**Literature review**			■	■	■	■	■										
2	**Design of MD System**				■	■	■	■	■									
3	**Experimental Design**								■	■	■							
4	**Setup construction**									△	△	△						
5	**Application of experimental matrix and Data collection**												△	△				
6	**Modelling/Analytical solution**									▭	▭	▭	▭	▭	▭			
7	**Analysis of Results and comparison**															⬯	⬯	
8	**Thesis writing and Defence**															⬯	⬯	

■ Fully Completed

△ Partially completed (20 % Left)

▭ Partially Completed (40 % Left)

⬯ Started (In beginning phase)

CHAPTER 5

EXPERIMENT RESULTS AND DISCUSSION

In this chapter, results obtained from experiments and modeling will be discussed in detail. Firstly results of direct contact membrane distillation system will be explained followed by validation with the theoretical results obtained from heat and mass transfer modeling of DCMD system. Then a comparative study was established between DCMD and AGMD system for the same operating and design conditions. Experimental data for AGMD was obtained from umar’s MS thesis [108]. Then in the second portion of the chapter, another comparative study between Water gap membrane distillation system (WGMD) and AGMD was conducted under the same operating and design conditions. Operating conditions include inlet feed temperature, coolant temperature, feed salinity, feed flow rate, and coolant flow rate. Design conditions include the gap width, membrane materials, membrane pore size.

5.1 Performance of DCMD system

There was a wide range of experiments covered in this section comprehensively. The inlet feed temperature was varied from 40 ^oC to 90 ^oC. The coolant temperature was varied between 5 ^oC to 25 ^oC. The feed flow rate and coolant flow rate was tested at three different levels each. Four different levels of feed salinity were tested; 143 mg/L, 2 g/L, 43 g/L and 100 g/L were examined. Two membrane materials of PTFE, PVDF with pore size of 0.45

µm and 0.22 µm were tested. A well elaborating relationship was developed between the theoretically predicted flux and experimental flux.

5.1.1 Effect of inlet feed temperature

The effect of inlet feed temperature over the permeate flux is studied over a range of temperature of 40 °C to 90 °C with an increment of 10 °C. It was observed that with increasing the inlet feed temperature, permeate flux increases. The change in inlet feed temperature was observed at varying permeate temperature with feed salinity of 2g/L. Figure 5.1.1 (a) to 5.1.1(e) shows the effect of feed temperature on flux at various cold permeate temperature (T_{bc}) of 5 °C, 10 °C,15 °C, 20 °C and 25 °C respectively. In all the figures the similar trend is observed with difference in numerical values. In fig 5.1.1(f) the combined effect is studied. From this figure it can be seen that increasing the inlet feed temperature, increases the flux. According to the Antoine equation (Equation no.2 and 3), the effect of temperature on vapor pressure is considerably low at lower feed temperature, and becomes very significant at higher temperature.

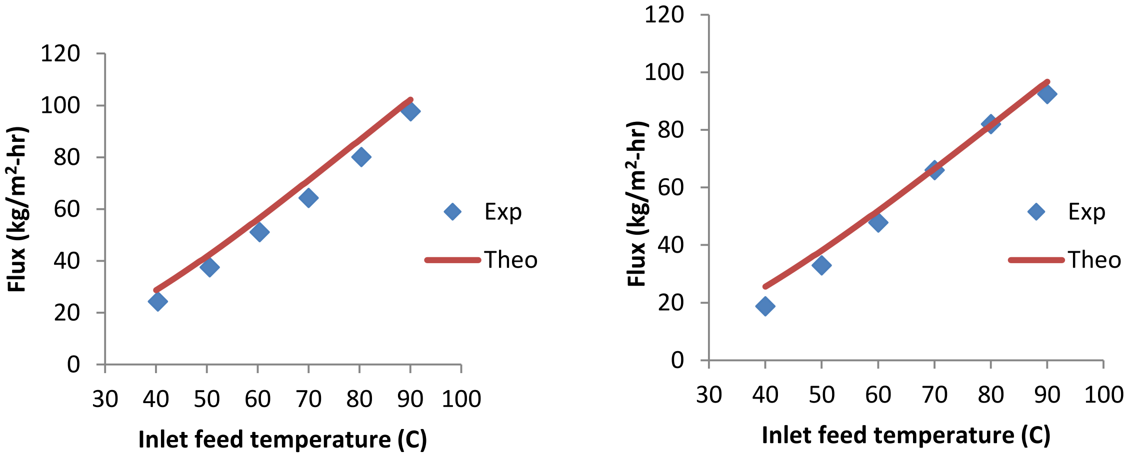

(a) At T_{bc}=5 °C

(b) At T_{bc}=10 °C

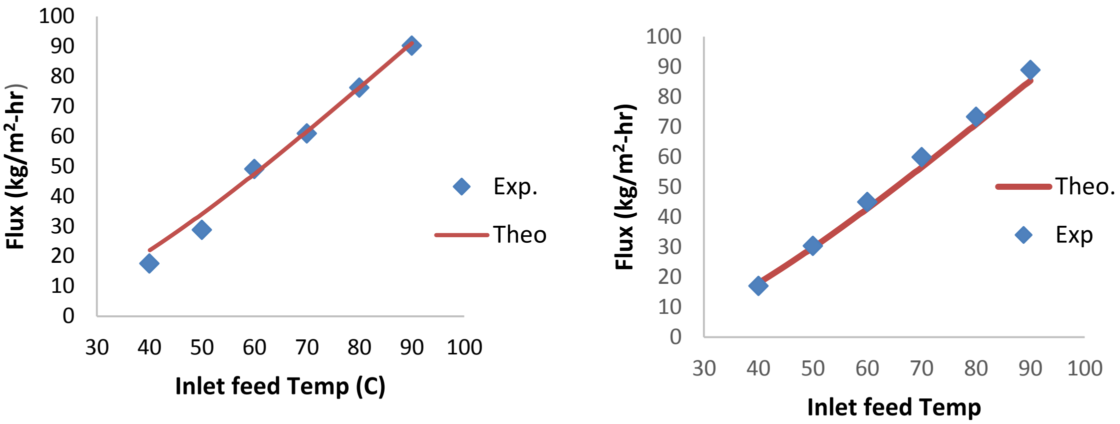

(c) At T_{bc}=15 °C **(d) At T_{bc}=20 °C**

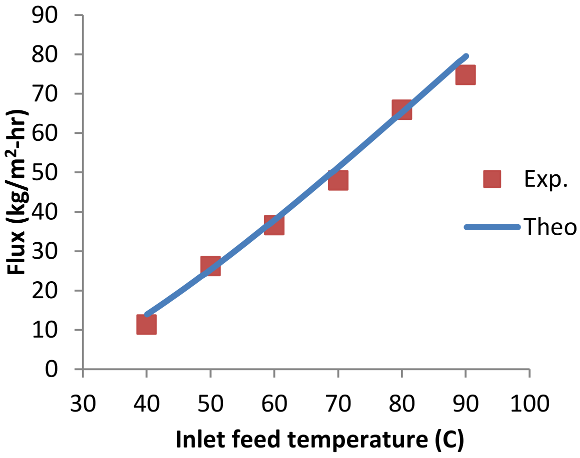

(e) At T_{bc}=25 °C

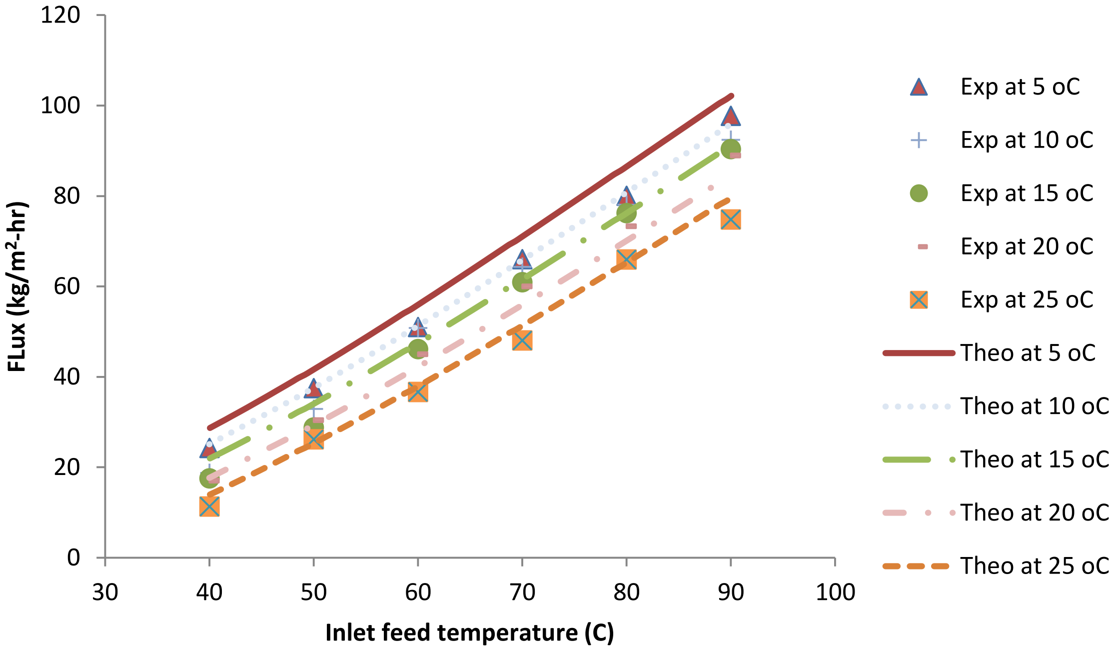

Figure 5.1 (f)

Figure 5. 1 Effect of feed temperature on permeate flux

Operating Conditions: PTFE 0.45 microns, 25 ^{o}C coolant temperature, feed flow rate 4.6 L/m, coolant flow rate 3.65 L/m , feed salinity 2 g/L

If we compare the percentage increase in flux when the cold permeate temperature was reduced from 25 ^{o}C to ^{o}C, then referring to figure 5.2, it shows the percentage increase in flux at various inlet feed temperatures, it is observed that at 40 ^{o}C percentage change in flux is more than 100 % which goes on declining until temperature arouses up to 80 ^{o}C and then at 90 ^{o}C percentage change again increases. Although operating at higher inlet feed temperature gives more flux, but the percentage increase in flux is higher at lower inlet feed temperature as compared to higher inlet coolant temperature.

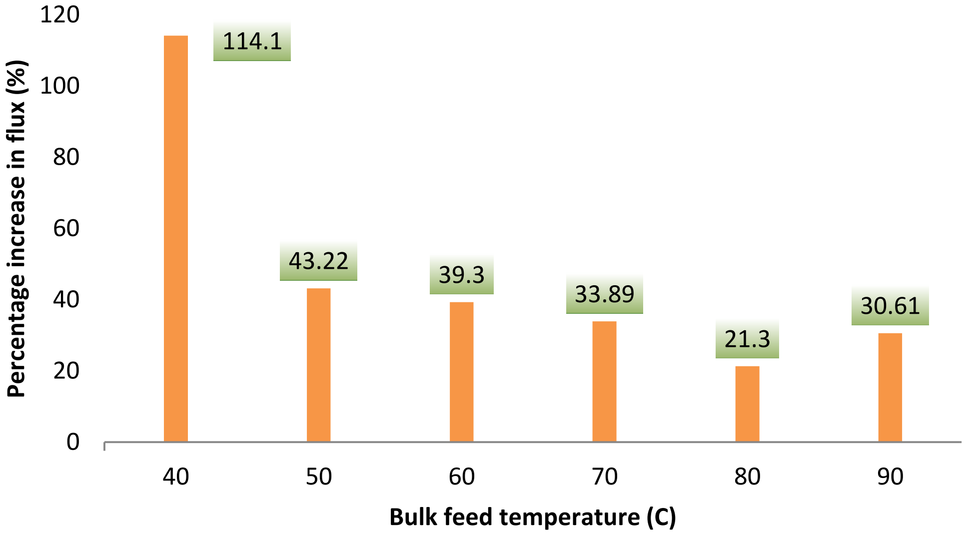

Figure 5. 2 Percentage increase in flux at different inlet feed temperatures

5.1.2 Effect of Cold permeate temperature

The effect of inlet coolant (Cold permeate) temperature on flux is shown in figure 5.3. The flux is increasing as the cold permeate temperature decreases. The coolant temperature was varied from 5^{o}C to 25^{o}C by the increment of 5^{o}C and feed temperature was held constant at 90 ^{o}C. Actually the flux is a function of diffusion co-efficient and differential transmembrane partial pressure. Increasing the cold permeate temperature causes a decrease in driving force which is difference of partial pressure, that leads to a reduction in permeate flux. So at lower coolant temperature the flux is higher and vice versa. Experiments show that comparatively inlet coolant temperature is less effective as compared to inlet feed temperature for flux enhancement.

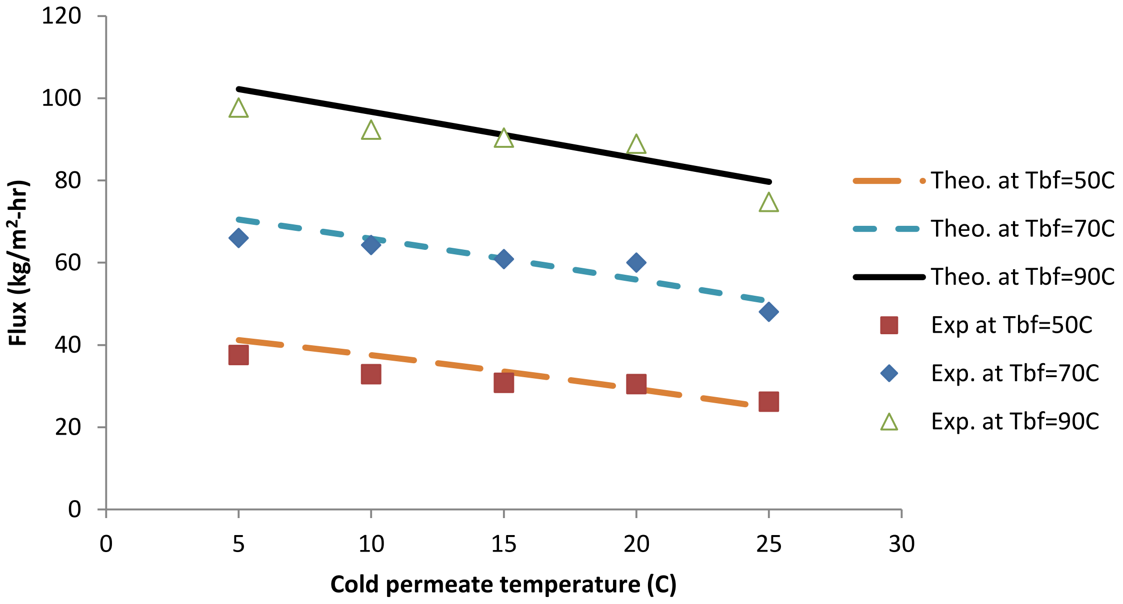

Figure 5. 3 Effect of coolant temperature on permeate flux

Operating Conditions: PTFE 0.45 microns, feed flow rate 4.6 L/m, coolant flow rate 3.65 L/m, feed salinity 2g/L

Figure 5.4 shows the effect of coolant temperature on percentage increase in flux at different coolant temperature when the feed temperature is changed from 40^{o}C to 90 ^{o}C. It is illustrating that at lower coolant temperature, the percentage increase in flux is lower as compared to higher value of coolant temperature. At low coolant temperature 5^{o}C, the percentage increase in flux is 302 % as compared to the flux at 40 ^{o}C that goes on increasing until coolant temperature increases up to 25 ^{o}C as shown in fig 5.4 , and then at this temperature percentage increase in flux is 560 % almost. So one conclusion can be made here that although operating DCMD system at low inlet coolant temperature can yield us high value of flux but percentage increase in flux is higher for higher inlet coolant temperature instead of low coolant temperature.

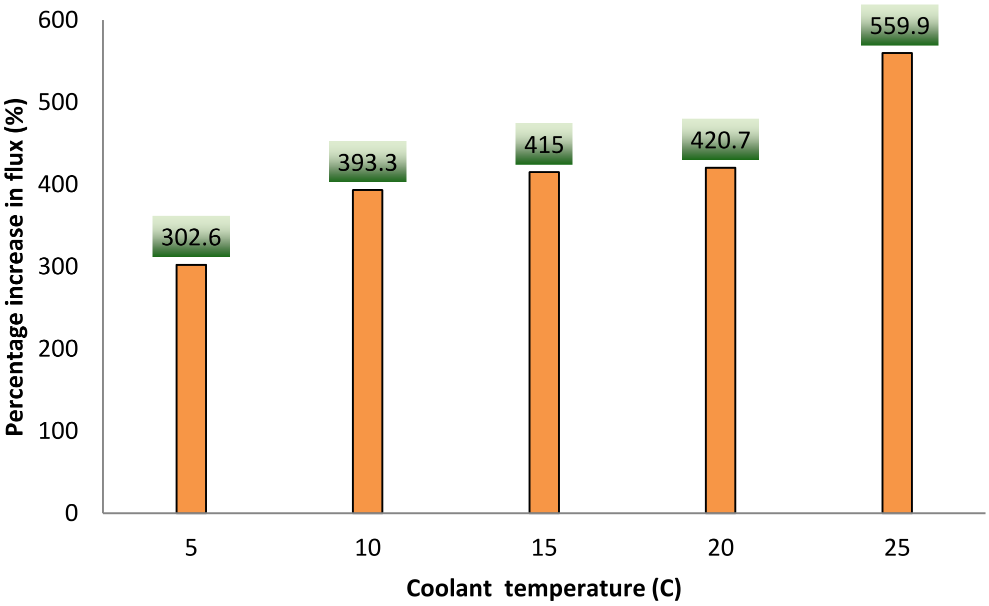

Figure 5. 4 Influence of inlet coolant temperature on percentage increase in flux

Figure no. 5.5 represents the effect of temperature ratios (Ratio of feed temperature over cold permeate temperature i.e. T_f/T_c) over flux theoretically and validated experimentally at different cold permeate temperature. The experimental operating conditions were taken as: PTFE membrane with 0.45 pore size, feed temperature was varied from 40 ^{o}C to 90 ^{o}C, with feed salinity of 43 g/L, feed flow rate 4.65 L/min, cold permeate flow rate 3.65 L/min. It was observed that, increasing the temperature ratio increases the flux exponentially with different inclination at different cold permeate temperature. The curves tend to move away from reference (origin) as the cold permeate temperature decreases from 25 to 5 ^{o}C. Also theoretical values were well validated by experiments.

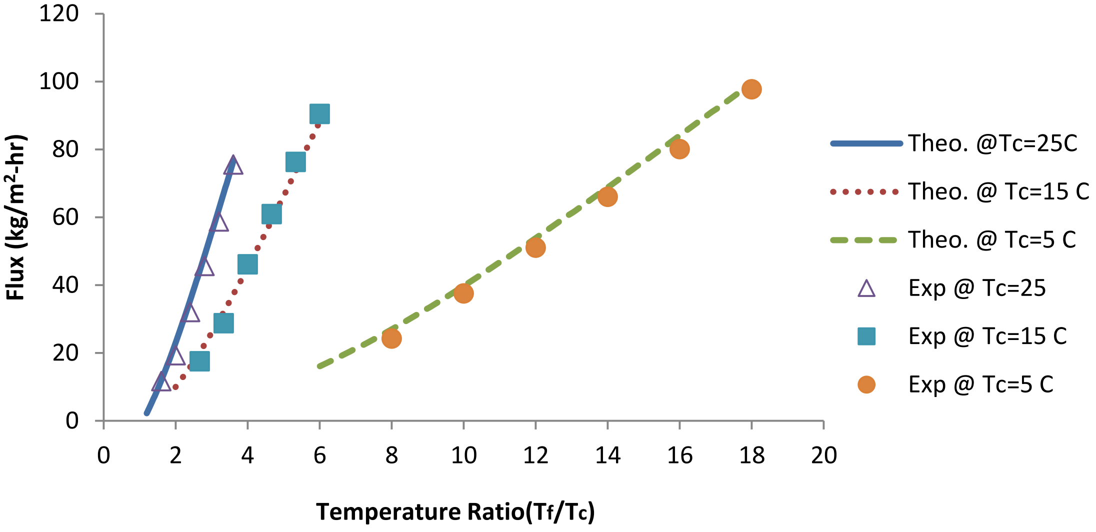

Figure 5. 5 Effect of temperature ratios on flux

Fig no. 5.6 represents the effect of resultant temperature difference between feed and cold permeate (T_f-T_c) on the flux on different cold permeate temperature theoretically and experimentally. The operating conditions were taken as; PTFE membrane with pore size of 0.45 microns, feed flow rate 4.65 L/min, cold permeate temperature 3.65 L/min, feed salinity 43 g/L. A good agreement was observed between theoretical and experimental values. It was seen that increasing the temperature difference increases the flux at different cold permeate temperatures. Another important observation to be made was that, at fixed temperature difference, higher cold permeate temperature yields higher flux. But lower cold permeate temperature yields lower flux at fixed temperature difference.

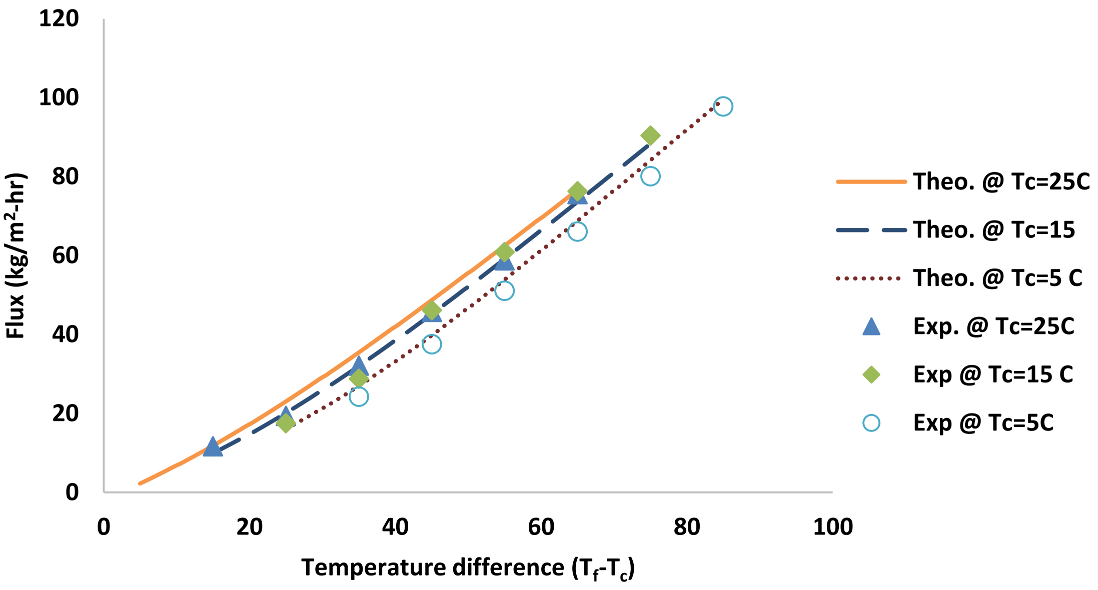

Figure 5. 6 Effect of temperature difference on flux

5.1.3 Effect of Feed flow rate

When the feed flow rate increases (keeping all other operating parameters constant), it increases Reynolds number, that generates more turbulences in the feed channel that assist heat transfer process by reducing the thermal boundary layer over the membrane surface. This decrement in thermal boundary layer also reduces temperature polarization co-efficient over the membrane surface. This effect can be visualized in the following fig. 5.7. It can be seen that by increasing the flow rate of feed, the flux is going to increase. The change in flux is prominent. For example flux is changing from 55 kg/m^2-hr to 75 kg/m^2-hr by changing flow rate from 2.5 L/min to 4 L/min.

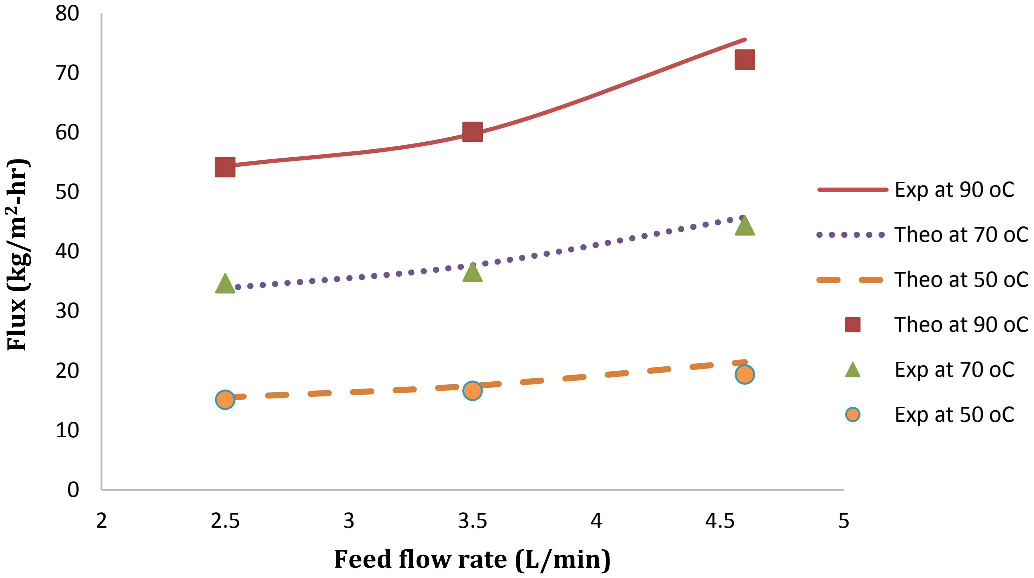

Figure 5. 7 Effect of feed flow rate on permeate flux

Operating conditions: coolant flow rate 3.65 L/m, inlet feed temperature 90 ^{o}C, coolant temperature 25 ^{o}C

In terms of percentage change in flux, when the inlet feed temperature is changed from 50 ^{o}C to 90 ^{o}C at different feed flow rates, fig 5.8 well explains this effect. The percentage change in flux from 2.5 to 4.5 L/m is not much as compared to their individual values. Keeping flow rate at 2.5 L/min. and changing feed temperature from 50 ^{o}C to 90 ^{o}C can give 258 % more flux and at 4.5 L/min, this percentage is merely 272 % which gives difference of 14 % only by changing feed flow rate from 2.5 to 4.5 L/min. One thing can be noticed that improvement in flux is highly pointed out at higher inlet feed temperature instead of lower feed temperature. So one can suggest that making larger feed flow rate is more beneficial at higher feed temperature instead of lower feed temperature.

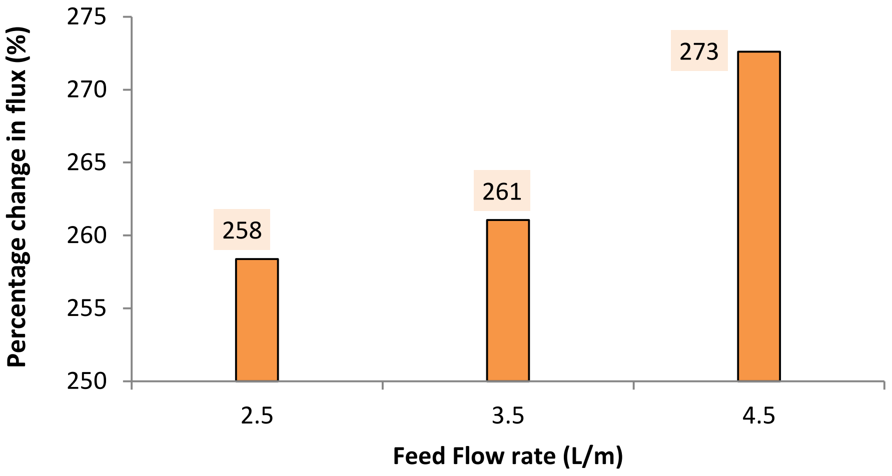

Figure 5. 8 Percentage change in flux at different feed flow rate

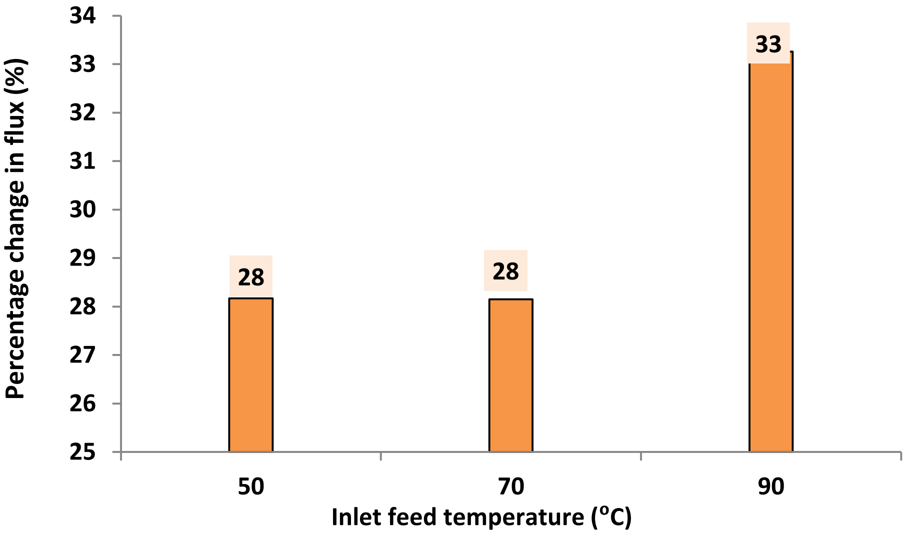

Figure 5. 9 Percentage increase in flux at different feed temperature

The importance of feed flow rate can also be shown in fig. 5.9. Operating the system at low feed temperature say 50 ^{o}C, it can govern 28 % increment in flux as compared to the flux at 2.5 L/min by changing the flow rate from 2.5 to 4 .5L/min. But at higher feed temperature 90 ^{o}C, it can result in 33.2 % more flux. So a percentage difference of 5 is observed by changing the feed temperature from 50 ^{o}C to 90 ^{o}C.

5.1.4 Effect of permeate flow rate

As the permeate flow rate increases the system generates more flux permeation as shown in fig 5.10. For different feed temperatures of 50 °C, 70 °C and 90 °C, the flux increases by increasing coolant flow rate. Although the change is not much significant but the trend is rising in both; experimental and theoretical results as it is depicted from the fig 5.10. A mere difference of 2-4 kg/m^2-hr can be observed from three different feed temperatures as shown in fig 5.10. The reason for not being much significant is that the hot feed is the main source of the vapor flux rather coolant. So the effect of coolant flow rate is not significant in enhancing the flux as compared to the feed flow rate.

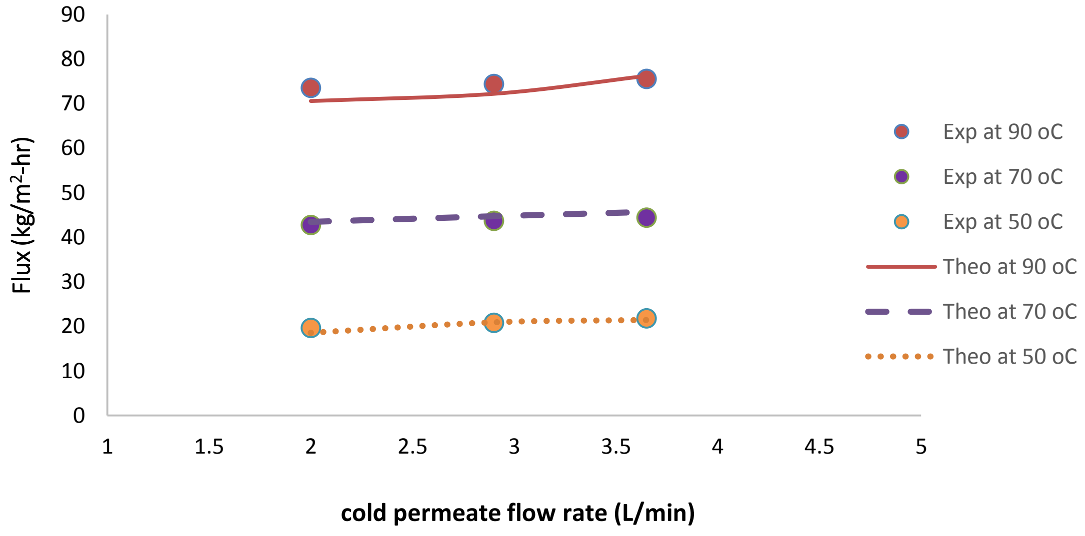

Figure 5. 10 Effect of coolant flow rate on permeate flux

Operating Conditions: PTFE 0.45 microns, coolant temperature 25 °C, feed flow rate 4.65 L/min. , feed salinity 2g/L

Figure 5.11 is showing the percentage change in flux for different coolant flow rate over complete range of feed temperature from 50 °C to 90 °C. This figure shows that at low cold permeate flow rate, the change in percentage is high as compared to high cold permeate flow rate. Varying the coolant flow rate from 2L/min to 3.65 L/min, only changes 10.3 % compared to the reference value which is the flux at 40 °C. Therefore, cold permeate flow rate is not much significant in increasing the flux.

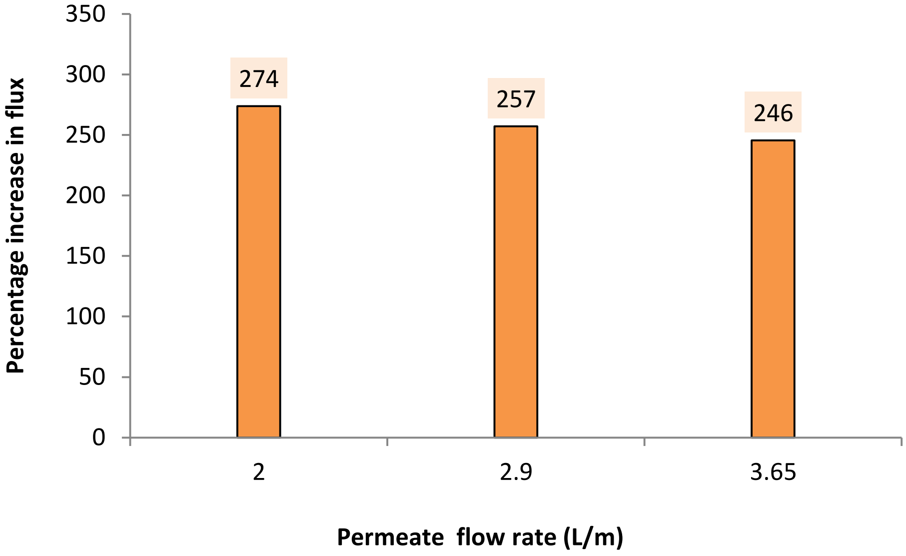

Figure 5. 11 Percentage increase in flux at different permeate flow

Figure No. 5.12 shows the effect of volume flow rate ratio (Feed flow rate over cold permeate flow rate i.e. V_f/V_p) on flux experimentally and theoretically on selected permeate flow rate of 2 L/min, 2.9 L/min and 3.65 L/min. The operating conditions were taken as , PTFE membrane with pore size of 0.45 microns, inlet feed temperature 90 °C, permeate temperature 25 °C, feed salinity 43 g/L, and feed flow rate was varied from 2.5 L/min to 4.65 L/min. It was observed that increasing the VFR (volume flow rate ratio) increases the flux at any cold permeate flow rate parabollicaly. For fixed value of VFR, higher permeate flow rate yields more flux output. Also a good coherence was seen between theoretical values and experimental values of flux at all permeate flow rate.

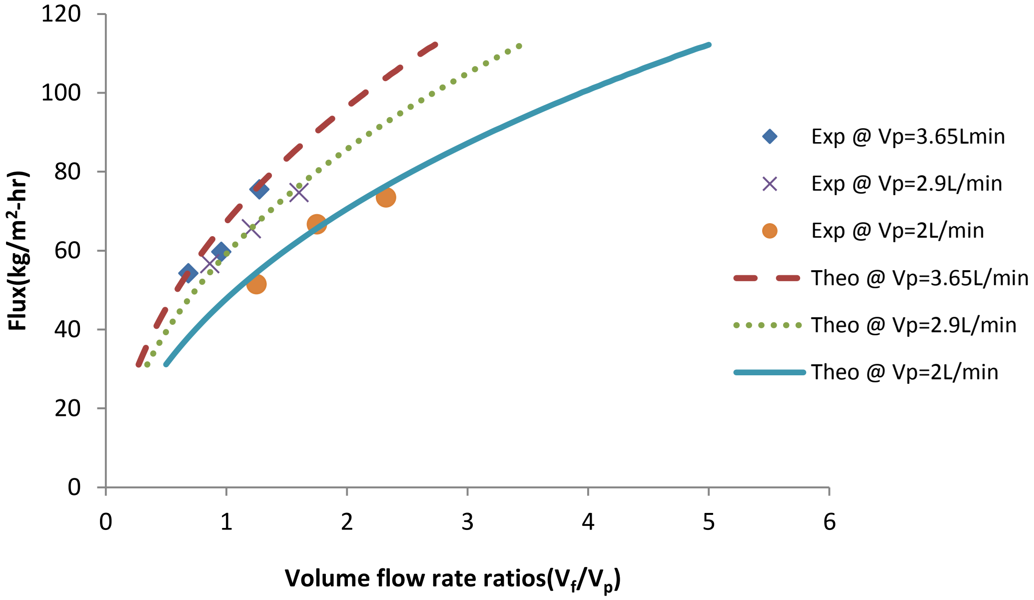

Figure 5. 12 Effect of volume flow rate ratio on flux

5.1.5 Effect of membrane pore size

Membrane pore size is an important property of the membrane morphology. In order to investigate the effect of membrane pore size on flux, two different pore size of PTFE membrane were tested, PTFE 0.45 µm, PTFE 0.22 µm, other properties like tortuosity, membrane thickness, water contact angle etc. are almost similar (Table 4.2). It can be seen in figure 5.13 that by increasing the inlet feed temperature, experimental and theoretical both fluxes increased. This is another observation from fig 5.13 that for 0.45 microns pore size PTFE the flux is higher for membrane as compared to 0.22 microns. The reason behind this is that for bigger size of pore, the flux permeation is more as compared to small pore size, slight increase in porosity yields in higher flux for 0.45 microns membrane. Although the air resistance inside the pores is larger in bigger size membrane, but the driving force between the two surfaces causes more flux permeation through pores. It can also be observed that smaller pore sizes can lead to more molecule-wall collision that can increase the resistance for permeation, but in larger pore size the resistance can be reduced.

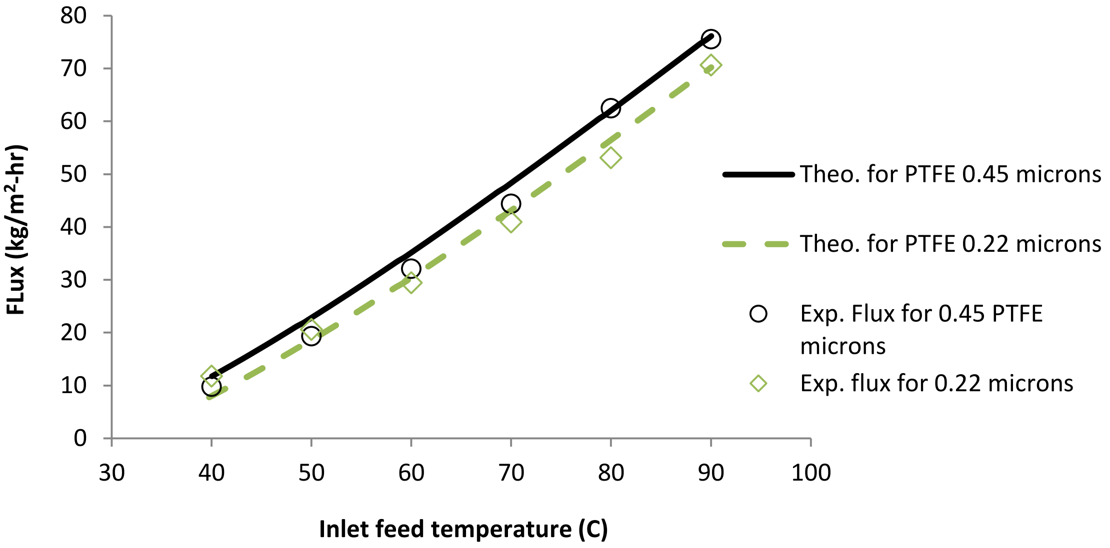

Figure 5. 13 Effect of membrane pore size on permeate flux

Operating Conditions: Inlet coolant temperature 25 °C, feed flow rate 4.65 L/m, coolant flow rate 3.65 L/m, feed salinity 43 g/L.

Fig 5.14 is representing the percentage difference in flux for both membranes at different feed temperatures with the reference values of fluxes at 40 °C. As the feed temperature increases, the difference in percentage flux is also increasing. This means that the effect of pore size is more prominent at high feed temperature as compared to lower feed temperature.

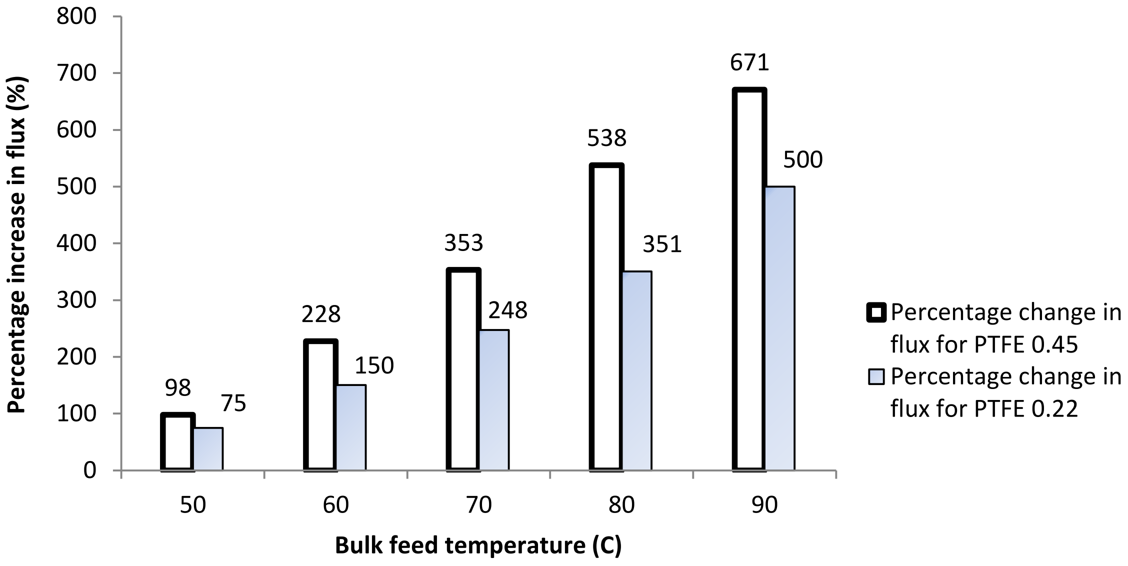

Figure 5. 14 Percentage change in flux for PTFE 0.45 and PVDF 0.45

Figure 5.15 represents the effect of membrane pore size on the flux theoretically. The membrane pore size was varied between 0.1 µm to 5 µm keeping all other morphological properties (hydrophobicity, void volume fraction, membrane thickness etc.) constant. It was observed that increasing pore size increases the flux up to certain value and then pore size doesn't increase the flux. Increasing the pore size from 0.1 to 0.6 increases the flux (1.75%) but after that increasing pore size from 0.6 µm to 5 µm, yields only 0.3 % increase in flux. So theoretically it seems pore size is only effective within the range of 0.1 µm -0.5 µm. Practically speaking, literature says membrane pore size shouldn't exceed 1 µm , after that surface energy of membrane materials decreases, and hydrophobicity decreases, which leads to pore wetting phenomenon which greatly retards the performance of MD [109].

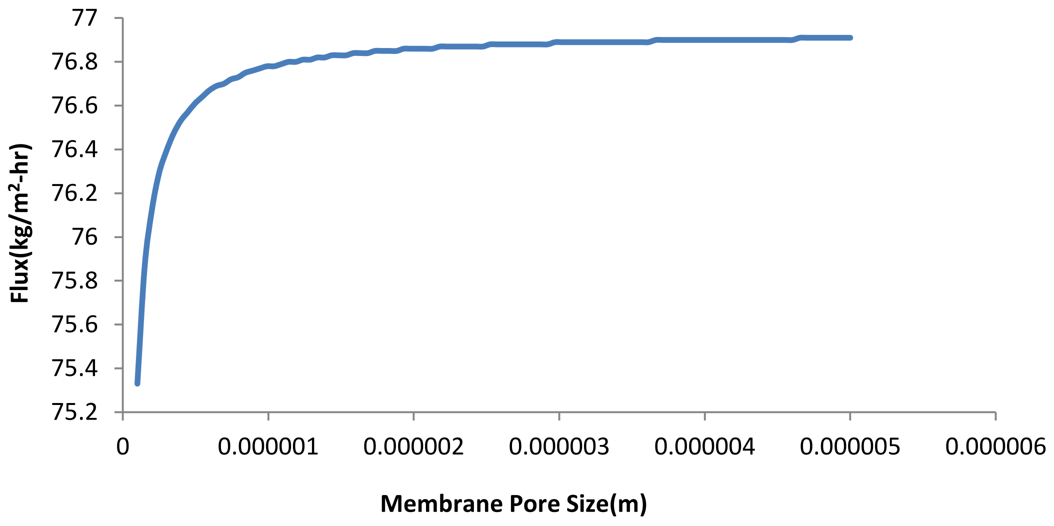

Figure 5. 15 Effect of membrane pore size on flux

5.1.6 Effect of membrane materials

Two membranes of different material PTFE and PVDF were tested to investigate the influence on the flux. From fig 5.16, it can be deduced that PTFE membrane is giving more flux as compared to PVDF membrane. It could be inferred to the effect of porosity, thickness and contact angle as PTFE has more porosity and hydrophobicity (water contact angle) than PVDF as can be seen from table 4.2. The used PTFE membrane is having higher contact angle than the PVDF membrane. The higher contact angle leads to more repulsive force between the liquid water molecules and membrane surface. Also higher contact angle leads to more hydrophobicity of membrane that gives more surface energy to membrane and it repels water molecules to come into contact. PTFE also shows more hydrophobic nature as compared to PVDF membrane. Apart from hydrophobicity, porosity (Volume void fraction) is another factor that can be related to more flux output. PVDF membrane having lower porosity of 60% as compared to PTFE with higher porosity of 80 % causes lower flux permeation through pores. The PVDF membrane is thicker as compared to PTFE membrane. Thicker membrane generates more resistance to vapor to pass through as they have to travel more distance inside the pore and increased resistance gives lessened flux. At all the tested feed temperatures, PTFE membranes yields more flux than PVDF membranes.

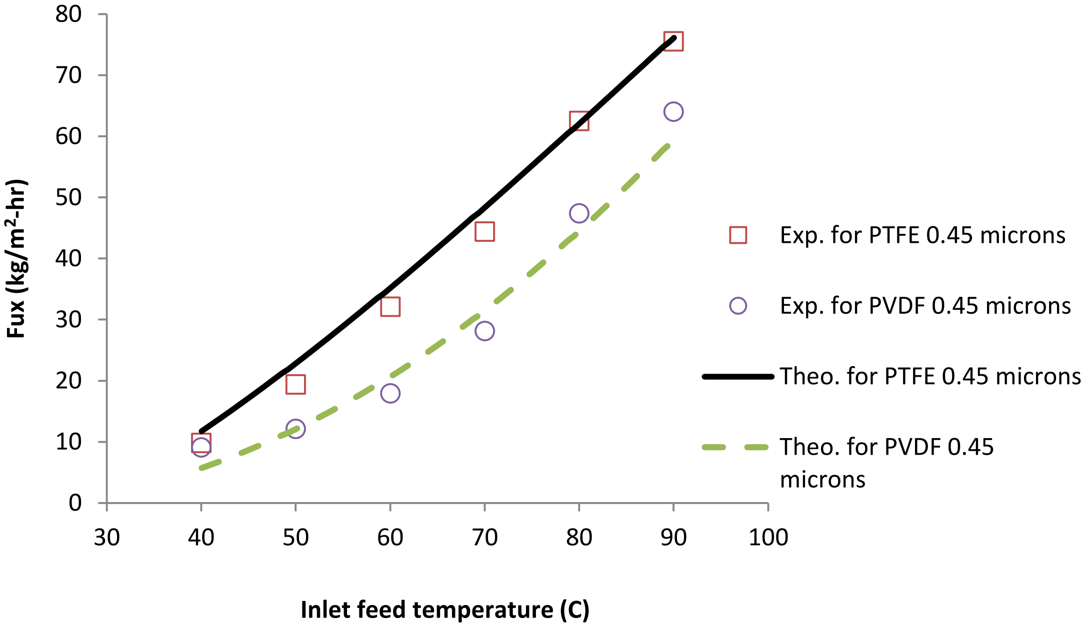

Figure 5. 16 Effect of membrane material on flux

Operating conditions: Inlet coolant temperature 25 ^{o}C, feed flow rate 4.65 L/m, coolant flow rate 3.65 L/m, feed salinity 43 g/L

Fig 5.17 illustrates percentage change in flux at different inlet feed temperatures when using PTFE membrane as compared to PVDF membrane. The resulted curve in figure 5.17

can be divided into two regions; Region 1 where inlet feed temperature increases from 40 ^{o}C to 60 ^{o}C and it yields percentage increase in flux and region 2 where inlet feed temperature increases from 60 ^{o}C to 90 ^{o}C and in this region percentage change in flux goes on decreasing. At low feed temperature (40^{o}C), there is no much difference in flux for both membrane materials. But as the feed temperature goes on increasing until 60 ^{o}C, percentage increase goes on elevating and then until 60^{o}C feed temperature is achieved, it goes on decreasing. From the resulted curve it is clear that the effect of membrane material is featuring more at 60 ^{o}C. But at lower or higher feed temperatures this effect is not much prominent.

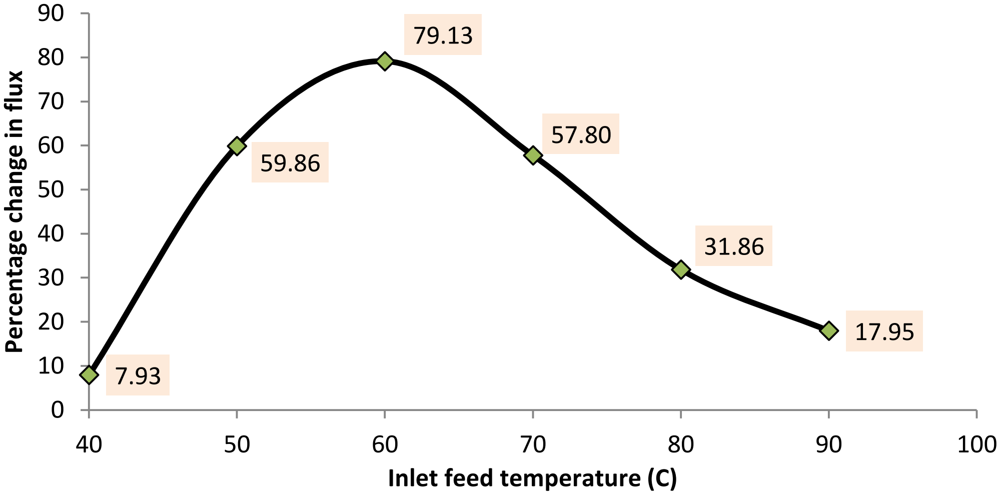

Figure 5. 17 Percentage change in flux for PTFE and PVDF membranes

5.1.7 Effect of feed concentration

Four levels of feed salinity were tested, sweet tap water having concentration of 140 mg/L, aqueous salt solution of 2 g/L, sea water collected from Arabian Gulf Al-Khobar Kingdom of Saudi Arabia with 43 g/L salt concentration and NaCl salt solution of 100 g/L prepared. The conditions of this experiment were taken as; feed flow rate 4.65 L/min, coolant flow rate 3.65 L/min, and coolant temperature was taken as 25 ^{o}C. Fig. 5.18 shows that as the feed salinity was increasing, the permeate flux was continuously decreasing because of membrane pores blocking by salts precipitation, that reduce flux permeation through membrane pores. The basic factor in reduction of flux is salt concentration polarization, salts sticks onto the membrane surface, covering some effective area of membrane, and causes reduction in partial pressure in the feed side that retards the permeation process so ultimately the flux is decreased. Scaling and fouling on the membrane surface that can also reduce the flux.

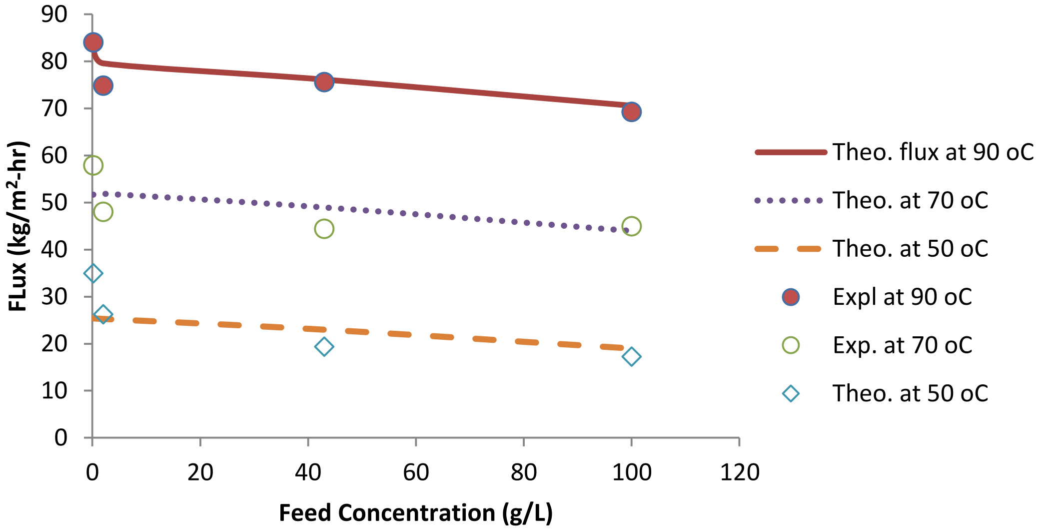

Figure 5. 18 Influence of feed concentration of flux

Operating conditions: PTFE 0.45 microns, coolant temperature 25 ^{o}C feed flow rate 4.65 L/m, coolant flow rate 3.65 L/m

Fig 5.19 represents percentage increase in flux at different feed concentration maintaining constant range of inlet feed temperature (50^{o}C -90^{o}C). From the bar charts It can be seen that for sweet water to be used as feed, flux collected at 90 ^{o}C is 140 % more than at 40 ^{o}C. But when we increase the feed salinity this percentage also goes on increasing from 140 to

302 % for varying salinity from 0.140g/L to 100g/L. So inlet feed temperature can be more effective for high feed salinity as compared to low feed salinity in terms of percentage increment in flux.

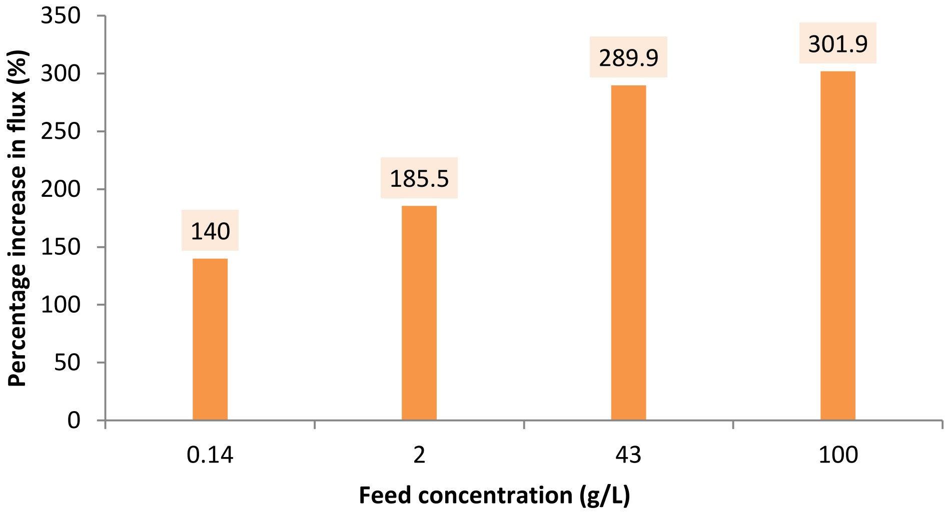

Figure 5. 19 Percentage change in flux for different feed concentration

Fig 5.20 is showing the percentage change in flux for different inlet feed temperature when the feed concentration is changed from 0.14 g/L up to 100 g/L (0.14 g/L,2g/L,43g/L and 100g/L). So as it is obvious from the chart that running the experiment at low feed temperature can yields more percentage increase in flux but as the feed temperature increases, the percentage increase in flux decreases. So another conclusion can be derived from here that effect of feed concentration is not much important at high feed temperature as compared to operating at low feed temperature. Another conclusion to be derived from this experiment is that its better to operate on higher feed temperature when the feed salinity is high or there is big variation in the feed salinity.

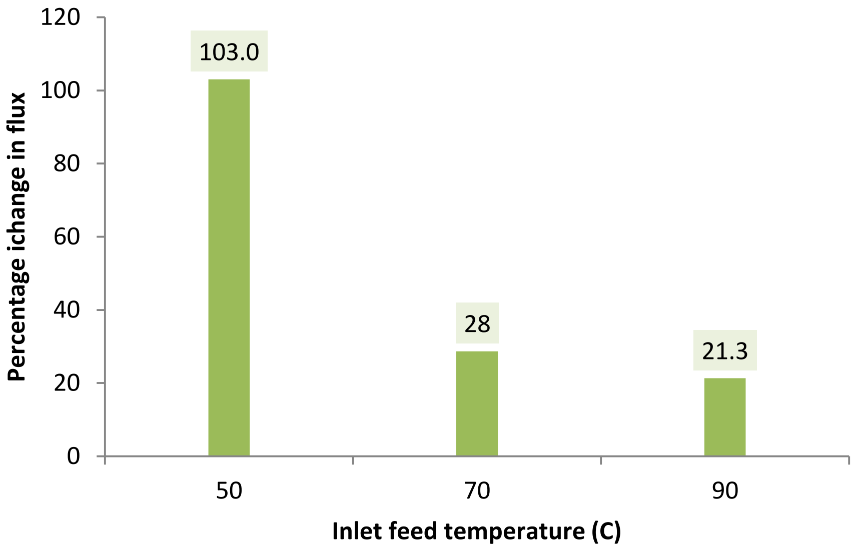

Figure 5. 20 Percentage change at different inlet feed temperature when the feed salinity changed from 0.140g/L to 100g/L

5.1.8 Quality of flux

Quality of flux is defined in terms of TDS (totally dissolved solids). Another dimensionless parameter 'salt rejection factor' is utilized to define the quality of permeate as compared to feed salinity . Salt rejection factor is given as

$$SRF = \frac{Feed\ Concentration - Permeate\ Concentration}{Feed\ Concentration} * 100$$

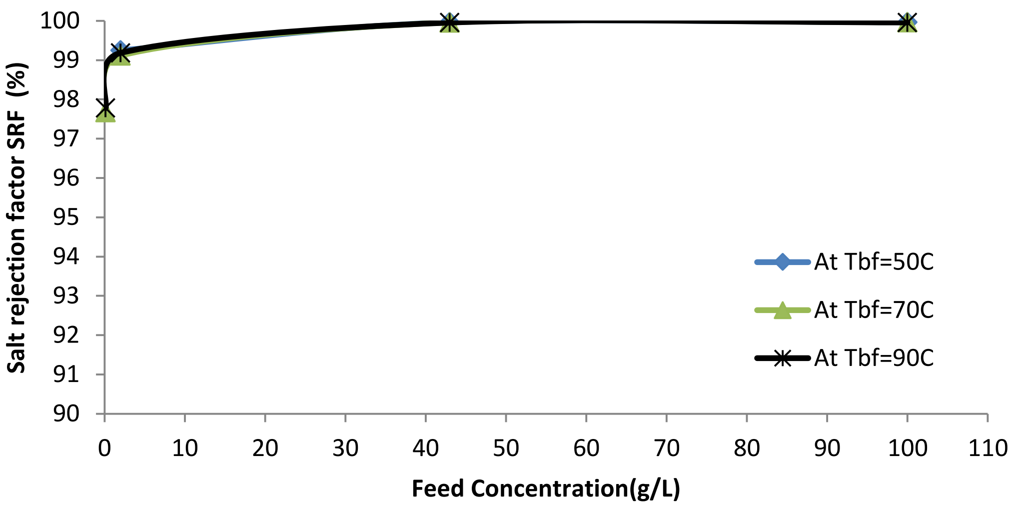

Figure 5. 21 Influence of feed concentration on quality of permeate

Operating Conditions: PTFE 0.45 µm, feed flow rate 4.65 L/m, coolant flow rate 3.65 L/m

To check the effect of feed salinity on the quality of flux, a wide range of feed concentration was tested. Four levels of feed concentration (0.140g/L, 2g/L, 43g/L and 100 g/L) were tested. Starting from sweet tap water (140mg/L) ,preparing a solution of NaCl (2g/L) and raw sea water collected from Arabia Gulf in Al-Khobar Kingdom of Saudi Arabia, and reaching a very high value of feed concentration of 100g/L. Figure 5.21 is shows the effect of feed concentration on salt rejection factor. As the feed concentration increases from 0.140 g/L to 2 g/L, SRF increases. When sea water (43g/L) was used as feed, salt rejection factor was almost 99.8% and then it becomes constant for very high feed concentration even for 100 g/L. For most of the experiments salt rejection factor was very high reaching almost 99.9 %. But for low concentration of feed (0.140 g/L) salt rejection factor was quite below, about 97.8 %.

5.1.9 Membrane Degradation test Long run experiment

Long-time experiment was conducted to investigate the effect of membrane continuous operation on system flux and to observe the degradation of membrane subjected to DCMD system. A long run experiment was run for 47 hours without interruption. The experiment was performed by using PTFE 0.45 membrane, with sweet tap water having concentration of 140mg/L as feed, with flow rate of 3.75 L/min and coolant flow rate of 3.65 L/min, inlet feed temperature 60 ^oC, inlet coolant temperature 20 ^oC. In the start of experiment, maximum flux was obtained, then almost after 3 hours a sudden decrement in flux was observed then after that flux almost remained constant for one complete day and then a slight variation occurred until the experiment was run for another 24 hours. There was not much variation seen in flux over the whole experiment. Again there is a sudden reduction in flux percentage in first three hours that continued with a slight variation till the half way of experiment and then at the end of experiment this percentage reduction was limited to 19 % almost. Fig 5.22 shows the variation in percentage change in permeate flux with respect to time.

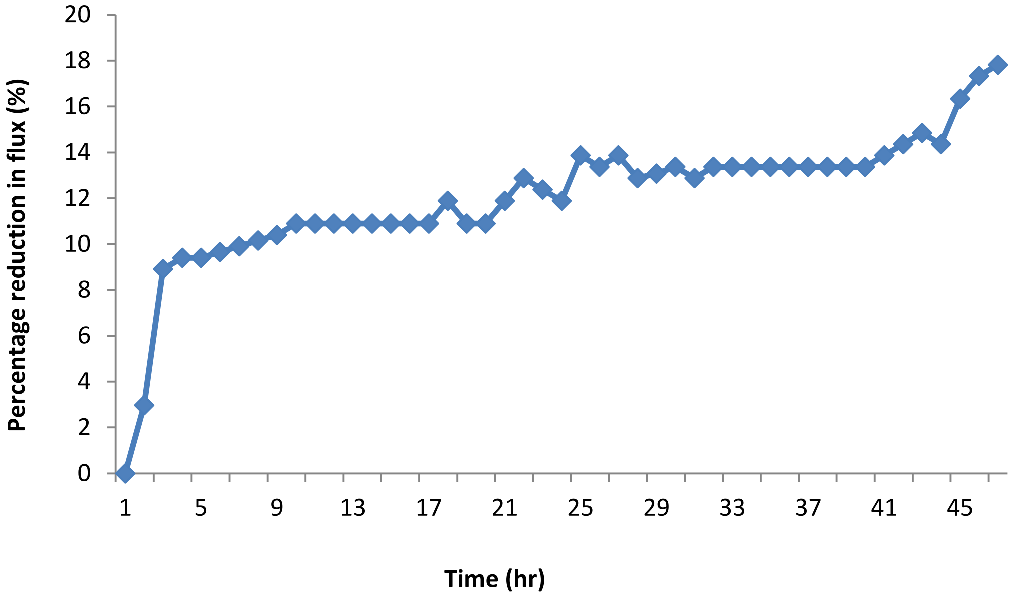

Figure 5. 22 Percentage reduction in flux with respect to time elapsed

Now let's consider the membrane degradation test with sea water as feed; another long term DCMD experiment was carried out for the PTFE 0.45 microns membrane with sea water as feed. It is worth mentioning that the used seawater was neither filtered nor was it pre-treated. The hot feed side temperature was raised up to 60 ^{o}C, the cold side temperature was kept at 20 ^{o}C. While the feed flow rate was maintained about 3.65 L/min and coolant flow rate was about 3.7 L/min. The sea water collected from Arabian Sea near Corniche (KSA). The setup was allowed to run continuously for 48 hours without break.

In order to compare the membrane degradation subjected to two different kinds of feed are available; tap water and sea water. The fixed test conditions were taken as ; inlet feed temperature 60 ^{o}C, inlet coolant temperature 20 ^{o}C, feed flow rate 3.75 L/min, coolant flow rate 3.75 L/min, PTFE 0.45 m membrane. The experiment was allowed to run for 2 days and nights almost. The setup was run for 47 hours without any interruption. Figure 5.23

shows the flux variation with time for both experiments. For Sea water; in the start of experiment, the flux is maximum (32 kg/m^2-hr) which goes on decreasing until the experiment ended. The initial flux is 42.4 % as high as the flux on the termination of experiment.

Figure 5.23 shows the comparison between the flux values of two feed systems. it can be seen that as the time passes by the flux decreases. For both feed systems, as the experiment goes on running the flux decreases. Although the declining curve is more steeper in case of sea water as compared to tap water The declines in permeate flux may be attributed to membrane fouling and scaling. Fouling has been a pressing issue in MD. Running the system at constant feed flow rate for long period could leads to deposition of salts over membrane surface. This could result in increased concentration polarization effect that could lead to reduction in the permeate flux. On the opposite end, this feed flow rate (3.75 L/min) can also assist in removing salt particles deposited on the membrane active surface. This removal of salt particles can be governed to eddies and turbulences generated by the feed itself because of the meshed net. The reduction in flux is governed because of salt precipitation over the membrane surface which blocks the pore of membrane that retards the flux. Also salt precipitation over the membrane active surface generates salt concentration polarization. Although the feed flow rate is high enough to remove some salts from the membrane surface because of turbulences induced by meshed net

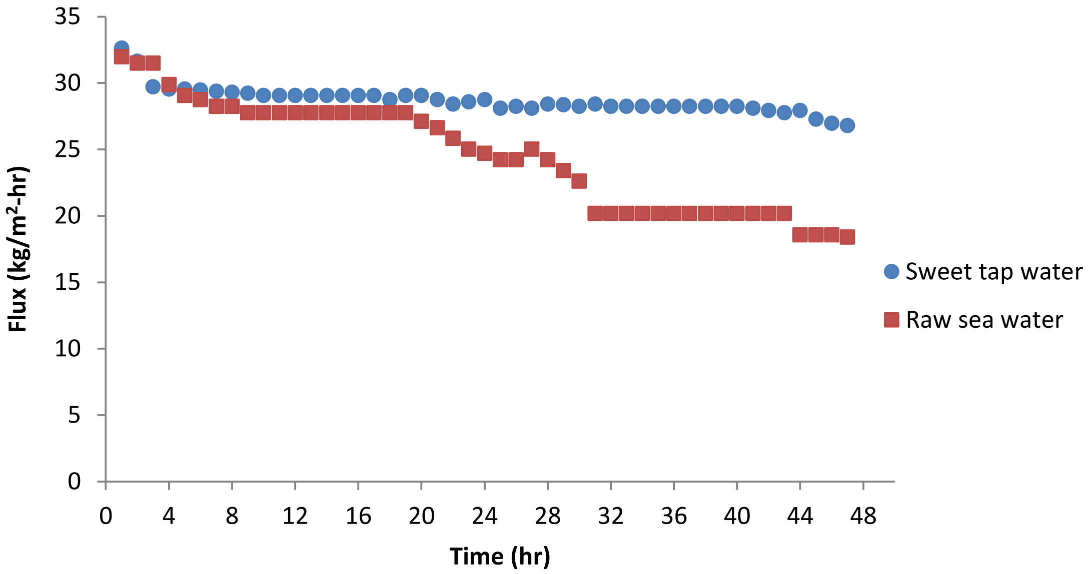

Figure 5. 23 Membrane degradation test flux VS time elapsed

The next figure 5.24 represents the similar idea but in terms of percentage flux. This figure depicts that as the time increases the percentage reduction in flux also increases. The important thing to note here is the magnitude of percentage reduction in flux. At the end of experiment, sea water system was subjected to 45 percent reduction in flux as compared to the flux at the start of experiment. But the tap water feed system was only supposed to have a reduction of 17 % at the termination of experiment.

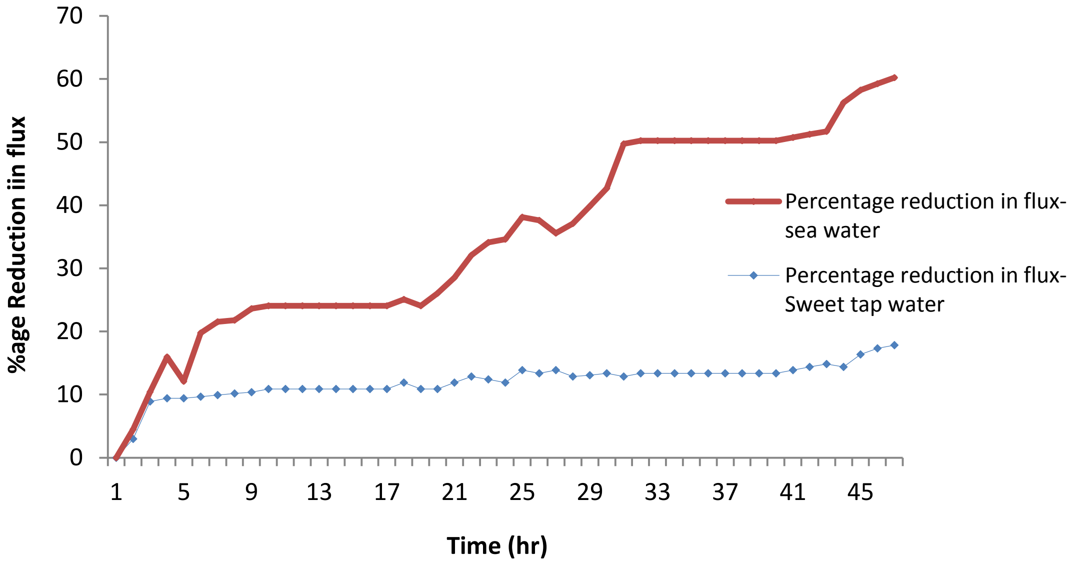

Figure 5. 24 Membrane degradation test; %age reduction in flux VS time elapsed

Quality of flux is defined in terms of TDS (totally dissolved solids). Another dimensionless parameter ‘salt rejection factor’ is also utilized to define the quality of flux. Salt rejection factor is given as

$$SRF = \frac{Feed\ Concentration - Permeate\ Concentration}{Feed\ Concentration} * 100$$

Salt rejection factor is a criterion to check that how much pure the permeate is, as compared to the intake feed .Discussing about the quality of permeate collected for longer run, figure 5.25 shows the salt rejection factor with time for which the experiment was continued for tap water and sea water. In the start of experiment the salt rejection factor is almost 98 % that goes on decreasing with the passage of time of tap water but for sea water SRF remains within 99.5 to 9.99 %.. For tap water in first four hours rejection factor slightly decreases, then remains constant for almost 16 hours then for another 12 hours similar trend is repeated then finally for 20 hours or so the quality of permeate remains constant. Still running after 47 hours we were able to have salt rejection factor of 96.5 %, giving percentage difference of 3.4 only, which shows that the quality of permeate is still good. But for sea water SRF remains within 99.99 % to 99.95 %. Most strikingly only 0.04% SRF change is observed for 48 hours long experiment which shows the consistency of DCMD technology for sea water. This reduction in salt rejection factor can be attributed to the feed salinity.

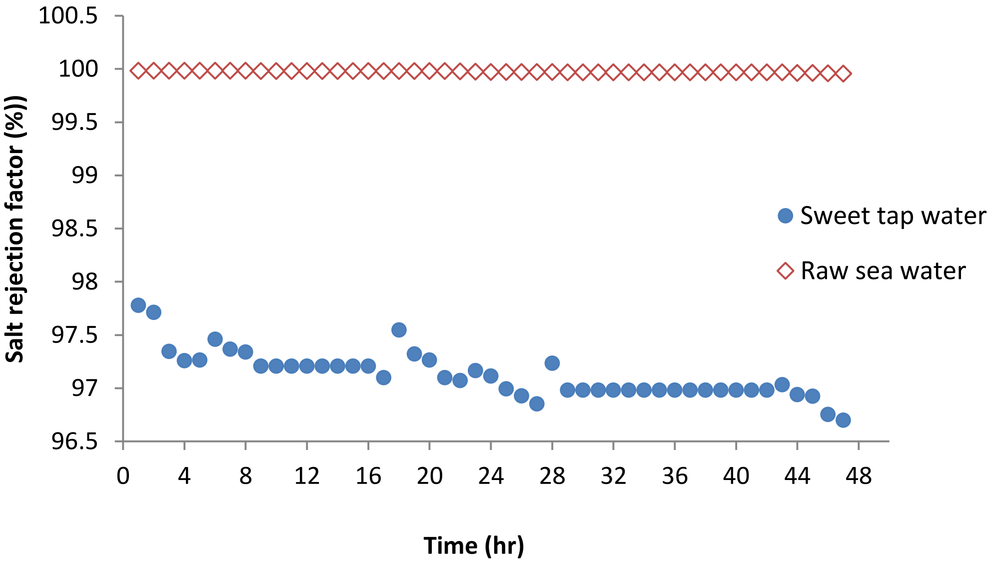

Figure 5. 25 Quality of permeate vs time elapsed

Figure 5.26 shows the TDS of permeate obtained from both feed systems. This is another representation to see the quality of permeate. TDS of permeate goes on increasing gradually with the passage of time for both of systems. But higher value of TDS of permeate for raw sea water shows that DCMD configurations performs well for sea water feed instead of tap water to be used as feed.

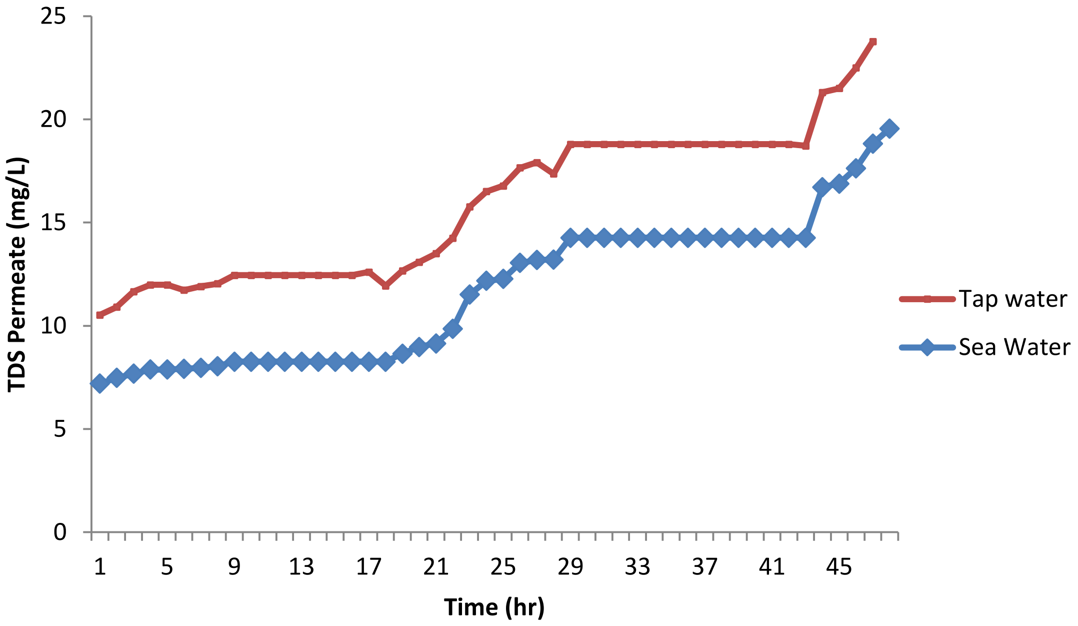

Figure 5. 26 TDS of permeate VS time elapsed

Figure 5.27 shows the TDS of feed (sea water) over the entire span of time of experiment. This figure is drawn to make sure that feed concentration remains within permissible limits for the whole experiment. With the passage of time quantity of feed was decreasing and the concentration was increasing slightly. There was a back up provided so that the level of feed may not fall below the operating limits. Make up feed was of the same characteristics as the original feed was being used and at the same temperature as of the original feed i.e. 43 g/L and 60 ^{o}C. TDS of feed remains between 43 and 46.4 g/L. In the first half of hours (up to 24 hours) only 5.8 % change in feed salinity was observed and until the termination of experiment this percentage was raised up to 7.8 %.

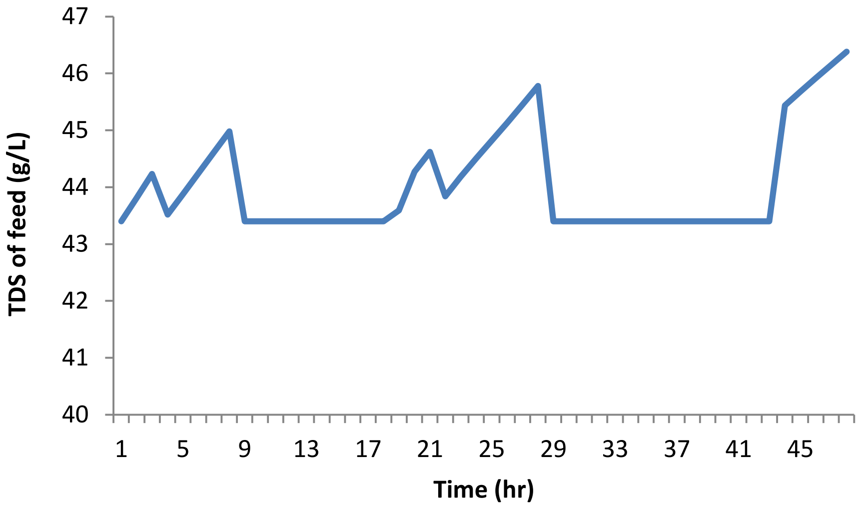

Figure 5. 27 TDS of feed (sea water) VS time elapsed

5.2 Comparative Study between DCMD and AGMD configurations

In this section, experimental comparison of the performance of two configurations, DCMD and AGMD will be made. In order to compare the performance of DCMD and AGMD systems with the same module design under the same operating and design conditions, all the experiments were done for DCMD system as done for AGMD by Lawal and Khalifa [108] . The operating conditions include, feed temperature, coolant temperature, feed salinity, feed flow rate, coolant flow rate. The design conditions include , the gap width (Fixed for AGMD design only), same module channel design with similar dimension, type of feed and coolant flow(Counter flow arrangements). In general, It was seen that DCMD gives more fluxes as compared to AGMD at all tested conditions. The reason behind this is the method of condensation. In AGMD, water vapours has to cross the air barriers then after coming intact with condensation plate, they are condensed. But in DCMD there is no air barrier, as vapours came out of membrane surface, flowing cold water mix them to condense.

5.2.1 Effect of feed temperature

The first parameter to be compared is the effect of inlet feed temperature. The operating conditions for this experiment were taken as; feed flow rate 3L/min, coolant flow rate 3 L/min, feed concentration of 75 mg/L, PTFE 0.45 µm membrane, inlet feed temperature was changed from 40 ^{o}C to 80 ^{o}C. For the whole experiment the coolant temperature was set to (T_{bc}) 15 ^{o}C -25 ^{o}C. Also for AGMD, the gap width was taken as 3mm. Figure 5.33 (a),(b),(c) shows the effect of inlet feed temperature on flux at different coolant temperature of 15,20 and 25 C respectively. It can be seen that increasing the inlet feed temperature increases the flux for both (DCMD, AGMD) configurations. Figure 2.25 (d) shows the effect of inlet feed temperature at various coolant temperatures collectively. After performing the experiment, it was perceived that increasing the inlet feed temperature increases the flux. The understandable reason behind this technique is the increase in difference of temperatures across the membrane that governs increase in difference of partial pressures over the surface. The observed increment in permeate flux due to increasing the transmembrane temperatures that enhances the driving force responsible for permeation

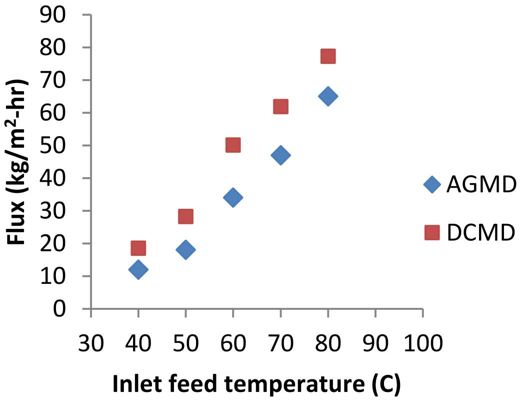

(a) At T_{bc}=15 C

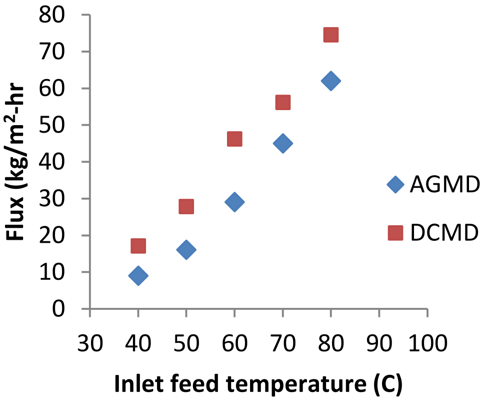

(b) At T_{bc}=20 C

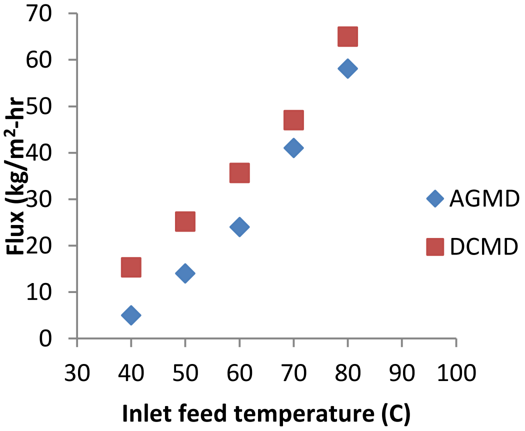

(c) At T_{bc}=25 C

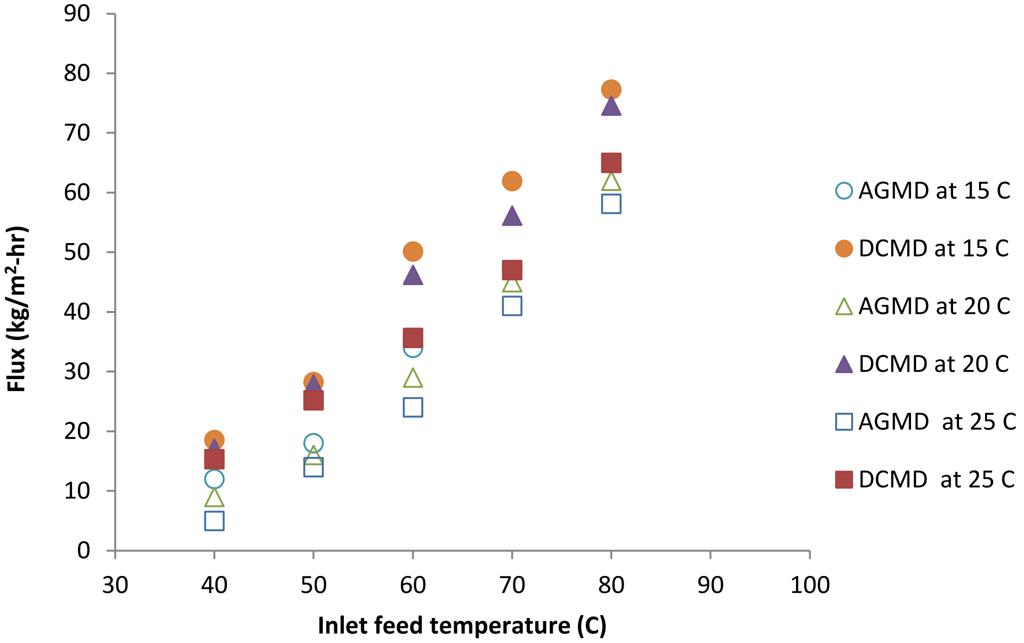

(d) Combined effect

Figure 5. 28 Effect of inlet feed temperature on flux; DCMD vs AGMD

Operating Conditions; Tbc=15 -25 C; Feed flow rate=3L/m, coolant flow rate=3L/m, feed concentration 75 mg/L,PTFE 0.45 microns,3mm gap for AGMD

5.2.2 Effect of coolant temperature

The second parameter to be compared was the effect of coolant temperature. The operating conditions for this experiment were taken as; feed flow rate 3L/min, coolant flow rate 3 L/min, feed concentration of 75 mg/L, PTFE 0.45 µm membrane, inlet feed temperature (T_f)was changed from 40 °C to 80 °C for three different sets of experiments . The experiment was carried out at three different coolant temperatures of 15 °C, 20 °C and 25 °C. Also for AGMD, the gap width was taken as 3mm. After performing the experiment, it was perceived that increasing the coolant temperature decreases the flux. The observed reduction in permeate flux due to increasing coolant temperature, and this reduction is best attributed to the reduction in transmembrane driving force responsible for permeation.

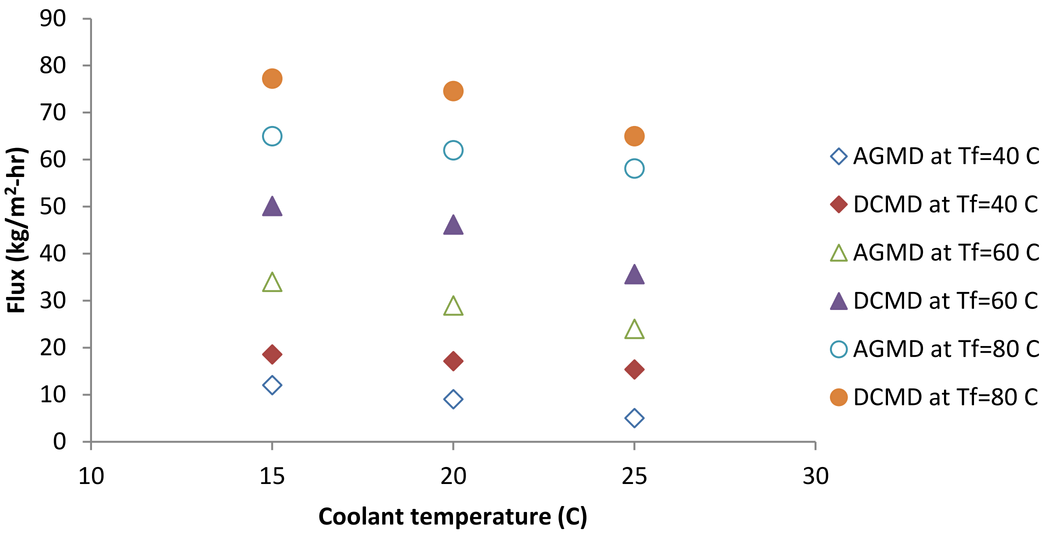

Figure 5. 29 Effect of inlet coolant temperature on flux; DCMD vs AGMD

Operating Conditions; T_f=40 -80 C; Feed flow rate=3L/min, coolant flow rate=3L/min, feed concentration 75 mg/L,PTFE 0.45 microns,3mm gap for AGMD

AGMD flux goes on decreasing as coolant temperature increases from 15 to 25 ^{o}C at every tested feed temperature (T_f). At 40 ^{o}C, percentage decrease of 58.3 is observed wile at 60 ^{o}C percentage decrease of 29.4 % is observed and at 80 ^{o}C percentage decrease of 10.6 is observed. So it can be said that coolant temperature is more effective at low feed temperature as compared to higher feed temperature. For DCMD, flux goes on decreasing as coolant temperature increases from 15 to 25 ^{o}C at every tested feed temperature (T_f). At 40 ^{o}C, percentage decrease of 16.3 is observed wile at 60 ^{o}C percentage decrease of 28.9 % is observed and at 80 ^{o}C percentage decrease of 15.93 is observed. So it can be said that coolant temperature yields maximum percentage reduction in flux at 60 and is not as much effective as in AGMD configuration.

5.2.3 Effect of feed flow rate

The third parameter to be investigated for the performance of the two configurations was the effect of feed flow rate. The operating conditions for this experiment are taken as; feed temperature 70 °C, coolant temperature 20 °C, coolant flow rate 3 L/min, feed concentration of 75 mg/L, PTFE 0.45 µm membrane, the gap width was taken as 3mm for AGMD. The experiment shows that increasing the feed flow rate increases the flux for both configurations either DCMD or AGMD. DCMD configuration gives more flux as compared to AGMD configuration at all tested conditions of flow rate; (2.5 L/min, 3.65 L/min and 4.65L/min). In terms of percentage increase in flux, DCMD yields 13.8 % while AGMD yields 9.7 % with reference fluxes at flow rate of 2.5 L/min. When the feed flow rate increases (keeping all other operating parameters constant), it increases Reynolds number, that generates more turbulences in the channel that assist evaporation process by decreasing the thermal boundary layer over the membrane surface. The observed rise in permeate flux as a result of increasing feed flow rate is due to reduction in temperature and concentration polarization effects. Increasing the feed flow rate encourages turbulence level in the flow and increases heat transfer coefficient of the feed boundary layer. Besides, increasing the feed flow rate also reduce water resistance time in the feed channels and make the feed bulk temperature in the feed channels closer to the feed inlet temperature.

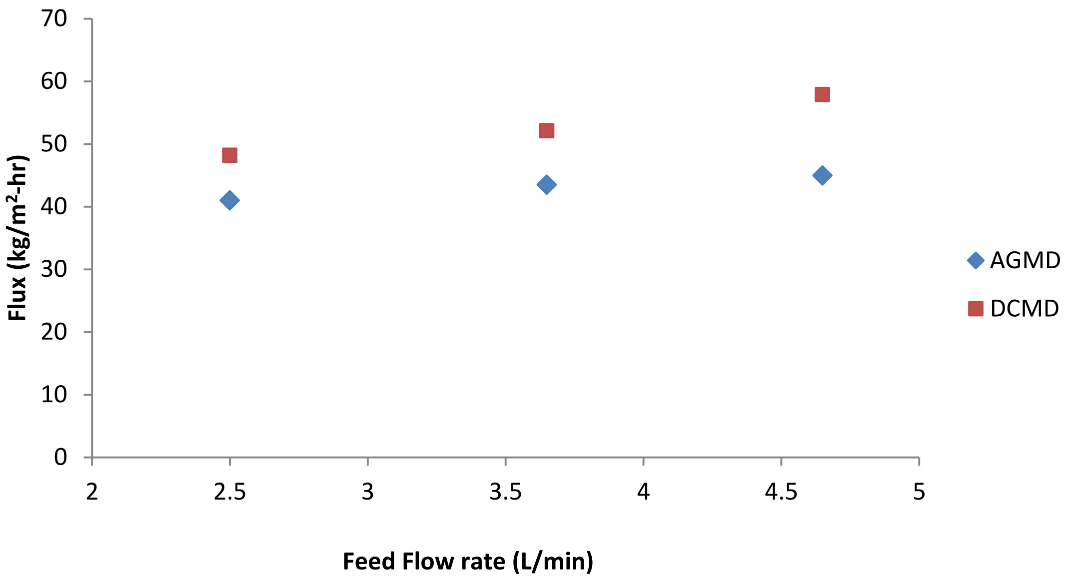

Figure 5. 30 Effect of feed flow rate on flux; DCMD vs AGMD

Operating Conditions; T_{bf}=70 °C; T_{bc}=20 °C coolant flow rate=3L/m, feed concentration 75 mg/L,PTFE 0.45 microns,3mm gap for AGMD

5.2.4 Effect of coolant flow rate

The other parameter to be analyzed was the effect of coolant flow rate. The fixed test conditions are; feed temperature 80 °C, coolant temperature 20 °C, feed flow rate 3 L/min, feed concentration 75 mg/L, PTFE membrane with pore size 0.45 microns,3mm gap for AGMD and coolant flow rate was changed from 1 to 3.5 L/min gradually for the whole of experiment with tested conditions of operations are 1L/min, 2L/min, 3L/min, and 3.5L/min. However, little or no effect were observed in flux when we increase the coolant flow rate from 1 L/min to 3.5 L/min as shown in fig. 5.36. Although the change is not much significant but the trend is rising in both configurations. Gradual increase can be observed in flux for DCMD configuration, (Only percentage increase in flux is only 6.3 %) but for AGMD this increment seems more lessened (only 1.98 % increment in flux). So it can be deduced that coolant flow rate is not very much significant for flux in both configurations. But if comparing the performances of both systems, then in DCMD coolant flow rate plays more important role as compared to AGMD. The reason for not being much significant is that the feed is the main source from which the vapor flux is to be produced rather coolant. So the coolant flow rate is not much more important in order to produce more flux than feed flow rate. We must understand that increasing cooling water flow rate mean increasing the cooling water heat transfer coefficient of the cooling surface. It is obvious from figure 5.36 that coolant flow rate has negligible effect on flux in AGMD. The effect of coolant flow rate is meaningless as far as we have minimum flow to conduct the heat from the condensate surface.

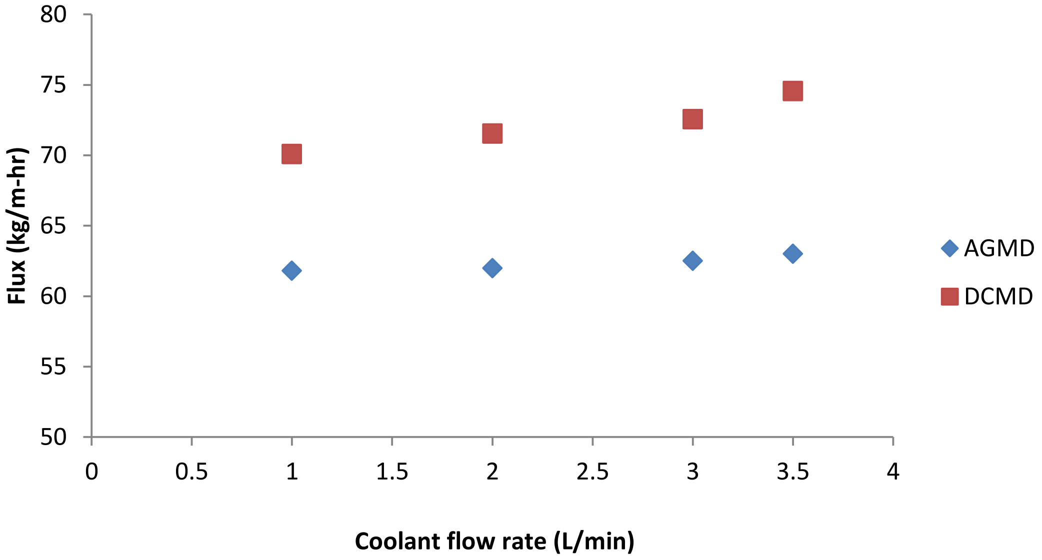

Figure 5. 31 Effect of coolant flow rate on flux; DCMD vs AGMD

Operating Conditions; T_f=70 ºC; T_c=20 ºC coolant flow rate=3L/m, feed concentration 75 mg/L,PTFE 0.45 microns,3mm gap for AGMD

5.2.5 Effect of membrane pore size

Membrane pore size is an important property of the membrane morphology. In order to investigate the effect of membrane pore size on flux, two different pore sized of PTFE membrane were tested, PTFE 0.45 µm, PTFE 0.22 µm, other properties like tortuosity, membrane thickness, water contact angle etc. are same. The fixed test conditions for the experiment were; coolant temperature 20 ^{o}C, feed flow rate 3 L/min, coolant flow rate 3L/min, feed concentration 75 mg/L,PTFE 0.45 microns,3mm gap for AGMD, and feed temperature was varied from 40 ^{o}C to 80 ^{o}C for the whole experiment. For 0.45 microns pore size PTFE the flux is higher for membrane as compared to 0.22 microns irrespective of configuration either DCMD or AGMD. Although it seems that the effect of pore size is more prominent at higher feed temperature as compared to lower feed temperature, but the percentage difference in flux is 56.49% at feed temperature of 40 ^{o}C and at higher feed temperature 80 ^{o}C this percentage increase in flux is 20 %. The reason behind this is that for bigger size of pore, the flux permeation is more as compared to small pore size. Although the air resistance inside the pores is larger in bigger size membrane, but the driving force between the two surfaces causes the more evaporation to occur that governs more flux permeation through pores. This can also be observed that smaller pore sizes can lead to more molecule-wall collision that can increase the resistance for permeation, but in larger pore size the resistance can be reduced.

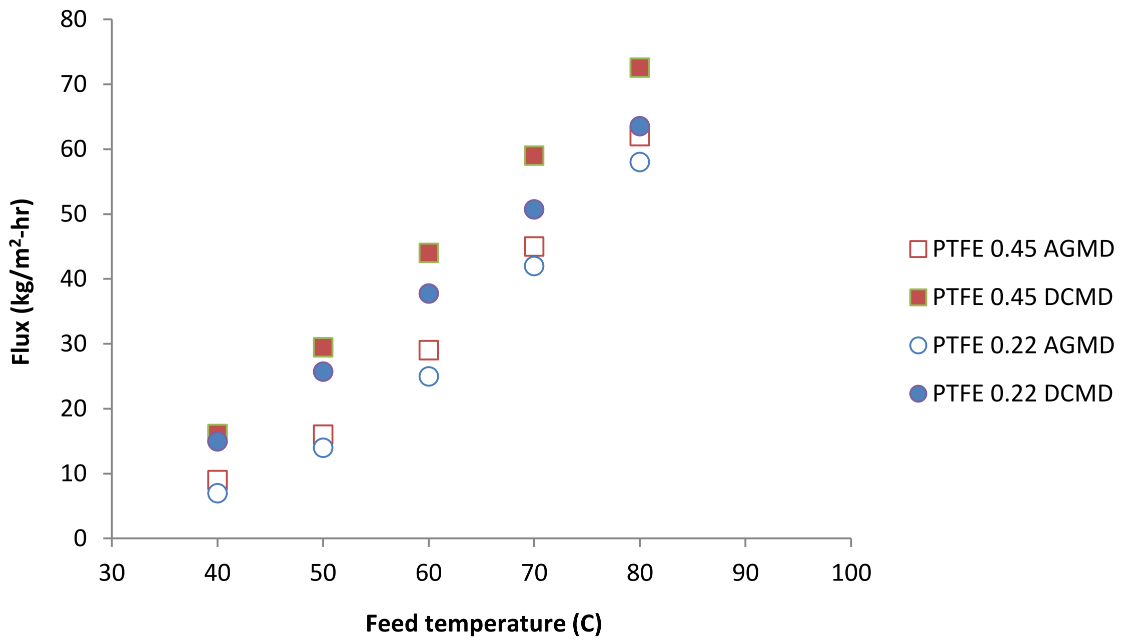

Figure 5. 32 Effect of membrane pore size on flux; DCMD vs AGMD

Operating Conditions; T_c=20 ^{o}C feed flow rate 3 L/min, coolant flow rate=3L/min, feed concentration 75 mg/L,PTFE 0.45 microns,3mm gap for AGMD

CHAPTER 6

COMPARATIVE STUDY BETWEEN WATER GAP AND AIR GAP CONFIGURATIONS

6.1 introduction

In this chapter experimental comparison of the performances between two other MD configurations will be made. These configurations are Water Gap Membrane Distillation (WGMD) and Air Gap Membrane Distillation AGMD. In order to compare the performance of WGMD and AGMD systems with the same module design 2 channel HDPE as shown in figure 4.8 (But different from DCMD module that is 3 channel Plexiglas) under the same operating and design conditions. The operating conditions include, feed temperature, coolant temperature, different membrane materials but with same pore sizes, and same membranes with different pore sizes. The design conditions include, the gap width, same module channel design with similar dimension, type of feed and coolant flow(Counter flow arrangements, dead end flow directions). In general, It was seen that WGMD gives more fluxes as compared to AGMD at all tested conditions. The reason behind this is the method of condensation. In AGMD, water vapours have to cross the air barriers then after coming intact with condensation plate, they are condensed. But in WGMD there is no air barrier, stagnant layer of condensed vapour make condensation quicker and efficient as shown in fig 4.6.

6.2 Effect of feed temperature on Flux; WGMD and AGMD

Fig 6.1 shows the effect of feed temperature over the permeate flux. Feed temperature is one of the most important parameter in MD technologies. In order to investigate the effect of inlet feed temperature on water gap membrane distillation flux and air gap membrane distillation flux, this experiment was conducted. The effect of feed water temperature on the permeate flux is examined for air gap design first and then system was allowed to run until the cavity is filled by distilled water and extra pure water starts coming out of the permeate cavity. The feed temperature is varied from 50 to 90 ^{o}C and the coolant temperature was selected 5 to 24 ^{o}C. The experiment was run with the following conditions; 2 mm gap width (Fluids filling the gap can be water or air), tap water of 140 mg/L , with flow rate of 1.5 L/min and coolant flow rate of 2L/min was employed. The membrane used for this test was PTFE membrane with pore size 0.45 microns. Coolant temperature was fixed at 5 ^{o}C, 15 ^{o}C and 24 ^{o}C. it is quite obvious from the experiments that increasing the feed temperature increases the permeate flux, for both configurations WGMD and AGMD. But the rise is exponential in AGMD with increasing feed temperature, whereas in WGMD the rise seems curvilinear with high inclination. When cumulative plot is drawn for the flux, it is very clear that WGMD flux is more than AGMD flux at every feed and coolant temperature. The rise in flux for WGMD can be attributed to the media filling the gap. In AGMD, this medium is air, and in WGMD it is distilled water which is stagnant. Air offers more resistance to the water vapours to be condensed while water assists condensation process. So air barrier is the basic reason behind the reduction in flux for AGMD as compared to WGMD.

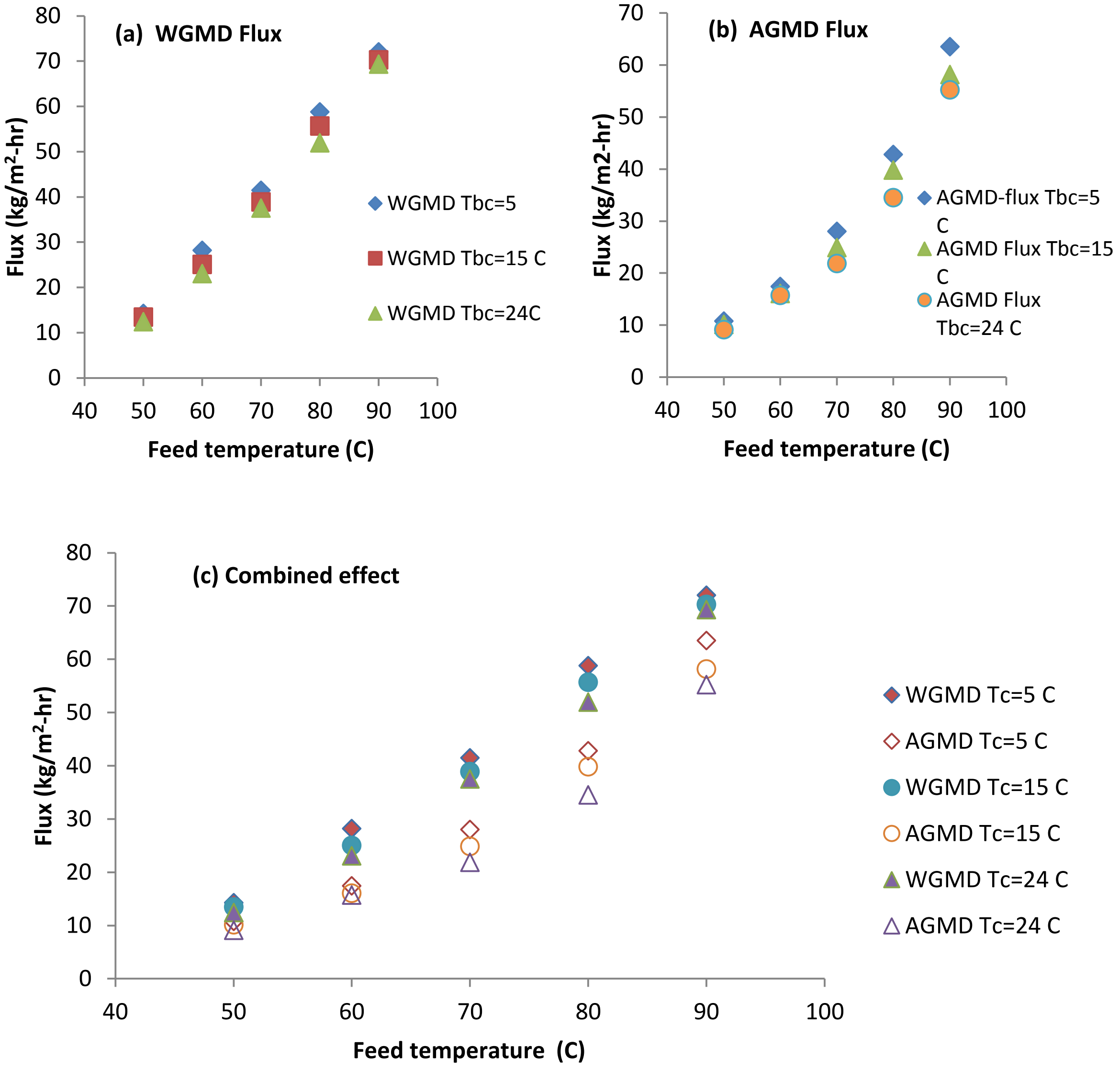

Figure 6. 1 Effect of inlet feed temperature on flux ; WGMD and AGMD

Operating Conditions: PTFE 0.45 µm , feed flow rate 1.5l/m, coolant flow rate 2L/m, feed concentration 140 mg/L, gap width 2mm

The importance of feed temperature on system flux can be observed as; WGMD yields 435 % increase in flux at coolant temperature of 5 ^{o}C with reference value of flux at feed temperature 50 ^{o}C. AGMD yields 535 % increase in flux at coolant temperature of 5 ^{o}C with reference value of flux at feed temperature 50 ^{o}C.

6.3 Effect of coolant temperature on Flux; WGMD and AGMD

Coolant temperature is another paremeter to check the performance of WGMD and AGMD configurations. Fig no. 6.2 represents the effect of bulk coolant temperautre over the flux for both configurations. The operating conditions for the experiment were taken as follows; feed flow rate 1.5 L/min, coolant flow rate 2 L/min, gap width 2 mm, tap water of 140 mg/L was used as feed. Different feed temperatures of 50 ^{o}C,70^{o}C and 70^{o}C are considered. The results show that for all tested feed temperatures, (50 ^{o}C,70 ^{o}C,90 ^{o}C), the flux decreases by increasing the coolant temperature for both configurations. The reduction in flux is because of incresing the coolant temperature, which reduces the transmembrane temperature difference, or alternatively decreases the difference of vapour partial pressure across the membrane surface. From the experimental results it seems that inlet coolant temperature is not much significant at any feed temperature for any configuration. For AGMD; percentage increase in flux is 18.3 at feed temperature of 50 ^{o}C, 12.79 ^{o}C at 70 ,and 15 at 90 ^{o}C refrence to the flux at 24 ^{o}C of coolant temperature. For WGMD; percentage increase in flux is 14.8 at feed temperature of 50 ^{o}C, 10.56 at 70 ^{o}C and only 3.9 at 90 ^{o}C refrence to the flux at 24 ^{o}C of coolant temperature. Maximum of 18.3 % change in flux is observed (for AGMD) at 50 ^{o}C and minimum of 3.9 % is observed for WGMD at 90 ^{o}C feed temperature.

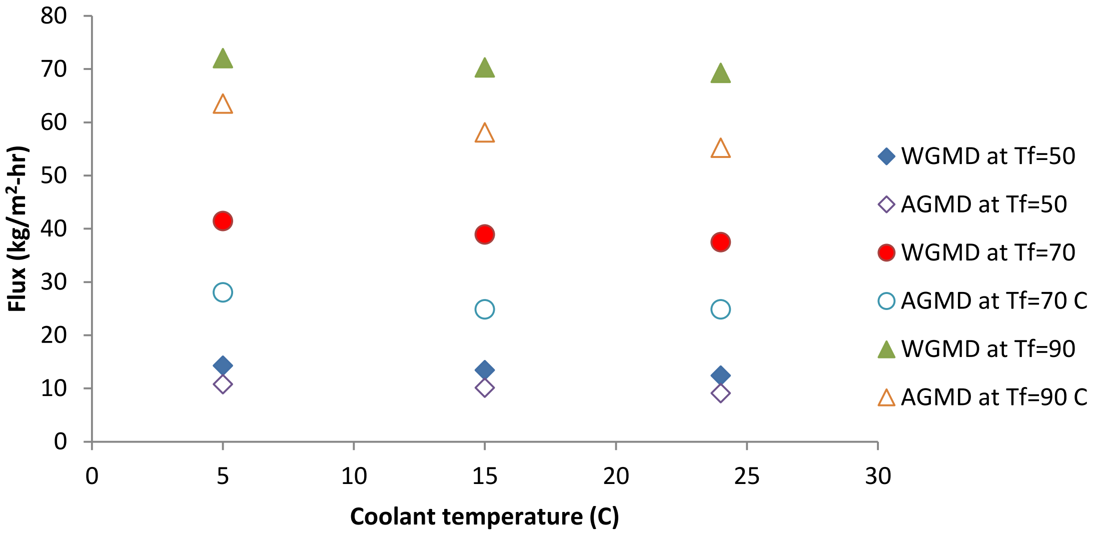

Figure 6. 2 Effect of coolant temperature on flux ; WGMD and AGMD

Operating Conditions: PTFE 0.45 µm , feed flow rate 1.5l/m, coolant flow rate 2L/m, feed concentration 140 mg/L, gap width 2mm

6.4 Effect of membrane material on flux;WGMD and AGMD

Membrane material is an important parameter in MD operation. In our experimentation, two kinds of membrane mateial were tested; Polytetraflouroethylene (PTFE) and polyvinyl diflouride (PVDF). Both membranes have same pore size of 0.45µm. The experiment was conducted for the following conditions of operation; inlet coolant temperature was decreased upto 5 ^{o}C, feed flow rate of 1.5 L/min, coolant flow rate 2 L/min, and tap water of concentration of 140mg/L was used as feed, provided by a gap width of 4 mm filled by air in AGMD and by distilled water in WGMD. Firstly WGMD were tested followed by AGMD configuration. For WGMD, it is clearly seen in fig 6.3 that PTFE gives more flux as compared to PVDF at every feed temperature. The same trend can be seen for AGMD, but in AGMD, the effect of membrane material is more prominent at high feed temperature instead of low feed temperatures. Figure 6.3 shows that PTFE membrane produces higher perameate flux as compared to PVDF in both configurations WGMD and AGMD respectively at all tested temperatures. The enhanced flux in PTFE membrane can be attributed to the following reasons; high hydrophobicity of PTFE as compared to PVDF, more void volume fraction in PTFE as compared to PVDF, less thickness in PTFE as compared to PVDF. All these features coming together gives more flux in PTFE as compared to PVDF. Comparing the performances of both membranes (PTFE & PVDF), PTFE seems more effective than PVDF irrespective of MD configuration. For WGMD configuration; PTFE 0.45 gives 296 % increase in flux as compared to flux at 50 ^{o}C, PVDF 0.45 gives 862 % increase in flux compared to flux at 50 ^{o}C. But for AGMD configuration; PTFE 0.45 gives 477 % increase in flux as compared to flux at 50 ^{o}C, PVDF 0.45 gives 433 % increase in flux compared to flux at 50 ^{o}C. So it seems that PTFE 0.45 yields higher values of flux but in terms of percentage PVDF 0.45 gives maximum value for WGMD configuration.

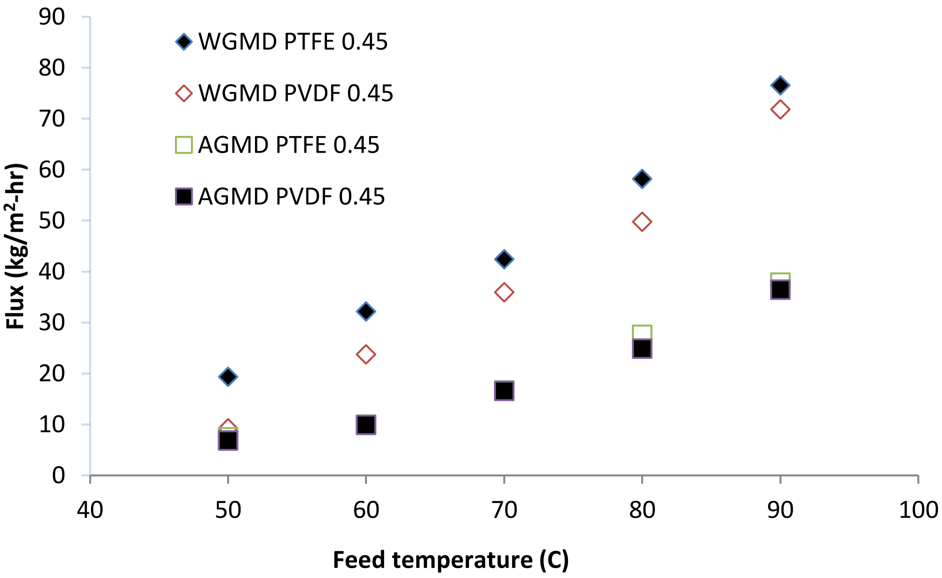

Figure 6. 3 Effect of membrane material on flux ; WGMD and AGMD

Operating Conditions: Tc=5 ^{o}C, Feed flow rate 1.5L/min, coolant flow rate 2L/min, feed concentration 140 mg/L, gap width 4mm

6.5 Effect of membrane pore size on flux; WGMD and AGMD

In order to see the effect of membrane pore size, two membrane of similar properties were tested. These PTFE membranes have all similar properties (Hydrophobicity, porosity, thickness) only differ in pore size as can be seen in table 4.2. From fig 6.4 , it can be predicted that increaseing the feed temperature increases the permeate flux .The operating conditions for the experiment were taken as; Coolant temperature (T_c) 24 ^{o}C, feed flow rate is 1.5 L/min, coolant flow rate 2 L/min, tap water of salinity of 140 mg/L, with a gap width of 4mm and then the system was run for a range of feed temperature of 50 ^{o}C to 90 ^{o}C. Figure 6.4 shows that for both configurations (WGMD and AGMD), increasing the feed temperature increases the flux. It also shows that membrane with the bigger pore size gives more flux in both types of configurations which means membrane with pore size of 0.45 microns yields more system flux as compared to membrane with pore size of 0.22 microns independent of the system configurataion. It can also be observed that the effect of pore size if more prominent at low feed temperature (60 ^{o}C) instead of higher feed temperature (90 ^{o}C) in both systems Although bigger pore size offers more resistance to the vapours to pass through because of air resistance existing between the pores but it also changes the type of diffusion from knudsen to molecular. But in theoretical modelling of DCMD system , combined knudsen and molecular diffusion was taken into accout.

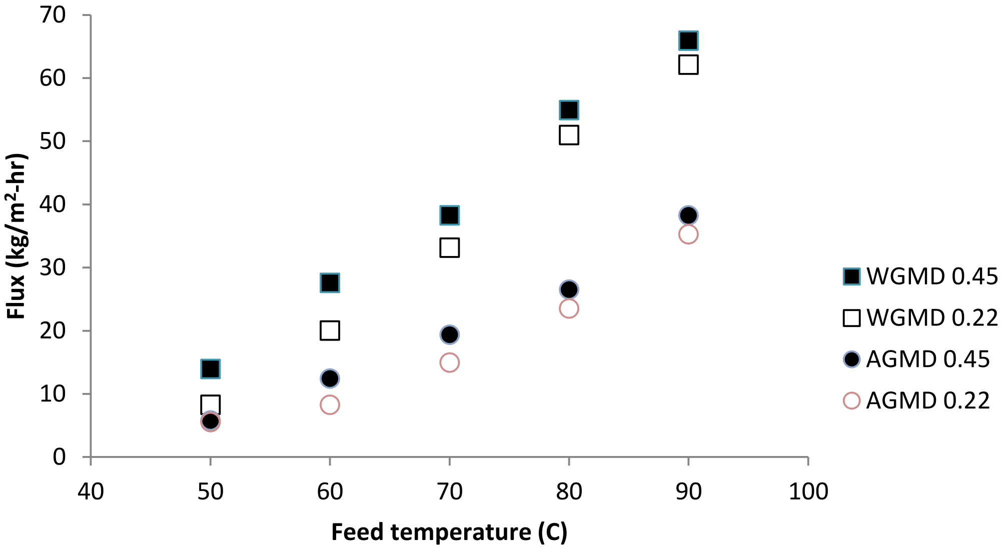

Figure 6. 4 Effect of membrane pore size on flux

Operating Conditions: Coolant temperature 24 °C, Feed flow rate 1.5L/m, coolant flow rate 2L/m, feed salinity 140mg/L,4mm gap width

6.6 Effect of gap width on flux; WGMD and AGMD

The distance between perforated supporting plate and the condensation plate is treated as gap width as can be seen in fig. 4.6. This gap width is an important design parameter in the evaluating the performance of WGMD and AGMD configurations. In order to investigate the influence of gap width on the system flux, an experiment was conducted for a series of gap widths; 2mm, 4mm, 6mm, 8mm and 12 mm. The operating conditions are; PTFE membrane of pore size of 0.45 microns, coolant temperature was fixed at 24 °C, feed flow rate 1.5L/min, coolant flow rate 2 L/min, feed salinity 140 mg/L. The gap width was changed by changing the gap gasket as shown in fig. 4.6.Figure 6.5 (a),(b) shows the effect of gap width of system flux for AGMD and WGMD respectively. It is visualized that increasing the gap width decreases the flux very effectively in AGMD but in WGMD the decrease is not very prominent. In AGMD flux is showing exponential trend with the increase in feed temperature at lower value of gap width. But in WGMD, it can be seen that the resulting curve (Fig 6.5 b) can be divided into two regions; Region 1 where feed temperature varies from 50 ^{o}C to 70 ^{o}C and a curve facing down is generated, in region 2 feed temperature varies from 70 ^{o}C to 90 ^{o}C and a curve facing up is generated. Figure 6.5 (c) shows the cumulative results of (a) and (b). Comparison shows WGMD gives more system flux as compared to AGMD. It can also be deduced that AGMD configuration becomes very efficient at lower gap width (2mm) by generating more flux as compared to higher gap width.

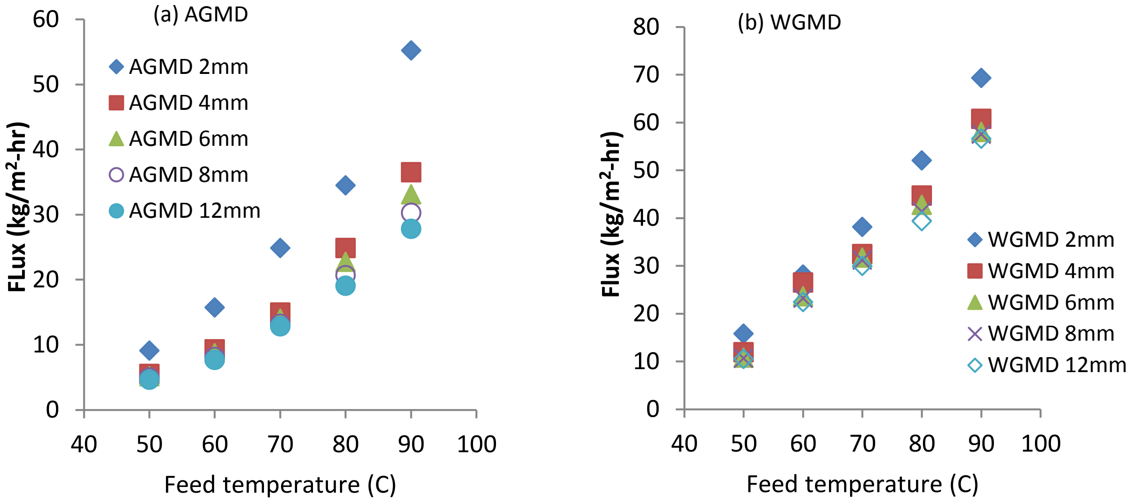

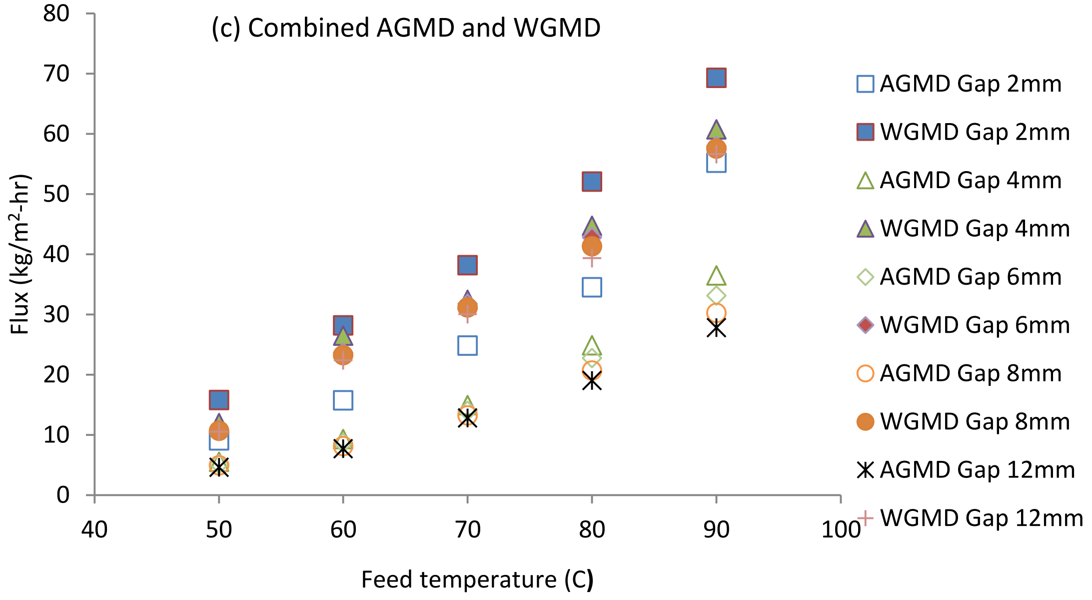

Figure 6. 5 Effect of gap width on flux; WGMD and AGMD

Operating Conditions: PTFE 0.45 µm, bulk coolant temp 24 C, feed flow rate 1.5L/m, coolant flow rate 2L/m, feed concentration 140mg/L

Figure 6.6 shows the effect of gap width on permeate flux for WGMD and AGMD configurations. It can be seen that increasing the gap width decreases the permeate flux in both configurations. In WGMD, the flux trend seems gradually decreasing and then becomes quite constant. Increasing the gap width from 2mm to 4mm reduces the flux by 12.31 % and then decreases by 6.79 % as we increase the gap width from 4 mm to 12 mm. So it seems that permeate flux is not much sensitive to gap width in WGMD. Now coming to AGMD, a more steeper curve can be seen, which means the gap width is more important in AGMD. By increasing the gap width from 2 mm to 12mm , reduces the flux by 58.74 % which drastically renders the performance of AGMD configuration. So the conlusion from this experiments is that the gap width is more important in AGMD as compared to WGMD. The basic reason is that air offers more resistance to water vapours to be condensed as compared to distilled water which is present in the gap. The more gap offers more resistance for the vapours to be condensed over the cooling plate or condensation plate Water has four times more specfic heat(4.18 kJ/kg-K) [110] than air which means it requires more heat to change its temperature by unit degree as compared to air. Air gets heatedquicker than water, so it decreases the efficiency of condensation process. Air molecules don't allow the vapors to pass through the gap and it decreases the flux.Another parameter is thermal conductivity of the water and air. Air has 0.0092 W/m-K and water has 0.6 W/m-K [110] which means water will require to heat to change its temperature as compared to air.

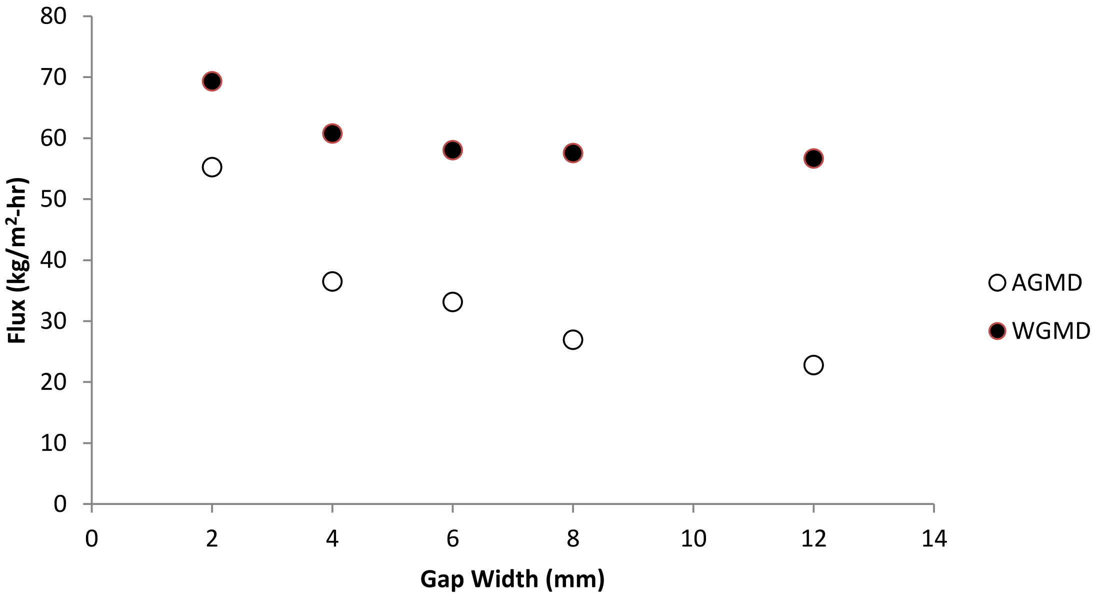

Figure 6. 6 Effect of gap width on flux WGMD and AGMD

Operating Conditions: PTFE 0.45 µm, inlet feed temperature 90 C, bulk coolant temp 24 C, feed flow rate 1.5L/m, coolant flow rate 2L/m, feed concentration 140mg/L, gap width 2mm,4mm,6mm,8mm and 12mm

CHAPTER 7

ENERGY ANALYSIS

7.1 Analysis of DCMD

In this section, comprehensive energy and exergy analysis of DCMD system is discussed. Energy analysis was done on experimental basis but exergy analysis was done theoretically. Energy analysis include performance parameters like thermal efficiency, gain output ratio while exergy analysis includes the effect of some operating parameters on exergy destruction.

7.1.1 Thermal efficiency

As the inlet feed temperature is increasing, it increases the partial pressure of water vapour in the feed side that enhances the difference of partial pressure across the membrane sides, which exaggerates the evaporation process, causing more vapor molecules to permeate through the membrane pores. Increasing inlet feed temperature increases evaporative efficiency as shown in fig. 7.1.

Thermal or evaporative efficiency is the ratio of latent heat of vaporization across the membrane surface to the sum of conductive and evaporative heat through membrane as can be seen in the following equation

$$\%EE = \left(\frac{Q_v}{Q_m}\right)*100 = \left(\frac{J_w * \Delta H_v}{U*(T_{b,f} - T_{b,p})}*100\right) \tag{48}$$

From figure 7.1 it can be seen that increasing inlet feed temperature increases the evaporative efficiency because of flux increasing that enlarges the numerator, in result of which efficiency increases. Now discussing the effect of cold permeate temperature, it can be seen that at lower permeate temperature, the efficiency is low because of the low flux generation or lower value of latent heat of vaporization associated with the vapour molecules. An interesting information can be taken from fig 7.1 that evaporative efficiency is higher at higher cold permeate temperature, and vice versa. Referring to fig 5.3 it can be stated that flux is higher at low cold permeate temperature.

In terms of percentage change it can be observed that at 40 ^{o}C, percentage change in evaporative efficiency is 12.63 % when the permeate temperature is changed from 5 ^{o}C to 25 ^{o}C, but as the inlet feed temperature increases, this percentage increase diminishes, and at 90 ^{o}C, this percentage increases only left with 2 % only. So from this statistical analysis, one can result that operating the system at higher feed temperature is not highly affected by inlet coolant temperature, but if the system is running at low inlet feed temperature , higher inlet coolant temperature is preferred for higher evaporative efficiency.

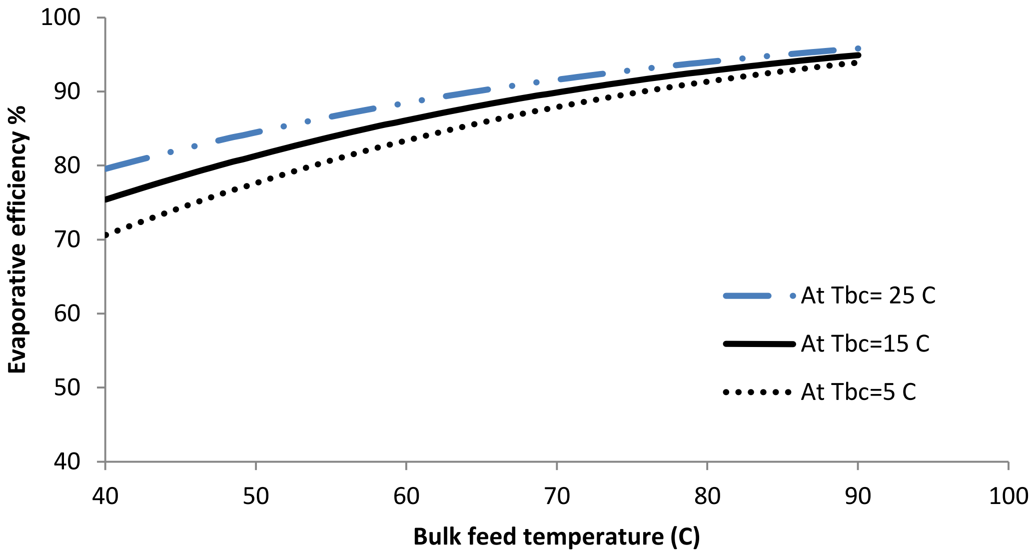

Figure 7. 1 Effect of feed temperature on evaporative efficiency

Operating Conditions: PTFE 0.45 µm, feed flow rate 4.65 L/m, coolant flow rate 3.65 L/m, feed concentration 140 mg/L, coolant temperature T_{bc}=5,15,25 °C

7.1.2 Gain Output Ratio

Gain output ratio (GOR) is another measure of performance of the DCMD system. It is the ratio of latent heat of vaporization of distillate produced to the heat input to the system in the form of heat [114].For any system GOR is defined as [115]

$$GOR = \frac{m_d * \Delta H_v}{m_f * c_{pf} * \Delta T_{\text{mod}ule}} \tag{49}$$

Where

m_d is the mass of permeate produced (kg/s)

ΔH_v is the latent heat of vaporization (J/kg)

m_f is mass flow rate of feed (kg/s)

C_{pf} is the specific heat of feed (J/kg-K)

ΔT_{module} is the temperature difference between inlet and outlet of hot side of module.(°C or K)

The operating conditions for the experiment can be seen below fig 7.2.

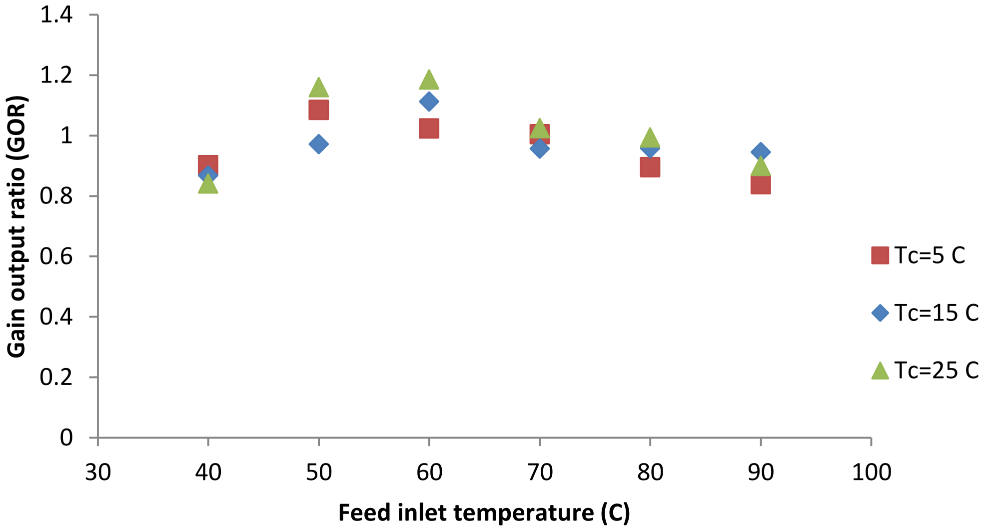

Figure 7. 2 Effect of feed temperature on GOR for DCMD

Operating conditions: PTFE membrane of 0.45 µm, feed flow rate 4.65 L/min, cold permeate flow rate 3.65 L/min, feed salinity 2 g/L, and selected cold permeate temperature T_c=5,15,25 °C.

Figure 7.2 shows the effect of feed inlet temperature on the gain output ratio at different cold permeate temperatures. It is observed that increasing the inlet feed temperature up to 60 °C, increases the gain output ratio of the module but after that gain output ratio decreases until feed inlet temperature reaches up to 90 °C. Experiments shows that working at higher cold permeate temperature results in higher value of GOR than at lower cold permeate temperature. GOR remains in between 0.8 and 1.2. Maximum value of GOR was obtained at 25 ^{o}C cold permeate temperature is 1.2. But Summers et. Al. [111]suggested GOR values of 0.25-4.5 subjected to a very long membrane of 100 m and very low mass flow rate.

7.1.3 Exergy analysis

Exergy analysis is an important parameter to analyse the performance of thermal systems [112]. Exergy of an open or closed system is an intensive property which depicts maximum obtainable work from the system per unit mass. More briefly exergy was defined by Molinari et al [113] as the maximum useful work a system can do when it passed from an actual state to the reference state where it is in equilibrium with the surrounding state. Friction is the basic cause of degradation and this degradation is represented in terms of heat dissipation. Dissipation of heat caused by irreversibilities, which represents entropy generation and second law of thermodynamics (Exergy analysis) is to be considered. Anergy and Exergy are the two parts of energy, which are in degradable and useful form [114]. In an open system exergy of system depends upon three parameters; temperature, pressure, and concentration gradient [112, 113, 115] . The exergy (Ex) of an open system can be written as sum of all exergetic terms [115]

$$Ex = Ex^{Temperature} + Ex^{Pressuree} + Ex^{concentration} \tag{50}$$

As DCMD system was run with sea water as feed with concentration of 43000 ppm and on atmospheric pressure so exergy destruction because of pressure term can be nullified, only the effect of concentration and temperature will stay there. Exergy destruction because of temperature gradient and concentration gradient can be given as [112, 116];

$$Ex^{Temperature} = m \times cp \times \left[(T - To) - To\ ln\left(\frac{T}{To}\right)\right] \tag{51}$$

$$Ex^{concentration} = m \times [n_{solv} \times R \times To \times ln(x_{solve})] \qquad (52)$$

Where; T_o is the reference temperature, m is mass flow rate (feed or cold permeate), c_p is specific heat of the fluid at the given temperature, n_{solve} is chemical potential differences. Exergetic analysis was made by using Engineering Equation Solver software V9.698. The SeaWater.lib built-in function in EES library provides thermophysical property data for sea water. This library was developed by John Lienhard and his co-workers at MIT [117]. In this way exergy of the four streams was found out by computation and then net exergy was calculated by the following expression [112, 116];

$$Ex_{destroyed} = \Sigma Ex_{in} - \Sigma Ex_{out} \qquad (53)$$

And inlet exergy is produced because of two inlet streams which are feed and cold permeate in and can be given as;

$$\Sigma Ex_{in} = Ex_{feed,in} + Ex_{cold\ permeate,in} \qquad (54)$$

And outlet exergy is produced because of two outlet streams which are feed and cold permeate out and can be given as;

$$\Sigma Ex_{out} = Ex_{feed,out} + Ex_{cold\ permeate,out} \qquad (55)$$

Figure 7.3 shows the effect of feed flow rate on exergy destroyed. As it can be seen that increasing the feed flow rate, increases the exergy destruction linearly. The trend is linear because mass flow rate (or feed flow rate) is a linear function of exergy destruction as can be seen in equation 51 and 52. It happens because the increase in feed flow rate increases the mass flow rate, which leads to more friction losses that increases the heat loss,, due to which exergy destroyed increases and entropy generation increases.

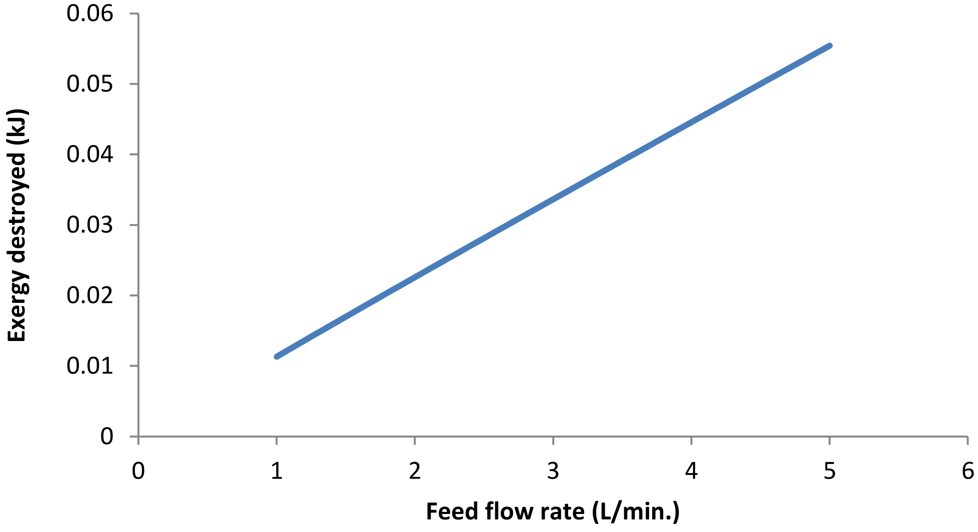

Figure 7. 3 Effect of feed flow rate on exergy destroyed

Operating Conditions: PTFE 0.45 microns, inlet feed temperature 50 ºC, cold permeate temperature 25 ºC, coolant flow rate 3.65 L/m , feed salinity 140 mg/L,

Figure 7.4 represents the effect of inlet feed temperature on the exergy destruction. The trend is non-linear and can be justified by equation 51. As higher inlet temperature results in more heat transfer losses, which governs more irreversibilities that results in more entropy generation,

Furthermore, it can also be seen that increasing the feed temperature increases the exergy destruction exponentially. The exergy destruction equation 51 which has logarithmic factor that causes the exergy to be changed exponentially.

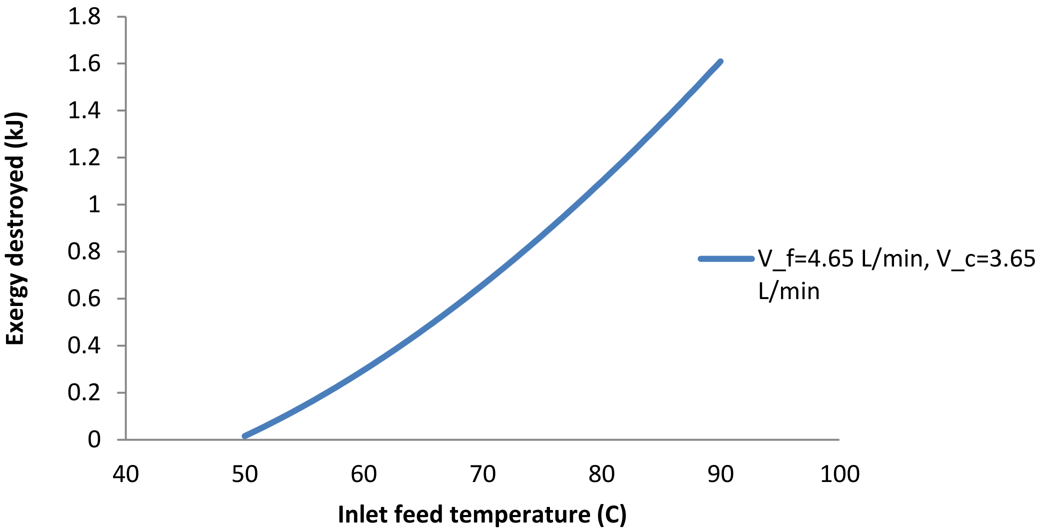

Figure 7. 4 Effect of feed temperature on entropy generation

Operating Conditions: PTFE 0.45 microns, cold permeate temperature 25 ^{o}C, feed flow rate 4.65L/min, coolant flow rate 3.65 L/m , feed salinity 140 mg/L

Figure 7.5 shows exergy analysis where combined effect of feed flow rate and inlet feed temperature was analysed collectively. In order to analyse the effect of feed flow rate, it was varied between 1 L/min to 5 L/.min, cold permeate flow rate was fixed at 3.65L/min, with cold permeate temperature was held at 25 ^{o}C, different feed temperature values were selected e.g. 50 ^{o}C to 90 ^{o}C with an increment of 10 ^{o}C. It is observed that increasing the feed flow rate increases the exergy destruction, also increasing feed temperature increases the exergy destruction as indicated earlier. Another observation can be made; i.e. as feed temperature is increasing, slope and radius of curvature of the lines is increasing e.g. at 50 ^{o}C, slope is $4.905x10^{-3}$ and at 90 ^{o}C, the slope is 0.0772.

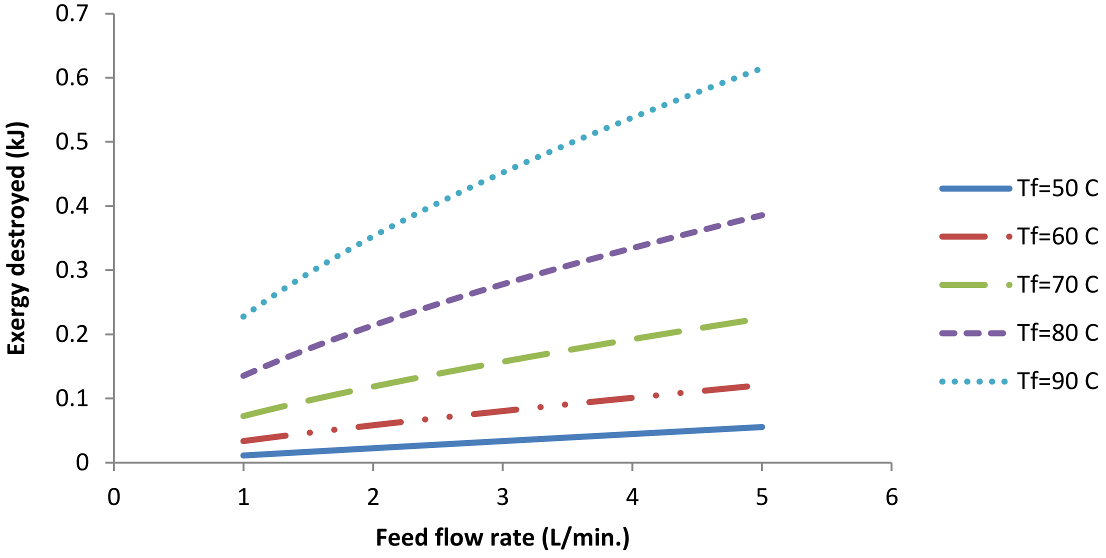

Figure 7. 5 Effect of feed flow rate on exergy destruction

Operating Conditions: PTFE 0.45 microns, cold permeate temperature 25 ^oC, cold permeate flow rate 3.65 L/min , feed salinity 140 mg/L

Figure 7.6 shows the influence of cold permeate flow rate on exergy destruction at selected inlet feed temperatures. As it is shown increasing the feed temperature, increases exergy destruction. Exergy destruction seems to be not sensitive to cold permeate flow rate. Increasing the flow rate from 1L/min to 5L/min doesn't show much variation in exergy destruction. Another observation can be made regarding fig. 7.6 that as inlet feed temperature increases from 50 ^oC to 90 ^oC the exergy destruction lines are shift up with increasing rate. E.g. if feed temperature is increased from 50 to 90 C, with step size of 10 C, the %age of exergy destruction decreases as 106 %, 88 %, 72.2 % and 59.98 % respectively reference to the lower feed temperature.

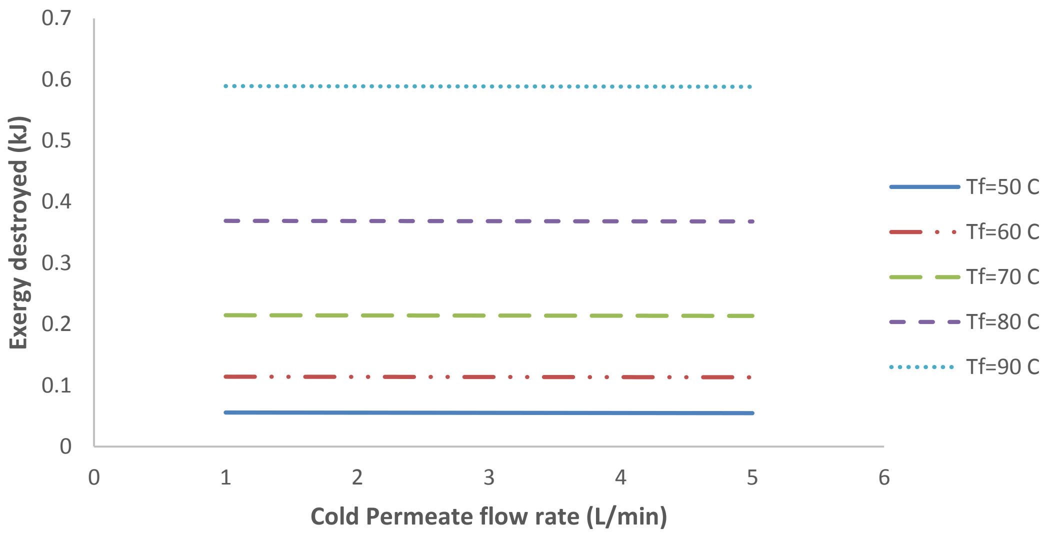

Figure 7. 6 Effect of cold permeate flow rate on exergy at different feed temp.

Operating Conditions: PTFE 0.45 microns, cold permeate temperature 25 ^{o}C, feed flow rate 4.65 L/min , feed salinity 140 mg/L

Figure 7.7 depicts the influence of cold permeate flow rate at various cold permeate temperatures. It is observed that at elevated cold permeate temperatures, exergy destruction is low but as soon as the cold permeate temperature drops to 20 ^{o}C from 25 ^{o}C, exergy destruction increases by 6.1%. Further if cold permeate temperature decreases from 20 ^{o}C to 10 ^{o}C, exergy destruction increases by 6.7 % only. In other words it can also be said that decreasing the cold permeate temperature, increases the temperature difference between feed and cold permeate sides, which increases the heat transfer because of which exergy destruction or entropy generation increases.

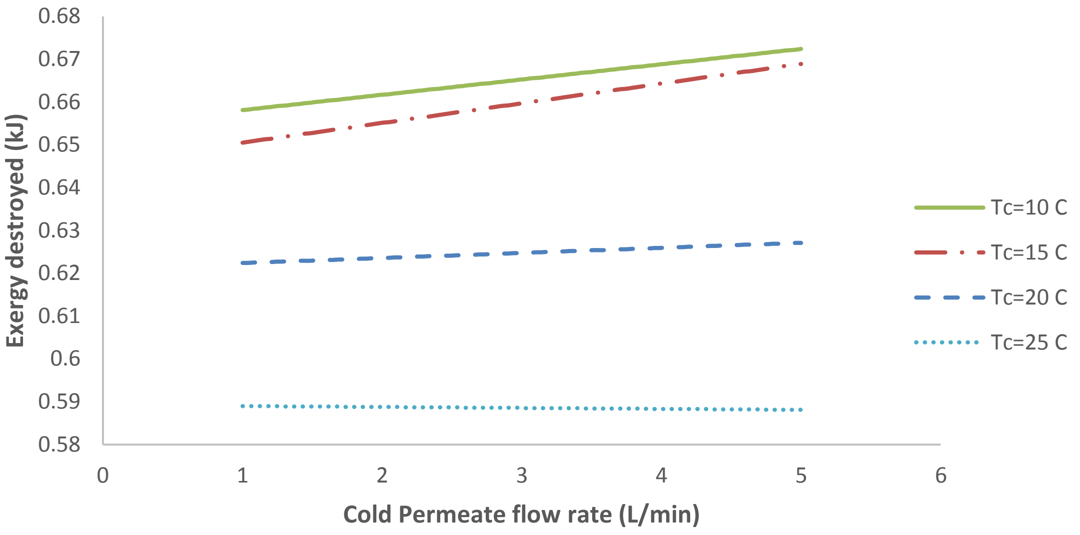

Figure 7. 7 Effect of cold permeate flow rate on exergy at different permeate temp.

Operating Conditions: PTFE 0.45 microns, feed temperature 90 °C, feed flow rate 4.65 L/min , feed salinity 140 mg/L

7.1.4 Heat analysis of DCMD

In order to analyse the heat required to produce fresh water under steady state conditions, thermocouples at the inlet and outlet of hot compartment of module were installed. Then heat input to the system (Q_{in}) is calculated by using the following equation

$$Q_{in} = m_f \times c_p \times \Delta T_{module} \tag{56}$$

Where

m_f ; mass flow rate of feed (kg/s);

C_p; specific heat of feed at given temperature and salinity (J/kg-K)

ΔT_{module} is temperature difference between inlet and outlet of feed (K)

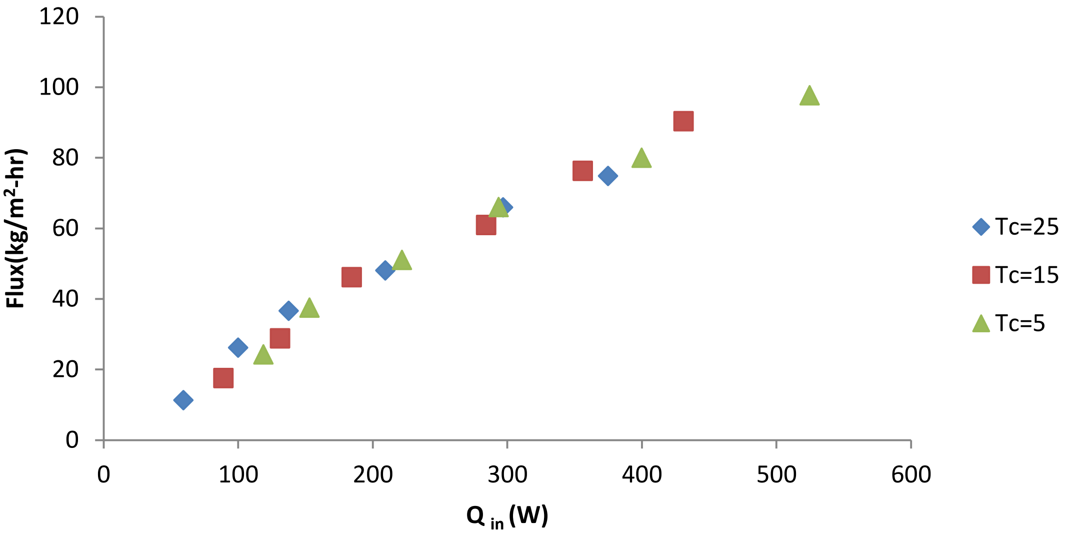

Figure 7. 8 Effect of heat input on the flux for DCMD

Operating Conditions: PTFE 0.45 microns, feed flow rate 4.65 L/min , feed salinity 2g/L, selected feed temperature 50,60,70,80,90 °C

As shown in fig. 7.8, increasing the input energy to the system, increases the flux production increases parabollicaly. It is happening because input energy is increased by increasing the inlet feed temperature (or the temperature difference between feed and cold permeate side) which leads to transmembrane temperature difference between feed and cold permeate side, which eventually is the driving force for the flux permeation. Further it can be seen that cold permeate temperature is not significant for input heat, as fig 7.8 shows three different result of input heat against flux output at three different cold permeate temperatures. Analysis shows that, 375 W of electrical energy is required to produce 75 kg of fresh water per hour per m^2 of effective membrane area. Or in simple words, 1.775 tons of fresh water can be produced per day for $1m^2$ of effective membrane area by consuming 9 kW of electrical energy subjected to the following conditions of operations; PTFE membrane with pore size of 0.45 microns, cold permeate temperature 25 °C, feed flow rate 4.65 L/min , feed salinity 140 mg/L was taken.

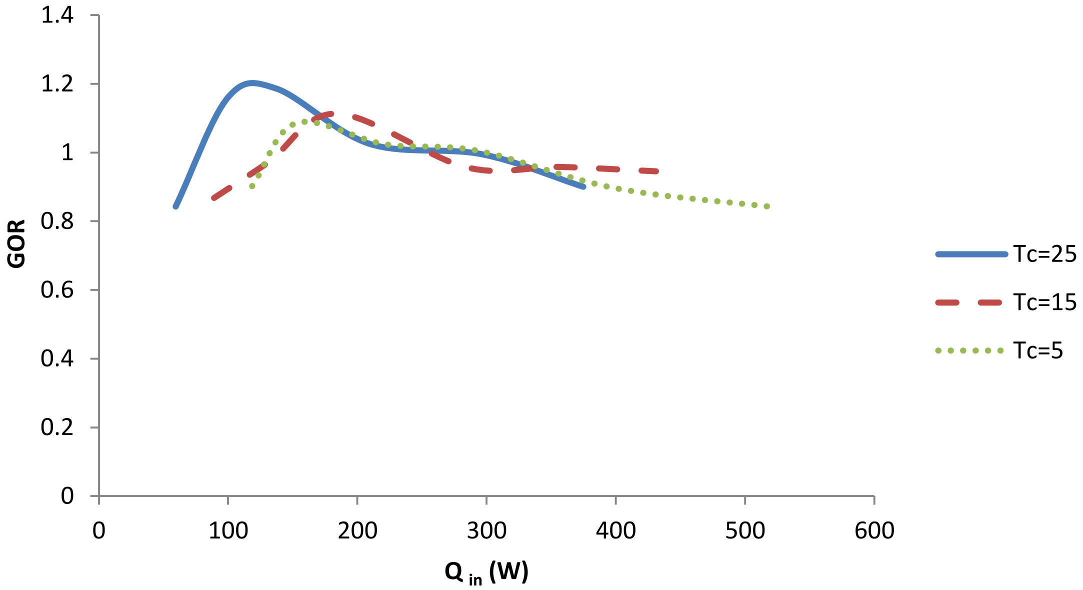

Figure 7. 9 Effect of input energy on GOR for DCMD

Operating Conditions: PTFE 0.45 microns, feed flow rate 4.65 L/min , feed salinity 2g/L, , selected feed temperature 50,60,70,80,90 ^{o}C

Figure 7.9 shows the effect of input energy on the gain output ratio at different cold permeate temperatures, under the same operating conditions as explained earlier. It shows that increasing the input energy increases the GOR up to certain value (150W) and then goes on decreasing as we increase the input heat. But the GOR value remains between 0.8 and 1.2 when the input energy was ranged between 59 W and 375W corresponding to cold permeate temperature of 25 ^{o}C. The reason behind this can be explained well on the basis of figure 5.28, which represents that GOR value increases up to 1.2 by increasing the feed temperature from 40 ^{o}C to 60 ^{o}C and then goes on decreasing. Because increasing the feed temperature above certain value, yields more temperature drop in the feed side or heat loss increases that results in lessened value of GOR at high feed temperature or at high input heat energy.

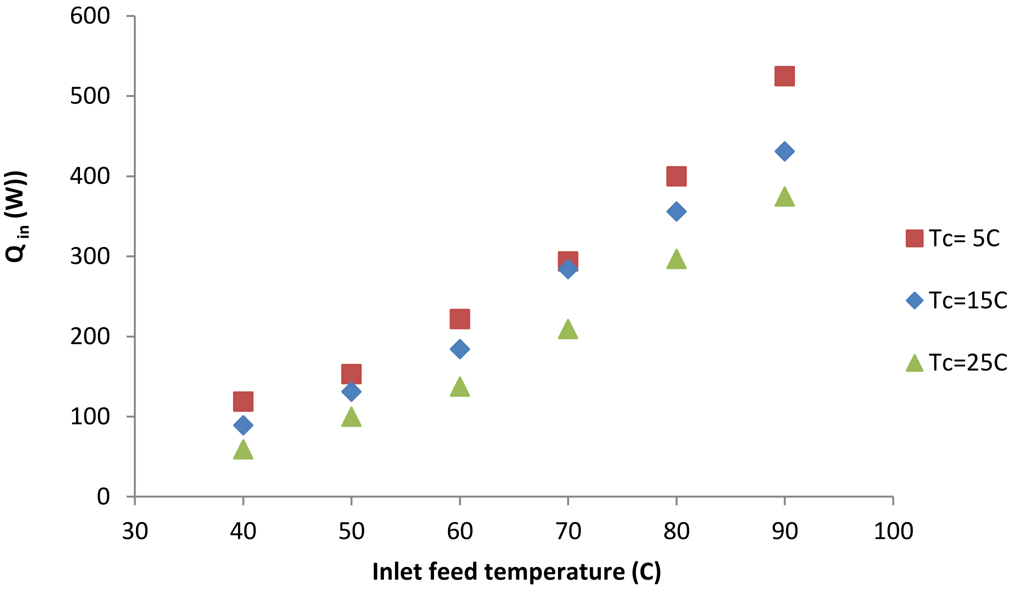

Figure 7. 10 Effect of feed temperature on input heat for DCMD

Operating Conditions: PTFE 0.45 microns, feed flow rate 4.65 L/min , feed salinity 2g/L, selected feed temperature 50,60,70,80,90 ^{o}C

Figure 7.10 represents the effect of inlet feed temperature on input heat supplied to the system at different cold permeate temperatures. Results show that increasing the feed temperature increases the input energy exponentially at all cold permeate temperatures. But if the cold permeate temperature is low, more input energy will be required to produce more flux due to which input energy will be increased. The reason behind this phenomenon is that as feed temperature exceeds 70 ^{o}C, internal heat losses of membrane module start to dominate over flux production as this phenomenon can be observed in fig 7.1, which represents that GOR increases with increases of feed temperature up to 60 ^{o}C then it starts to decrease until we reach 90 ^{o}C feed temperature.

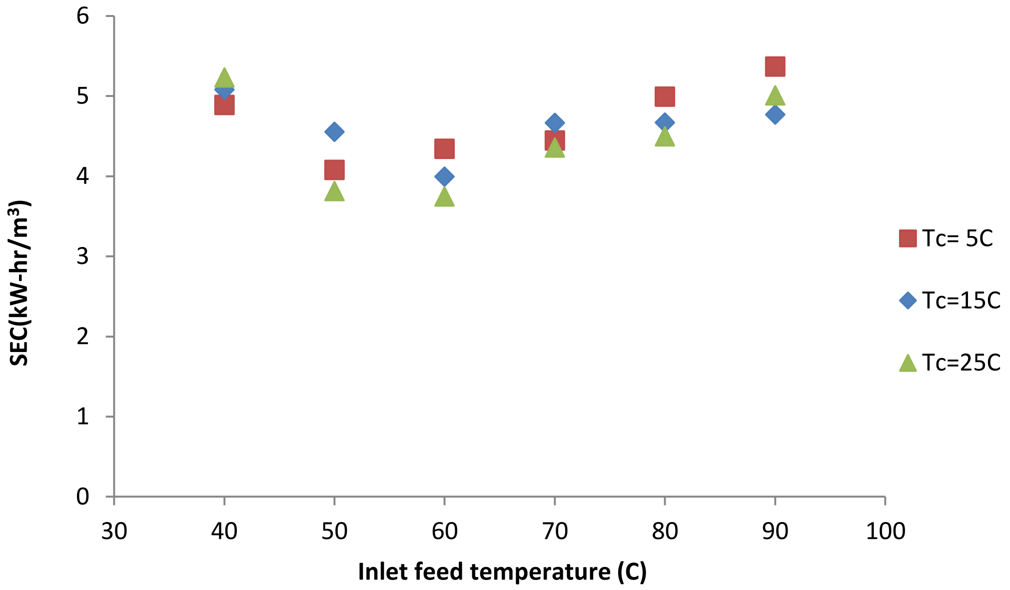

Figure 7. 11 Effect of feed temperature on SEC for DCMD

Operating Conditions: PTFE 0.45 microns, feed flow rate 4.65 L/min , feed salinity 2g/L

Figure 7.11 shows the influence of inlet feed temperature on specific energy consumption (Energy consumed to produce per m^3 of fresh water by DCMD) at different cold permeate temperature. It is observed that similar trend can be observed as was seen for GOR in fig 7.1. Increasing the inlet feed temperature, decreases the specific energy consumption up to 60 ^{o}C of feed temperature and then it goes on increasing until feed temperature was raised up to 90 ^{o}C. The same reason can be found, that increasing the feed temperature increases the flux and heat loss. So up to 60 of feed temperature, flux dominates over heat loss, but after 60 of feed temperature, heat loss is more as compare to flux production. That is why at low feed temperature, low specific energy will be consumed to produce fresh water but at high feed temperature, more energy will be required to produce fresh water.

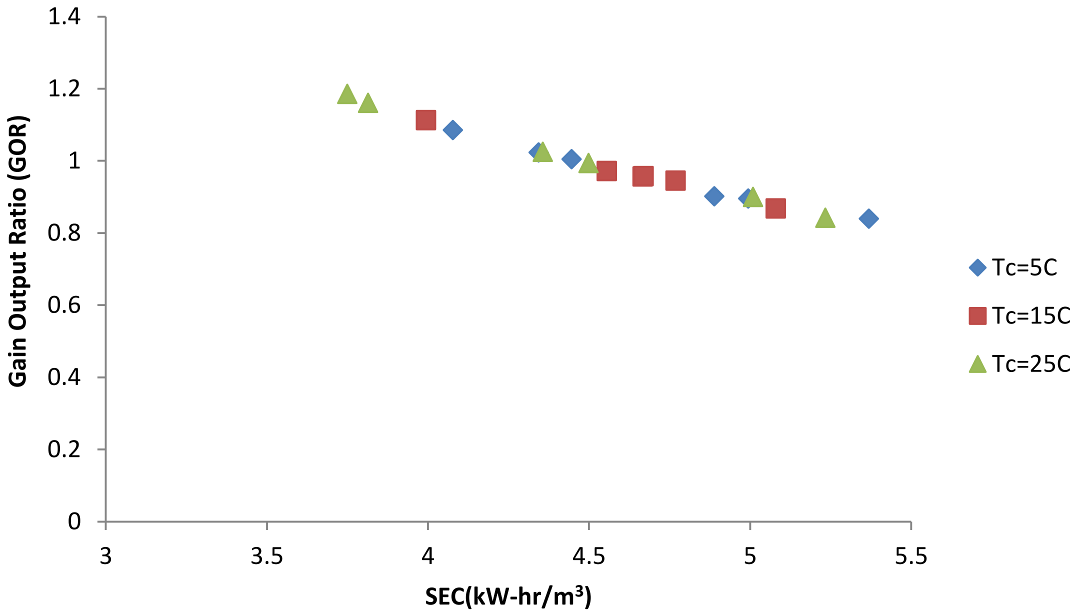

Figure 7. 12 Effect of SEC on GOR for DCMD

Operating Conditions: PTFE 0.45 microns, °C, feed flow rate 4.65 L/min , feed salinity 2g/L, , selected feed temperature 50,60,70,80,90 °C

Figure 7.12 represents relation between specific energy consumption against gain output ratio at different cold permeate temperature. Again it seems cold permeate temperature is not very important parameter, because specific energy consumption values are quite similar at different cold permeate temperatures. By increasing the specific energy consumption, GOR is decreasing. The basic factor in decreasing the GOR is the sum of conductive and evaporative heat loss across the membrane, which is going to increase at high feed temperature which increases input energy or specific energy consumption.

7.2 Comparative energy analysis of WGMD and AGMD

Figure 7.13 is representing the effect of inlet feed temperature on gain output ratio (GOR) for WGMD and AGMD comparatively. It is observed that increasing the inlet feed temperature, increases the GOR for WGMD and AGMD both. But for WGMD, GOR value increases up to 80 °C feed temperature and then stats to decreases after 80 °C. Similar sort of trend was observed for DCMD in fig 7.2. But for AGMD GOR values goes on increasing by increasing the inlet feed temperature. GOR values for WGMD remains in between 0.558 and 1.25 and for AGMD it remains between 0.81 and 1.3.

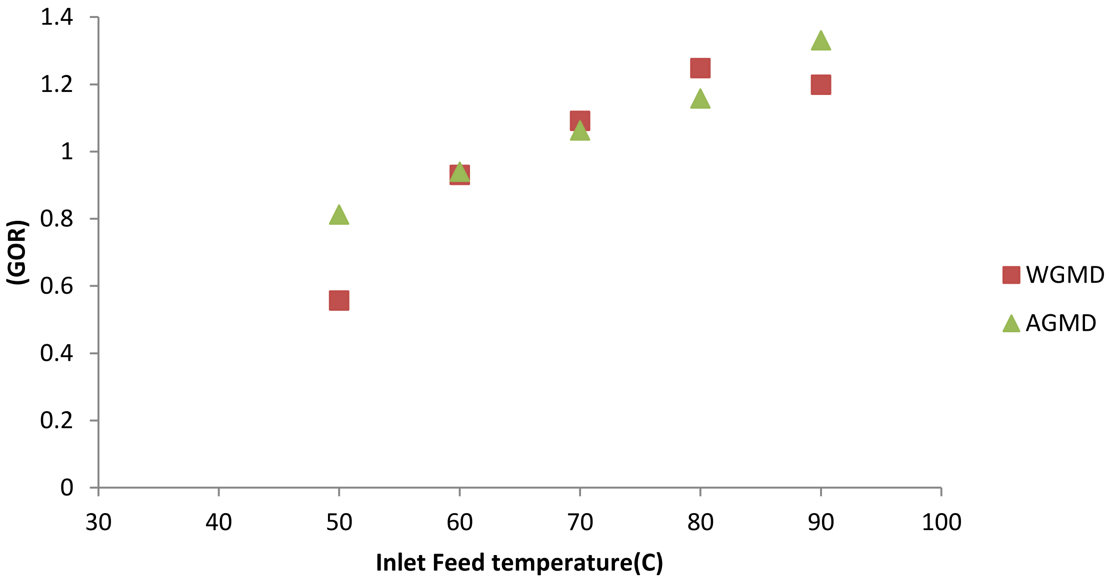

Figure 7. 13 Effect of feed temperature on GOR for WGMD and AGMD

Fig 7.14 shows the influence of inlet feed temperature on specific energy consumption for WGMD and AGMD comparatively. It is observed that at low feed temperature, specific energy consumption is more and then at high feed temperature, specific energy consumption is lower. So increasing the feed temperature decreases the specific energy consumption for both configurations. Also it can be observed that there is a visible difference of energy consumption between WGMD and AGMD at lower feed temperature as compared to higher feed temperature..

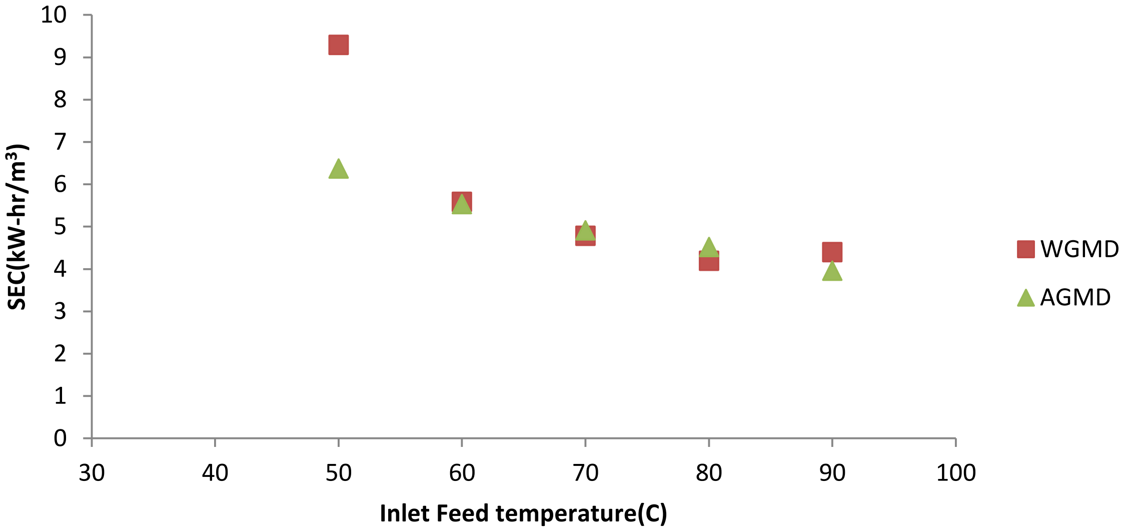

Figure 7. 14 Effect of feed temperature on SEC for WGMD and AGMD

Operating Conditions: Gap width 2 mm, PTFE 0.45 microns , 1.8L/min feed flow rate ,2L/min coolant flow rate, 180 mg/L salinity Coolant temperature 25 ºC

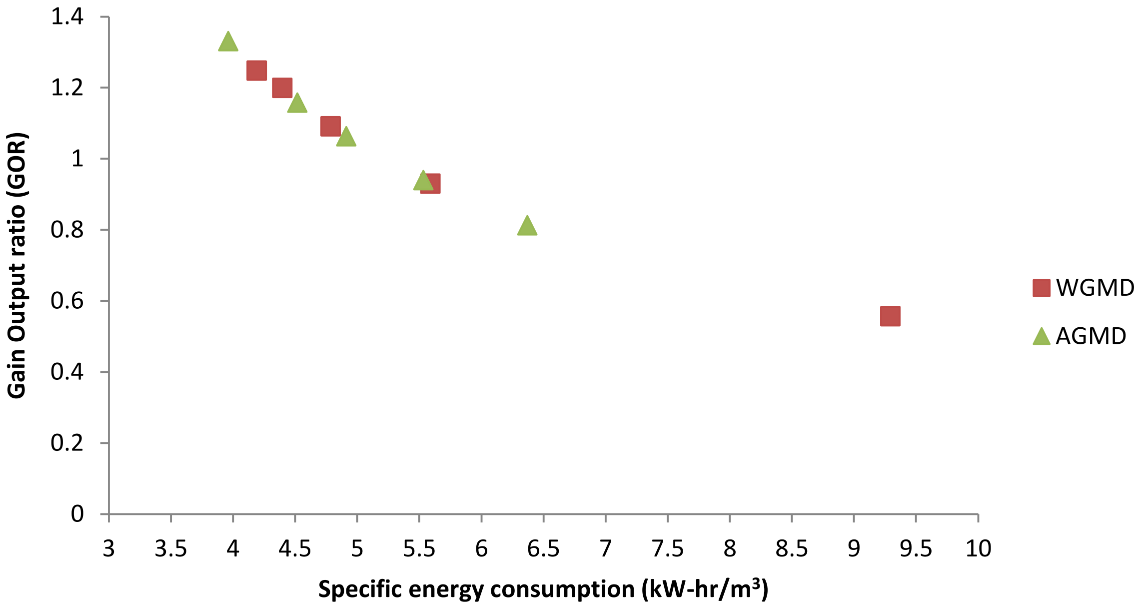

Figure 7. 15 Effect of specific energy consumption on GOR for AGMD and WGMD

Operating Conditions: Gap width 2 mm, PTFE 0.45 microns, 1.8L/m feed flow rate , 2L/min coolant flow rate, 180 mg/L salinity Coolant temperature 25 °C

Figure 7.15 describes the effect of specific energy consumption on gain output ratio at coolant temperature of 25 °C. It shows that increasing the specific energy consumption decreases the gain output ratio. This trend seems similar to DCMD trend fig 7.12.And the reason behind this can be the same as for DCMD, i.e. heat transfer across the membrane surface. More elaborately, increasing the inlet feed temperature, increases the input energy to the membrane module, which increases the energy consumption, which leads to more production in flux as well as more heat transfer loss across the membrane surface i.e. conductive and evaporative heat loss through the membrane surface. So heat transfer loss dominates over the flux production.

CHAPTER 8

CONCLUSION

Water desalination using direct contact membrane distillation, water gap membrane distillation and air gap membrane distillation had been investigated. The effect of DCMD, WGMD and AGMD operating parameters such as feed temperature, coolant temperature, feed flow rate, coolant flow rate and air gap width(for WGMD and AGMD) on the distillate water production had been investigated experimentally. The influence of membrane pore size and membrane material on permeate flux was also investigated. The impact of feed solution concentration and membrane usage time on permeate flux as well as on salt rejection factor (quality of the permeated liquid) were studied and presented.

Theoretical modelling of DCMD system has also been presented and successfully implemented using Engineering Equation Solver (EES). The effect of feed temperature, coolant temperature, feed flow rate, coolant flow rate on permeate flux was investigated analytically. The role of membrane pore size, membrane material on permeate flux was also investigated and presented. The DCMD thermal efficiency, Gained output ratio as well as temperature polarization coefficient was thoroughly investigated theoretically at different system operating parameters such as feed temperature, feed flow rate, coolant temperature and coolant flow rate.

The used membranes material are polyvinydiflouiride (PVDF) and polytetraflouroethylene (PTFE) having two different pore sizes of 0.45 μm and 0.22 μm. The tested feed solutions are tap water, laboratory prepared salt water solution and raw seawater. The tested feed water solutions concentrations are: 0.140 g/L, 2 g/L, 43 g/L, and 100 g/L.

Permeate flux increases with increasing feed temperature and feed flow rate. Increasing the coolant flow rate tends to marginally increase the system performance. For DCMD system the following conclusions can be made

- Feed temperature recorded the maximum of 302.5% increment in flux when it was increased from 40^0C to 90^0C at low inlet coolant temperature of 5 ^{o}C
- 30.6 % increase in flux is observed when inlet coolant temperature decreased from 25 ^{o}C to 5^{o}C.
- 39.1 % increase in flux percentage was observed when feed flow rate was increased from 2.5 L/min to 4.5 L/min..
- Only 4.79 % increases in flux is observed when coolant flow rate was increased from 2 L/min. to 3.65 L/min.
- The maximum and minimum percentage increase in flux was observed to be 671% and 98% for PTFE and 500% and 75% for PVDF as compared to their flux values at 40 ^{o}C under the following conditions; coolant temperature 25 ^{o}C, feed flow rate 4.65 L/m, coolant flow rate 3.65 L/m, feed salinity 43 g/L

Based on the aforementioned fact, the system performance is essentially dominated by the effect of both feed temperature and feed flow rate. Although feed flow rate carries less weightage as compared to feed temperature yet the effect of feed flow rate is visible. Coolant temperature have relative considerable effect on flux. While the effect of coolant flow rate on system performance is marginal or negligible. There was no clear difference in the quality of permeate flux produced using the two membrane materials off PTFE and PVDF.

Therefore, the conclusion is flux increases with increasing in membrane pore size.

Experimental comparison of DCDM and AGMD was also given with the following conclusions;

- Maximum percentage difference of flux was 54.67 % at 40 °C and minimum percentage difference was coming out to be 18.82 % only at 80 °C. It means DCMD was becoming more attractive at low feed temperature instead of high feed temperature.
- When checked the effect of inlet coolant temperature, percentage increase in flux was more at high inlet coolant temperature as compared to low coolant temperature for low feed temperature of 40 °C.
- Talking about the effect of coolant flow rate, the percentage difference in flux is slightly higher at high feed flow rate, but the difference in numerical values is not big. And the same conclusion can be drawn for the effect of coolant flow rate.
- PTFE membrane gives more flux as compared to PVDF for both DCMD and AGMD configurations

Another comparative study was made on the performance of WGMD and AGMD configurations, and the following conclusions can be made;

- By increasing the feed temperature, permeate flux increases irrespective of configurations. But AGMD gives rise 489.4 % of flux as compared to 50 °C flux , and WGMD gives 393.8 % increment in flux at 5 °C of inlet coolant temperature which senses that the inlet feed temperature is highly significant factor for both configurations.
- Similarly variation of inlet coolant temperature from 24 °C to 5°C yields 15.3 %

increase in flux for AGMD and only 3.93 % increase in flux for WGMD, which governs that effect of inlet coolant temperature is not highly significant.

- Regarding the effect of membrane materials (PTFE and PVDF), PTFE membrane gives more flux as compared to PVDF for both configurations.
- And the effect of pore size consequences that bigger pore size membrane yields more flux in both systems.
- The other important parameter is the air gap width, increasing the air gap width decreases the flux. For WGMD, decreasing the water gap width from 12 mm to 2mm outcomes the 22.3 % increase in flux. But for AGMD decreasing the air gap width from 12mm to 2mm increases the flux percentage by 142.3 %. So the importance of gap width is very high for AGMD as compared to WGMD.

Another comparison was made for DCMD, WGMD and AGMD finally. It was observed that for DCMD yields more flux than WGMD and AGMD at selected cold permeate temperatures of 5 ^{o}C, 15 ^{o}C and 25 ^{o}C.

In all the experiments it was seen that WGMD gives more flux as compared to AGMD system at all the feed and coolant temperatures. When effect of inlet feed temperature was observed over gain output ratio (GOR), it was concluded that DCMD yields GOR between 0.8-1.2, but WGMD and AGMD gives between 0.8-1.25. The similar trend for GOR was observed for DCMD and WGMD at selected cold permeate temperatures, i.e. GOR values increases with increasing feed temperature (up to 60 ^{o}C for DCMD and 80 ^{o}C for WGMD) and then decreases with the increase in feed temperature. Specific energy consumption (Energy consumed per m^3 of fresh water produced) were calculated for these three configurations. It was concluded that increasing the inlet feed temperature, decreases the specific energy consumption for AGMD and WGMD rapidly but trend is found quite smooth for DCMD. Specific energy consumption was 5.2 kW-hr/m^3 for AGMD , 5.1 kW-hr/m^3 for DCMD and 6.85 kW-hr/m^{3}for WGMD were calculated. Literature shows that specific energy consumption for RO process range between 4.22-7.9 kW-hr/m^3 and for MSF , specific energy consumption is 26.4 kW-hr/m^3 [115, 118]. Macedonio et.al. reported that for sea water desalination, RO consumes 2.2-6.7 kW-hr and MSF consumes 17-18 kW-hr of energy to produce m^3 of fresh water [119]. It was also noted down that increasing the specific energy consumption decreases the gain output ratio for all configurations.

REFERENCES

1. Bleninger, T., G. Jirka, and S. Lattemann, Environmental planning, prediction and management of brine discharges from desalination plants. Middle East Desalination Research Center (MEDRC): Muscat, Sultanate of Oman, 2010.
2. http://environment.nationalgeographic.com/environment/freshwater/freshwater-crisis/, Fresh Water Crisis.
3. Richard E. Smalley and Nobel Laureate, Seawater Desalination Department of Chemical and Environmental Engineering Yale University Menachem Elimelech. 2012.
4. Singh, R.P., Water Desalination "The Role of RO and MSF".
5. Mabrouk, A.-N.A., Techno-economic analysis of tube bundle orientation for high capacity brine recycle MSF desalination plants. 2013.
6. Toufic Mezher , H.F., Zeina Abbas, Arslan Khaled, Techno-economic assessment and environmental impacts of desalination technologies. 2010.
7. Kim Choon Ng , K.T., Youngdeuk Kim , Anutosh Chakraborty , Gary Amy, Adsorption desalination: An emerging low-cost thermal desalination method. 2012.
8. McClain, M.E., Balancing water resources development and environmental sustainability in Africa: a review of recent research findings and applications. Ambio, 2013. **42**(5): p. 549-65.
9. Report, U., The United Nation World Water Development Report 4, 2015, United Nations Educational,Scientific,and Cultural Organization: UNESCO.
10. Report, U., The Sources of Fresh Water-Modlule 7
11. Abdul Ghani I. Dalvi, R.A.A.-R.A.M.A.J., STUDIES ON ORGANIC FOULANTS IN THE SEAWATER FEED OF REVERSE OSMOSIS PLANTS OF SWCC.
12. Policy, U.E.P., Drinking Water Advisory:Consumer Acceptability Advice and Health Effects Analysis on Sodium. 2003.
13. Andrjesdóttir, Ó., et al., An experimentally optimized model for heat and mass transfer in direct contact membrane distillation. International Journal of Heat and Mass Transfer, 2013. **66**: p. 855-867.
14. Macedonio, F., et al., Direct contact membrane distillation for treatment of oilfield produced water. Separation and Purification Technology, 2014. **126**: p. 69-81.
15. Manawi, Y.M., et al., A predictive model for the assessment of the temperature polarization effect in direct contact membrane distillation desalination of high salinity feed. Desalination, 2014. **341**: p. 38-49.
16. Hsu, S.T., K.T. Cheng, and J.S. Chiou, Seawater desalination by direct contact membrane distillation 2002.

17. Boubakri, A., A. Hafiane, and S.A.T. Bouguecha, Direct contact membrane distillation: Capability to desalt raw water. Arabian Journal of Chemistry, 2014.
18. Lin, S., N.Y. Yip, and M. Elimelech, Direct contact membrane distillation with heat recovery: Thermodynamic insights from module scale modeling. Journal of Membrane Science, 2014. **453**: p. 498-515.
19. Srisurichan, S.J., R. Fane, A., Mass transfer mechanisms and transport resistances in direct contact membrane distillation process. Journal of Membrane Science, 2006. **277**(1-2): p. 186-194.
20. Naidu, G., S. Jeong, and S. Vigneswaran, Influence of feed/permeate velocity on scaling development in a direct contact membrane distillation. Separation and Purification Technology, 2014. **125**: p. 291-300.
21. Ho, C.-D., et al., Performance improvement on distillate flux of countercurrent-flow direct contact membrane distillation systems. Desalination, 2014. **338**: p. 26-32.
22. Qtaishat, M., et al., Heat and mass transfer analysis in direct contact membrane distillation. Desalination, 2008. **219**(1-3): p. 272-292.
23. U. Lawal, D. and A. E. Khalifa, Flux Prediction in Direct Contact Membrane Distillation. International Journal of Materials, Mechanics and Manufacturing, 2014. **2**(4): p. 302-308.
24. Francis, L., et al., Material gap membrane distillation: A new design for water vapor flux enhancement. Journal of Membrane Science, 2013. **448**: p. 240-247.
25. Khalifa, A.E., Water and air gap membrane distillation for water desalination – An experimental comparative study. Separation and Purification Technology, 2015. **141**: p. 276-284.
26. Essalhi, M. and M. Khayet, Application of a porous composite hydrophobic/hydrophilic membrane in desalination by air gap and liquid gap membrane distillation: A comparative study. Separation and Purification Technology, 2014. **133**: p. 176-186.
27. Khayet, M., C. Cojocaru, and C. Garcia-Payo, Application of response surface methodology and experimental design in direct contact membrane distillation. Industrial & engineering chemistry research, 2007. **46**(17): p. 5673-5685.
28. <Separation of binary mixtures by thermostatic sweeping gas membrane distillation I Theory and simulations .pdf>.
29. 2008, W.H.O.-G., Guidelines for Drinking water quality Vol. 1 [electronic resource] Recommendations. – 3rd ed., ISBN 92 4 154696
30. Igor Shiklomanov's chapter "World fresh water resources" in Peter H.Gleick (editor), 1993, Water in Crisis: A Guide to the World's Fresh Water Resources (Oxford University Press, New York).
31. World Bank development education program, beyond economic growth.

32. United Nations News Centre - Ballooning global population adding to water crisis, warns new UN report.
33. Gleick, P.H., Dirty Water: Estimated Deaths from Water-Related Diseases 2000-2020 Pacific Institute Research Report
34. UN World water development report.
35. Population institute report, J., <Water_and_population_2.pdf>.
36. Water in a changing world, The United Nations World Water Development Report 3.
37. Kyaw Thu, A.C., Young-Deuk Kim, Aung Myat, Bidyut Baran Saha and Kim Choon Ng, Numerical simulation and performance investigation of an advanced adsorption desalination cycle. 2012.
38. Group, W.R., A Comprehensive Report on Charting of Our Water Future.
39. Mohamed A. Eltawil, Z.Z., Liqiang Yuan, A review of renewable energy technologies integrated with desalination systems, Renewable and Sustainable Energy Reviews 13 (2009) 2245–2262
40. M, S., Perspectives and challenges for desalination in the 21st century, Desalination 165(2004)1–9.
41. Mahmoud Shatat, M.W.a.S.R., Opportunities for solar water desalination worldwide: Review, Sustainable Cities and Society 9 (2013) 67–80. .
42. A.Y.Hoekstra, M.M.M., Global water scarcity: the monthly blue water footprint compared to blue water availability for the world's major river basins, Value of water research report series no. 53, UNESCO-IHE Institute for Water Education. .
43. Mulla, M.A.D.a.M.M.A., Enviornmental Impacts of Seawater Desalination: Arabian Gulf Case Study, International Journal of Environment and Sustainability, Vol. 1 No. 3, pp. 22-37 (2012)
44. Dawoud, M.A., The role of desalination in augmentation of water supply in GCC countries, Desalination 186 (2005) 187–198
45. Fath, H., Sadik, Ashraf ,Mezher, Toufic, Present and future trend in the production and energy consumption of desalinated water in GCC countries. Int. J. of Thermal & Environmental Engineering, 2013. **5**(2): p. 155-165.
46. Yan, T.-x.H.a.L.-j., Application of alternative energy integration technology in seawater desalination Desalination 249 (2009) 104–108. .
47. Kalogirou, S.A., Seawater desalination using renewable energy sources, Progress in Energy and Combustion Science 31 (2005) 242– 281.
48. Xavier Bernat, O.G., and Carlos Campos, The economics of desalination for various uses Chapter 18.
49. M. A1-Shammiri, M.S., Multi-effect distillation plants: state of the art, Desalination, Vol. 126 pp. 45-59, (1999).
50. H.T. El-Dessouky, H.M.E., Multiple-effect evaporation desalination systems: thermal analysis, Desalination Vol. 125 pp. 259–276 (1999).

51. Hisham T. El-De ssouky, H.M.E., Faisal Mandani, Performance of parallel feed multiple effect evaporation system for seawater desalination, Applied Thermal Engineering, Vol 20 pp. 1679-1706, (2000).
52. Ali M. E1-Nashar, A.A.Q., Simulation of the steady-state operation of a multi-effect stack seawater distilla tion plant, desalination, Vol. 101 pp. 231-243, (1995). .
53. Ashour, M.M., Steady state analysis of the Tripoli West LT-HT- MED plant, Desalination 152 (2002) 191-194
54. Narmine H. Aly, M.A.M., Dynamic response of multi-effect evaporators, Desalination 114 (1997) 189-196
55. H.T. El-Des souky, H.M.E.y., Fundamentals of salt water desalination, Elsevier, Amsterdam, the Netherlands, (2002).
56. Akili D. Khawaji, I.K.K., Jong-Mihn Wie, Advances in seawater desalination technologies , Desalination 221 (2008) 47–69. .
57. Narmine H. Aly, A.K.E.-F., Thermal performance of seawater desalination systems, Desalination, Vol. 158 pp. 127-142 (2003). .
58. M. A1-Shammiri, M.S., Multi-effect distillation plants: state of the art, Desalination, Vol. 126 pp. 45-59, (1999).
59. Bart Van der Bruggen, C.V., Distillation vs. Membrane filtration: overview of process evolutions in seawater desalination, Desalination 143 (2002) 207-218. .
60. F.N. Alasfour, M.A.D., A.O. Bin Amer, Thermal analysis of ME-TVC+MEE desalination systems. 2004.
61. Al-Radif, A., Review of various combinations of a multiple effect desalination plant (MED) and a thermal vapour compression unit, Desalination, 93 (1993) 119-125.
62. X.L. Wang, K.C.N., Experimental investigation of an adsorption desalination plant using low-temperature waste heat, Appl. Therm. Eng. 25 (2005) 2780–2789.
63. X.L. Wang, A.C., K.C. Ng, B.B. Saha, How heat and mass recovery strategies impact the performance of adsorption desalination plant: theory and experiments, Heat Transfer Eng. 28 (2) (2007) 147– 153.
64. K.C. Ng, X.L.W., L.Z. Gao, A. Chakraborty, B.B. Saha, S. Koyama, A. Akisawa, T.Kashiwag, Apparatus and method for desalination, WO Patent Number 121414 (2006). .
65. K. Thu, A.C., Y.D. Kim, A. Myat, B.B. Saha, K.C. Ng, Numerical simulation and performance investigation of an advanced adsorption desalination cycle, Desalination, (2012). .
66. K. Thu, A.C., B.B. Saha, W.G. Chun, K.C. Ng, Life-cycle cost analysis of adsorption cycles for desalination, Desalination and Water Treatment, 20 (2010) 1-10. .

67. K. Thu, Y.-D.K., A. Myat, A. Chakraborty, K.C. Ng, Performance investigation of advanced adsorption desalination cycle with condenser–evaporator heat recovery scheme, Desalination and Water Treatment, (2012) 1-14.

68. K. Thu, K.C.N., B.B. Saha, A. Chakraborty, S. Koyama, Operational strategy of adsorption desalination systems, International Journal of Heat and Mass Transfer, 52 (2009) 1811-1816. .

69. K.C. Ng, K.T., A. Chakraborty, B.B. Saha, W.G. Chun, Solar- assisted dual-effect adsorption cycle for the production of cooling effect and potable water, International Journal of Low-Carbon Technologies, 4 (2009) 61-67. .

70. K.C. Ng, K.T., B.B. Saha, A. Chakraborty, Study on a waste heat- driven adsorption cooling cum desalination cycle, International Journal of Refrigeration, 35 (2012) 685-693.

71. Kyaw Thu, K.C.N., Bidyut B. Saha, Anutosh Chakraborty and Shigeru Koyam, Operational strategy of adsorption desalination systems, International Journal of Heat and Mass Transfer 52 (2009) 1811–1816. .

72. Wai Soong Loh, B.B.S., Anutosh Chakraborty, Kim Choon Ng, Wongee Chun, Performance analysis of waste heat driven pressurized adsorption chiller, Journal of thermal science and technology, Volume5, No. 2, 2010.

73. W.S. Loh, I.I.E.-S., Kim Choon Ng, Bidyut Baran Saha, Adsorption cooling cycles for alternative adsorbent/adsorbate pairs working at partial vacuum and pressurized conditions, Applied Thermal Engineering 29 (2009) 793–798

74. M.A. Darwish, N.M.A.N., Energy consumption by multi stage flash and reverse osmosis desalters 1999.

75. Akili D. Khawajia , I.K.K., Advances in seawater desalination technologies Desalination.

76. Mulla, M.A.D.a.M.M.A., Environmental Impacts of Seawater Desalination: Arabian Gulf Case Study.

77. Bleninger, D.-I.T. and P.G.H. Jirka, Environmental planning, prediction and management of brine discharges from desalination plants Final report Principal Investigators.

78. Khayet, M., Membranes and theoretical modeling of membrane distillation: a review. Adv Colloid Interface Sci, 2011. **164**(1-2): p. 56-88.

79. Essalhi, M. and M. Khayet, Self-sustained webs of polyvinylidene fluoride electrospun nanofibers at different electrospinning times: 2. Theoretical analysis, polarization effects and thermal efficiency. Journal of Membrane Science, 2013. **433**: p. 180-191.

80. Song, Z.W. and L.Y. Jiang, Optimization of morphology and perf ormance of PVDF hollow fiber for direct contact membrane distillation using experimental design. Chemical Engineering Science, 2013. **101**: p. 130-143.

81. Chen, T.-C., C.-D. Ho, and H.-M. Yeh, Theoretical modeling and experimental analysis of direct contact membrane distillation. Journal of Membrane Science, 2009. **330**(1-2): p. 279-287.
82. Khayet, M. and T.Matsuura, Membrane Distillation Principles and applications.
83. J. Phattaranawika, R.J., A.G. Fane, Effect of pore size distribution and air flux on mass transport in direct contact membrane distillation. 2002.
84. S.B. Iversen , V.K.B., K. Dam-Johansen , G. Jonsson Characterization of microporous membranes for use in membrane contactors. 1997.
85. Alkhudhiri, A., N. Darwish, and N. Hilal, Membrane distillation: A comprehensive review. Desalination, 2012. **287**: p. 2-18.
86. Phattaranawik, J., Effect of pore size distribution and air flux on mass transport in direct contact membrane distillation. Journal of Membrane Science, 2003. **215**(1-2): p. 75-85.
87. Yun, Y., et al., Direct contact membrane distillation mechanism for high concentration NaCl solutions. Desalination, 2006. **188**(1-3): p. 251-262.
88. J. Phattaranawika, R.J., A.G. Fane, Heat transport and membrane distillation coefficients in direct contact membrane distillation. 2002.
89. MartÍNez-DÍEz, L., F.J. Florido-DÍAz, and M.I. VÁZquez-GonzÁLez, Study of Polarization Phenomena in Membrane Distillation of Aqueous Salt Solutions. Separation Science and Technology, 2000. **35**(10): p. 1485-1501.
90. L Martínez-Díez and M.I. Vázquez-González, Temperature and concentration polarization in membrane distillation of aqueous salt solutions. 1998.
91. Banat, F.A. and J. Simandl, Desalination by Membrane Distillation: A Parametric Study. Separation Science and Technology, 1998. **33**(2): p. 201-226.
92. Masao Sudoh , K.T., Hiroshi Iizuka , Kotoku Nagamatsuya, Effects of thermal and concentration boundary layers on vapour permeation in membrane distillation of aqueous lithium bromide solution.
93. L. Martı´nez-Dı´ez , M.I.V.e., Effects of polarization on mass transport through hydrophobic porous membranes.
94. Mengual, J.I., M. Khayet, and M.P. Godino, Heat and mass transfer in vacuum membrane distillation. International Journal of Heat and Mass Transfer, 2004. **47**(4): p. 865-875.
95. HALLSTROM, V.G.a.B., Mass transfer in the membrane concentration polarization layer under turbulent cross flow Critical literature review
96. Kevin W. Lawson and D.R. Lloyd, Membrane distillation. 1996.
97. Srisurichan, S., R. Jiraratananon, and A. Fane, Mass transfer mechanisms and transport resistances in direct contact membrane distillation process. Journal of Membrane Science, 2006. **277**(1-2): p. 186-194.
98. P. Termpiyakul, R.J., S. Srisurichan, Heat and mass transfer characteristics of a direct contact membrane distillation process for desalination.

99. M. Tomaszewska, M.G., and A.W. Morawski, A study of separation by the direct contact membrane distillation process.

100. Izquierdo-Gil, M.A., C. Fernández-Pineda, and M.G. Lorenz, Flow rate influence on direct contact membrane distillation experiments: Different empirical correlations for Nusselt number. Journal of Membrane Science, 2008. **321**(2): p. 356-363.

101. SHOJI KIMURA, S.-I.N., Transport phenomena in membrane distillation.

102. M. Gryta *, M.T., A.W. Morawski, Membrane distillation with laminar flow.

103. G.C. Sarti, C.G., S. Matuili Low energy cost desalination processes using hydrophobic membranes Desalination.

104. Curcio, E. and E. Drioli, Membrane Distillation and Related Operations—A Review. Separation & Purification Reviews, 2005. **34**(1): p. 35-86.

105. Mohamed Khayet, A.V.z.a.J.I.M., Modelling mass transport through a porous partition effect of pore size distribution.

106. Manawi, Y.M., et al., Effect of operational parameters on distillate flux in direct contact membrane distillation (DCMD): Comparison between experimental and model predicted performance. Desalination, 2014. **336**: p. 110-120.

107. Zhang, J., S. Gray, and J.-D. Li, Predicting the influence of operating conditions on DCMD flux and thermal efficiency for incompressible and compressible membrane systems. Desalination, 2013. **323**: p. 142-149.

108. Lawal, D.U., MSc Thesis Report in Mechanical Engineering Department2015, King Fahd University of Petroleum and Minerals

109. Khayet, M. and T. Matsuura, Membrane distillation: principles and applications. 2011: Elsevier.

110. Kays, W., M. Crawford, and B. Weigand, Convective Heat and Mass Transfer. Fourth ed.: McGraw hill International Edition.

111. Summers, E.K., H.A. Arafat, and J.H. Lienhard, Energy efficiency comparison of single-stage membrane distillation (MD) desalination cycles in different configurations. Desalination, 2012. **290**: p. 54-66.

112. Sharqawy, M.H., J.H. Lienhard V, and S.M. Zubair, On exergy calculations of seawater with applications in desalination systems. International Journal of Thermal Sciences, 2011. **50**(2): p. 187-196.

113. Molinari, R., R. Gagliardi, and E. Drioli, Methodology for estimating saving of primary energy with membrane operations in industrial processes. Desalination, 1995. **100**(1): p. 125-137.

114. Macedonio, F., E. Curcio, and E. Drioli, Integrated membrane systems for seawater desalination: energetic and exergetic analysis, economic evaluation, experimental study. Desalination, 2007. **203**(1-3): p. 260-276.

115. Criscuoli, A. and E. Drioli, Energetic and exergetic analysis of an integrated membrane desalination system. Desalination, 1999. **124**(1): p. 243-249.

116. Al-Obaidani, S., et al., Potential of membrane distillation in seawater desalination: thermal efficiency, sensitivity study and cost estimation. Journal of Membrane Science, 2008. **323**(1): p. 85-98.
117. Sharqawy, M.H., J.H. Lienhard, and S.M. Zubair, Thermophysical properties of seawater: a review of existing correlations and data. Desalination and Water Treatment, 2010. **16**(1-3): p. 354-380.
118. E.Miller, J., Review of Water Resources and Desalination Technologies, 2003: U.S. Department of Energy. p. 55.
119. Macedonio, F. and E. Drioli, An exergetic analysis of a membrane desalination system. Desalination, 2010. **261**(3): p. 293-299.

VITAE

Name : Hafiz Muhammad Ahmad

Nationality : Pakistan

Date of Birth : 11/13/1989

Email : ahmadidrees89@gmail.com

Address : House no. 19 Street no. 5 Main Bazar Garhi Shahu Lahore

Academic Background: Master of Science (MSc.) Mechanical Engineering (Thermo-fluids) King Fahd University of Petroleum & Minerals Dhahran, Saudi Arabia

Bachelor of Science (BSc.) Mechanical Engineering

University of Engineering & Technology Lahore Pakistan

Publications : 1- H.M.Ahmad, A.E.Khalifa, M.A.Antar "Performance of Direct Contact Membrane Distillation system for water de-salination" (Submitted for publication, ASME-IMECE-2015 Texas US conference)

2- A.E.Khalifa, H.M.Ahmad, M.A.Antar, T.Laoui, M.Khayet "Experimental and theoretical investigation of

DCMD system for water desalination (In progress for publication in international journal of desalination & water treatment)

3- H.M.Ahmad, A.E.Khalifa “Water and air gap membrane distillation for water distillation- 2 an extended comparative study” (In progress for publication in international journal of separation & purification technology)

4- H.M.Ahmad, A.E.Khalifa “Comparative study of DCMD and AGMD system for water desalination” (In progress for publication in international journal of separation & purification technology)

5- H.M.Ahmad, A.E.Khalifa, M.A.Antar “1st and 2nd law analysis of DCMD,AGMD and WGMD configurations” (To be Submitted for publication, Saudi Scientific Conference SSC 7-2016 Kingdom of Saudi Arabia)